Contents

List of Figures

List of Tables

1. Chapter 1: Introduction and motivation for this project

A solar eclipse is a unique atmospheric experiment. It is an approximately circular shaped reduction of global solar radiation the diameter of which can range from several hundred to several thousand kilometres. This forcing travels at speeds of about 2000km/hr or even more which is a supersonic speed. Therefore, any local atmospheric reaction cannot be affected by areas further upstream. Moreover, the forcing is applied very rapidly and hence there cannot be any latent (condensation of vapour) or dynamic effects (meeting of air currents, etc.) playing major role in the atmospheric changes that occur during eclipses. At any one location on the Earth the measurable effect of the solar eclipse can last from just a few minutes up to 2 hours. Therefore, the eclipse is an external forcing applied on the atmosphere, which does not otherwise naturally occur and there is no other similar event that would affect the atmosphere in a way that a solar eclipse does. (Espenak, 2009)

1.1. Rarity of total solar eclipses and opportunities to study them

A total solar eclipse is a very rare event. In any single region on the planet a total solar eclipse occurs on average only once in every 360 years. Globally, there is one total solar eclipse every year on average. The area that a typical total solar eclipse covers is about 4.3 million kilometres squared. The surface area of the planet is about 510 million kilometres squares, which means that a typical solar eclipse covers about 0.85% of the surface of the Earth. On the Earth there is no preferred region for an eclipse and all regions have the same frequency of total solar eclipses. The Earth comprises of about 70% ocean and 30% land. About 1/3 of the land is populated and out of that third, less than 1/5 has a reliable and dense enough network of meteorological stations that regularly record several meteorological variables that are affected by the eclipse. Given all the information above it comes out that globally there is a total solar eclipse that passes over a region with a dense and regularly recording network of meteorological stations only once in about every 50 years on average. Therefore, it is extremely rare to have an opportunity to study atmospheric changes associated with a total solar eclipse over an area. Because of this rarity, studies of eclipses that do occur over regions with good networks of recording meteorological stations are especially treasured (Espenak, 2009)

On 11th August 1999 a total solar eclipse occurred over western and central Europe, which is a densely populated area with dense networks of regularly recording meteorological stations. The observed atmospheric changes associated with the 1999 total eclipse ranged from ionosphere via stratosphere to troposphere. It was not only an opportunity for atmospheric scientists but many studies in other areas were performed during this event as well.

1.2. Astronomy

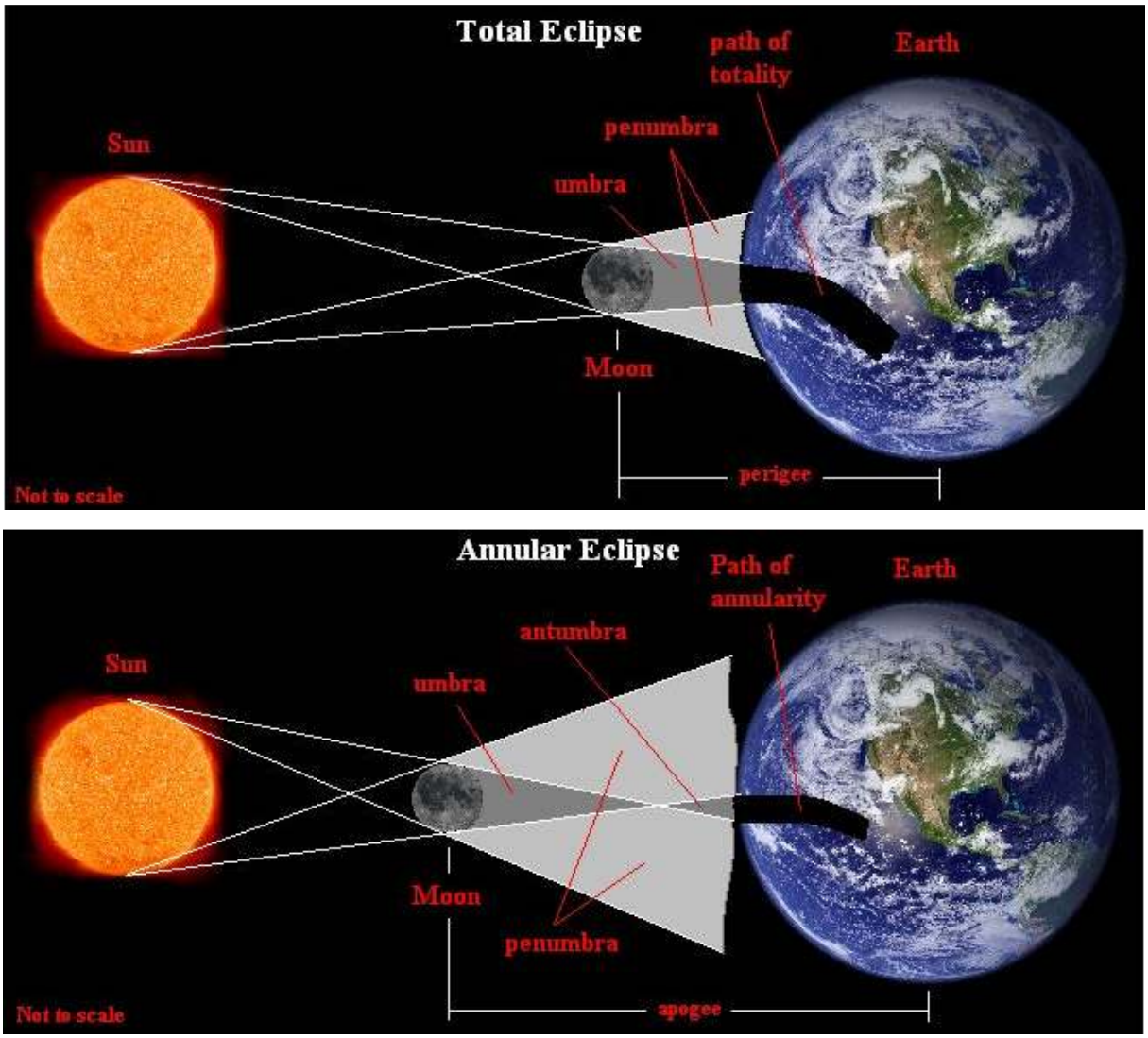

Figure 1.1: Diagram of the constellation of Sun, Moon and the Earth during a total solar eclipse (top) and annular solar eclipse (bottom) (from http://www.sems.und.edu/index_SolarEclipse.php downloaded on 3rd Mai 2010)

Solar eclipses occur when the moon's umbral, penumbral or antumbral shadow partly or wholly falls onto the Earth's surface as shown in Figure 1.1. If a location is placed within the moon's penumbral or antumbral shadow, the solar radiation is partly blocked whereas if a location is placed in the umbral shadow the solar radiation is wholly blocked and the radiation balance resembles that which occurs at night. There are however great differences between night and a total solar eclipse. The main of these is the fact that the transition between day and night is gradual and the reduction in solar radiation lasts several hours whereas in case of a total solar eclipse the transition takes an hour or less with the greatest changes in solar radiation within about 10 minutes before and after totality. Due to the geometries of and distances between the Earth, Sun and the Moon, the lunar penumbral shadow has a diameter of around 10.000km when it is wholly incident on the Earth surface. This diameter however slightly fluctuates between individual eclipses. The diameter of the umbral shadow varies greatly between eclipses and can be more than 300km diameter in some cases, while in others the umbra does not even touch the Earth's surface. In this case, the antumbral shadow falls upon the surface of the Earth and an annular solar eclipse can be observed within it. This is visible as the moon being in front of the Sun but its apparent radius being smaller than that of the Sun and hence a solar ring may be visible around the Moon. In some rarer cases the shadow cone of the Moon only briefly touches the Earth surface and a hybrid eclipse of the Sun occurs. This is visible as the moon and the sun having the same apparent diameter and while the Moon covers the Sun completely, the total eclipse lasts only a fraction of a second in this case. A hybrid solar eclipse is always visible as an annular eclipse in some parts of the world and total solar eclipse in other parts while the duration of both totality and annularity is typically very short (in the range of a few seconds). (Espenak, 2009)

The author of this project report travelled to two solar eclipse sites in 2010 in order to witness one annular and one total solar eclipse. Several photographs taken at these eclipses are shown in Figures 1.2 and 1.3 below.

Figure 1.2: Sunset total solar eclipse near El Calafate, southern Argentina, on 11th July 2010. Over 95% partial eclipse (top left), diamond ring effect (top right), totally eclipsed Sun above the Andes mountain range (bottom left), last few seconds of totality while the Sun was partially set (bottom right)

Figure 1.3: Annular solar eclipse in Male, Maldives, on 15th January 2010. About 50% partial eclipse (top left), annularly eclipsed Sun partly behind clouds (top right), projection of the partially eclipsed Sun (over 95% eclipse) through holes in vegetation (bottom left), projection of the annularly eclipsed Sun through holes in vegetation (bottom right)

1.2.1. The periodicity and timing of eclipses

The different properties of the umbral or antumbral shadow arise due to the fact that the Moon orbits the Earth on an ellipse, which is tilted by about 5 degrees with respect to the imaginary line that connects the centers of gravity of the Earth and the Sun. On this orbit, the distance of the centre of gravity of the Moon from that of the Earth varies between about 360.000km and 405.000km. The periods of these orbital properties are slightly different and together with the fact that the Earth orbits the Sun the Moon is apparently at a different location with respect to the Sun at each New Moon. In fact, if the Moon was at the same apparent location at each New Moon there would either be an eclipse with identical properties at every New Moon or, more likely, there would never be an eclipse. (Espenak, 2009)

The different orbital periods define three lunar months. The Synodic month is a period between New Moons and lasts 29,530589 days (which is 29d 12h 44m 03s). The anomalistic month is a period between perigees (the instants when the Moon is at its closest point to the Earth on its orbit) and lasts 27,554550 days (which is 27d 13h 18m 33s). The draconic month is a period between the same nodes (the instant when the Moon is at its greatest displacement from the Earth-Sun centre axis) and lasts 27,212221 days (which is 27d 05h 05m 36s). (Espenak, 2009)

After a certain period called a Saros these three months come together so that the Moon is almost at the same apparent location with respect to the Sun as it was before one Saros. A Saros is a period of 6.585,3 days (which is about 18 years 11 days and 8 hours). This is equal to (to within a few hours) 223 Synodic months, 239 anomalistic months and 242 draconic months. If there is an eclipse there will be another eclipse after a period of one Saros, which will have very similar geometrical properties (it will be at the same node, the Moon will be at a similar distance from the Earth and it will occur at nearly the same time of the year). (Espenak, 2009)

Because of this property of the lunar orbit all solar (and lunar) eclipses are grouped into Saroses and each Saros is given a unique number. Every Saros has a few tens of eclipses (usually between 70 and 90). The individual eclipses of a sub-sequence of eclipses separated by the 6.585,3 day period (1 Saros) one from the next also change slowly, with the characteristic decay time of about 1500 years. The solar eclipses of each Saros begin with a partial eclipse near one of the Earths poles with each subsequent eclipse being initially shifted towards the equator and then towards the other pole where the group ends with its final partial eclipse. Usually, about 50% of the eclipses of each Saros are partial (penumbral) and 50% umbral or antumbral (total or annular respectively). If an eclipse is umbral, the path of the following eclipse of that Saros will have very similar shape and will be shifted by about 120 degrees of longitude. The path will be slightly displaced either to the north or south, depending on the Saros. Also, the distance of the Moon will be very similar, but there will be a slight difference compared to the previous eclipse of that Saros. This difference is nearly the same between all member eclipses of that Saros and each Saros has either increasing or

decreasing distance. Therefore, most Saroses begin the umbral eclipse series with total eclipses and end it with annular eclipses and vice versa. There is typically one or a few hybrid eclipses between the annular/total ones as well. (Espenak, 2009)

2. Chapter 2: Eclipses and their atmospheric effects

2.1. Theory for reduction in solar radiation in the atmosphere

The lunar shadows (penumbra, umbra and antumbra) are nearly circular in shape. There are very small irregularities at the edges of the umbra/antumbra, in narrow regions called grazing zones. These irregularities (grazing zones) are caused by mountains on the surface of the Moon. Overall, the lunar shadow can be thought of as approximately circular forcing that reduces solar irradiance on the surface. The umbral shadow forcing totally blocks solar irradiance and hence changes the radiation regime from diurnal to nocturnal while the partial penumbral (or antumbral) shadow forcing reduces the solar radiation by a fraction, which can be related to the percentage of the Sun covered by the Moon. Abbot (1958) found during his experiments that the fractional decrease in global solar radiation was much larger than the percentage of the Sun being covered by the Moon. He suggested this was because of the lunar penumbra being in the atmosphere. Jagannathan *et al.* (1965) calculated the change in solar flux density during a partial eclipse to be

$$F(t) = \frac{1-A(t)}{(1-e(2\pi d/Y))^2}\cos[z(t)] \qquad (1)$$

and the reduction in total incoming energy due to the eclipse, Q, is given by integrating equation 1 above

$$Q = \int_{t1}^{t4} \frac{1-A(t)}{(1-e(2\pi d/Y))^2}\cos[z(t)]dt \qquad (2)$$

In these equations t1 and t4 are times of the beginning and end of the eclipse, which are also known as the first and fourth contact, A(t) is the fraction of the Sun obscured by the Moon, z(t) is the angular distance of the Sun from the zenith, e is the ellipticity of the Earth, d is the number of days from January 1 and Y = 365.26 days. Figure 1 below shows an example of a predicted reduction in global solar radiation during a solar eclipse. This one is for the 11th August 1999 eclipse for Reading, UK, which experienced a partial eclipse of about 97%.

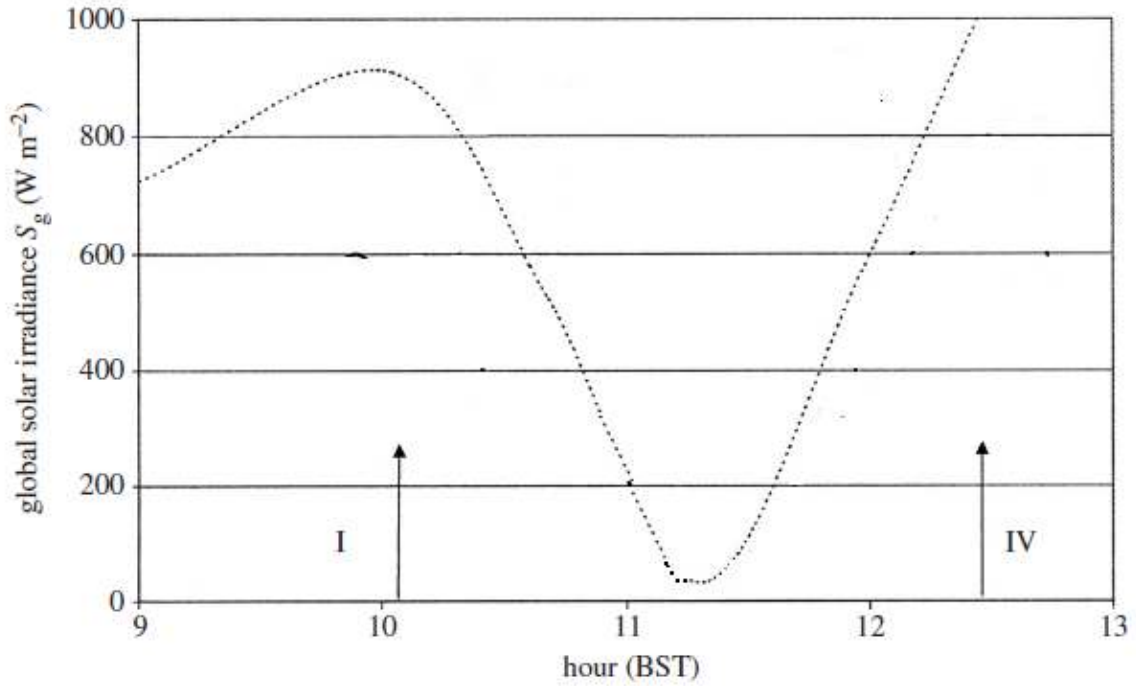

Figure 2.1: Theoretically predicted reduction in global solar radiation. I and IV are times of the beginning and end of the eclipse respectively (from Aplin and Harrison, 2002)

2.2. Changes in ionosphere associated with eclipses

Because of the forcing that solar eclipses impose on the atmosphere, it reacts and certain eclipse related changes occur. As discussed in chapter 1, these changes associated with the eclipse occur throughout the whole depth of the atmosphere and affect the ionosphere, stratosphere and the troposphere including processes in the boundary layer of the troposphere.

Ionosphere is one of the top layers of the atmosphere and consists mainly of ions and free electrons. The reason that ions and electrons co-exist in the ionosphere is the ionising radiation from the Sun, which strips electrons of atoms and creates ions (therefore the name ionosphere). The concentration of electrons, however, is not constant and greatly varies over time. The greatest variations in the concentration are diurnal variations, which are caused by the fact that there is no ionising solar radiation at night. Therefore, there is a minimum in the electron concentration in the morning and a maximum in the evening. Ionosphere temperature also depends on the intensity of solar radiation and its value has a similar diurnal cycle to that of the electron density. (H. Le, et al. 2008)

Because of this dependence of concentration of electrons on the solar radiation and its intensity, the concentration of electrons must also be affected by solar eclipses as they have a great effect on the intensity of solar radiation. Ionosphere eclipse induced electron concentration and temperature effects have been greatly studied by various methods in the past decade. These include the Faraday rotation measurement, ionosonde network, global positioning system (GPS), incoherent scatter radar (ISR) and various satellite measurements (H. Le, et al. 2008). All recent studies showed that there is a great decrease in electron density in lower ionosphere during a total eclipse while it is more complicated in the upper ionosphere where both a decrease and an increase in electron density have been observed during total eclipses. Variations in ionospheric electron density response to a solar eclipse have been observed with variations of latitude at which measurements were performed and different ionospheric response was detected at different locations during the same eclipse, which was likely caused due to variations in some local background parameters. (Adeniyi, et al. 2007, Tomas, et al. 2007, Farges, et al. 2001, Afraimovich, et al. 1998)

Huang et al. (1999) observed the lower ionospheric response to a total solar eclipse of 24th October 1995 and found that the electron concentration varied during this eclipse at one location. He concluded that there was an enhancement, followed by a depression, followed by a further enhancement, which was followed by further depression in Total Electron Concentration (TEC). These fluctuations were attributed to the occurrence of eclipse induced gravity waves in the ionosphere. (Gerasopoulos, et al., 2008)

2.3. Stratospheric changes associated with eclipses

Several eclipse related effects can be observed in the stratosphere. The most pronounced changes are in the total ozone column. There are several methods of measuring stratospheric ozone. Examples of this are Dobson spectrophotometric observations, which show an increase in total ozone near maximum eclipse (e.g. Bojkov, 1968). Other methods show both increases and decreases of total stratospheric ozone during eclipses of varying magnitudes (e.g. Mims and Mims, 1993; Chakrabarty et al., 1997). During the solar eclipse of 29th March 2006 data from the Greek UV network was analysed and did not hint on any consistent trend in changes of total ozone column. (Kazantzidis et al. 2007)

It was also suggested that the eclipse induced disturbance of the heat balance (local cooling) that travels at supersonic speed induces a gravity wave in the stratosphere. The source of the gravity wave was suggested to be the ozonosphere, which has the greatest temperature variations induced by the eclipse of the whole atmosphere. These gravity waves then propagate both upwards and downwards throughout the atmosphere. There were several attempts to measure or detect the evidence of this travelling bow-wave, but the results still remain equivocal (Eckermann et al. 2007). The only proper experimental evidence that the source of the gravity waves that propagate up- and downwards in the atmosphere is the cooling of the ozone layer was provided by Zerefos, et al. (2007), who performed measurements at three layers of the atmosphere and compared measurements during the eclipse and on a day before and after the eclipse (troposphere, stratosphere and ionosphere). Even though a distinct oscillation in surface temperature and humidity was measured, Zerefos, et al. (2007) concluded that the influence of gravity waves on the troposphere could not be deduced because of the small amplitude of these waves. (Gerasopoulos, et al., 2008)

2.4. Tropospheric changes associated with eclipses

Because of the reduction in solar irradiance, the heating of the surface is reduced and radiation cooling becomes more dominant, especially if skies are clear. The greater the fraction of the Sun covered by the Moon, the more pronounced this effect is. Therefore, surface temperature markedly drops as a result of the reduction in solar radiation. An example of this reduction is shown by the graph of temperature measured during a total eclipse below.

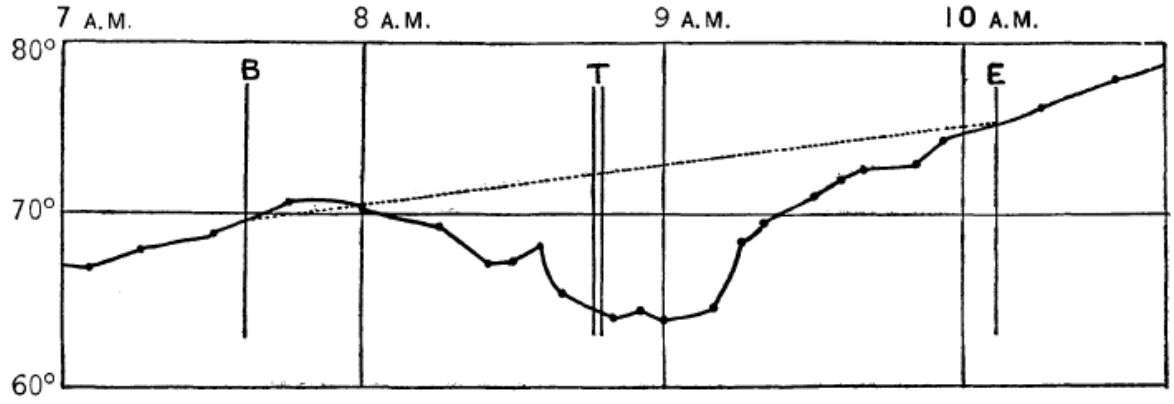

Figure 2.2: Graph of temperature (in Fahrenheit) against local time measured at Wadesboro, N. C., in the United States for the total solar eclipse of 28th May 1900. B stands for the first contact, E for the last (fourth) contact and the two lines by T are the boundaries of totality (second and third contacts). The dotted line represents a uniform interpolation of temperature so that the reduction of temperature can be separated from the diurnal changes (from Clayton, 1901)

It can be seen in Figure 2.2 that surface temperature begins to drop markedly about 20 minutes after the beginning of the eclipse. A minimum of temperature (greatest relative reduction) occurs about 15 minutes after maximum eclipse (in this case its magnitude is almost 10 degrees Fahrenheit) and the temperature sharply rises thereafter. (Clayton, 1901)

Because of the noticeable cooling in the umbral and deep penumbral regions, the air becomes denser and descends. This vertical motion near the centre of the shadow creates a region of slightly lower pressure usually very near the umbral shadow creating an eclipse cold core low. A pressure trace from the eclipse of 28th May 1900 may be seen in Figure 2.3 below.

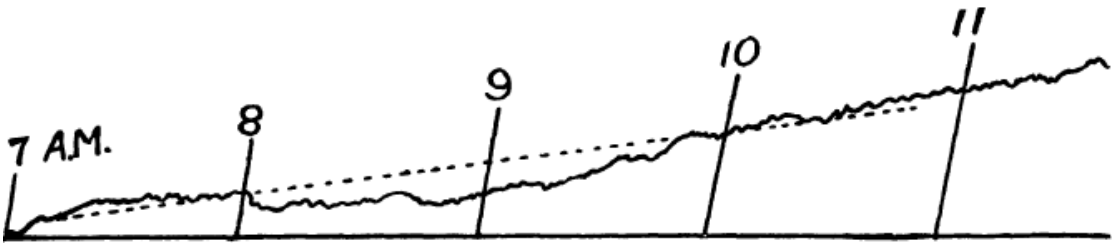

Figure 2.3: Trace of unreduced surface pressure from Toronto, Canada, during the eclipse of 28th May 1900 against local time. Dotted line represents interpolated pressure trace by assuming a uniform rise between the first and fourth contact (from Clayton, 1901)

Wind speed generally decreases during totality and at times close to totality, which is mainly caused by stabilization of the lowest levels of the boundary layer due to surface cooling, which inhibits turbulent mixing and also causes the boundary layer to be more detached from the general flow above it. (Clayton, 1901)

2.5. Clayton's (1901) conceptual model of tropospheric changes

The above described descent of air in the central parts of the lunar shadow provides an outflow of air, which is symmetrical about the centre of the umbral/antumbral shadow and hence takes the air away from the centre. This creates a region of local lower pressure. Clayton (1901) predicted that this lower pressure region would create a weak cyclonic circulation.

Clayton (1901) tested his hypothesis during the total solar eclipse that crossed the United States on 28th May 1900 by obtaining data for temperature, windspeed and wind-direction from a few reliable meteorological stations at that time. In order to verify if there was an eclipse induced wind, it would have been ideal if there was absolutely no synoptically induced wind in the region of the meteorological stations that were used. In reality, this is very rarely the case and hence Clayton (1901) used a parallelogram technique to separate an eclipse induced and synoptically induced wind.

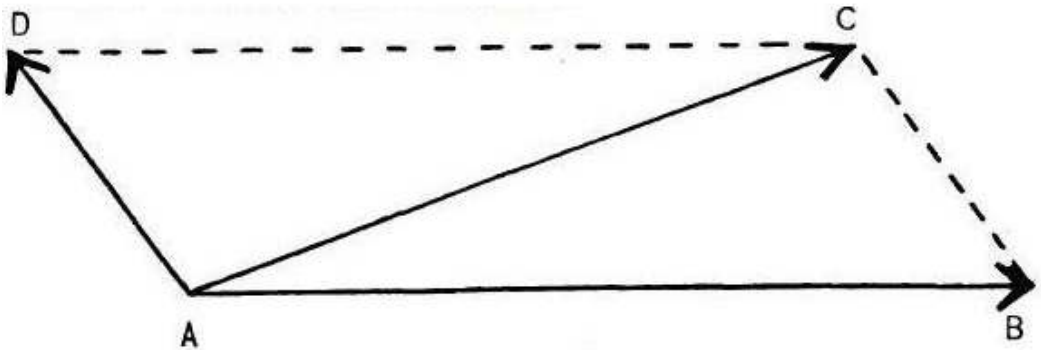

Figure 2.4: A simple diagram, where vector AB is the synoptically induced wind, vector AC the measured wind and vector AD the eclipse induced wind (from Clayton, 1901)

It can be deduced from Figure 2.4 that the more perpendicular the eclipse induced wind to the synoptic wind is the easier it would be to measure the magnitude and direction of it. The eclipse induced wind is sometimes described as the eclipse wind as some people tend to observe a wind blowing shortly after totality. Clayton (1901) tested this by producing a plot of temperature and wind changes for 8:15am and 9:00am local time, which corresponded to the umbral shadow being west of the US and east of the US respectively. Figure 2.5 below shows the plots that were obtained by using the above described technique.

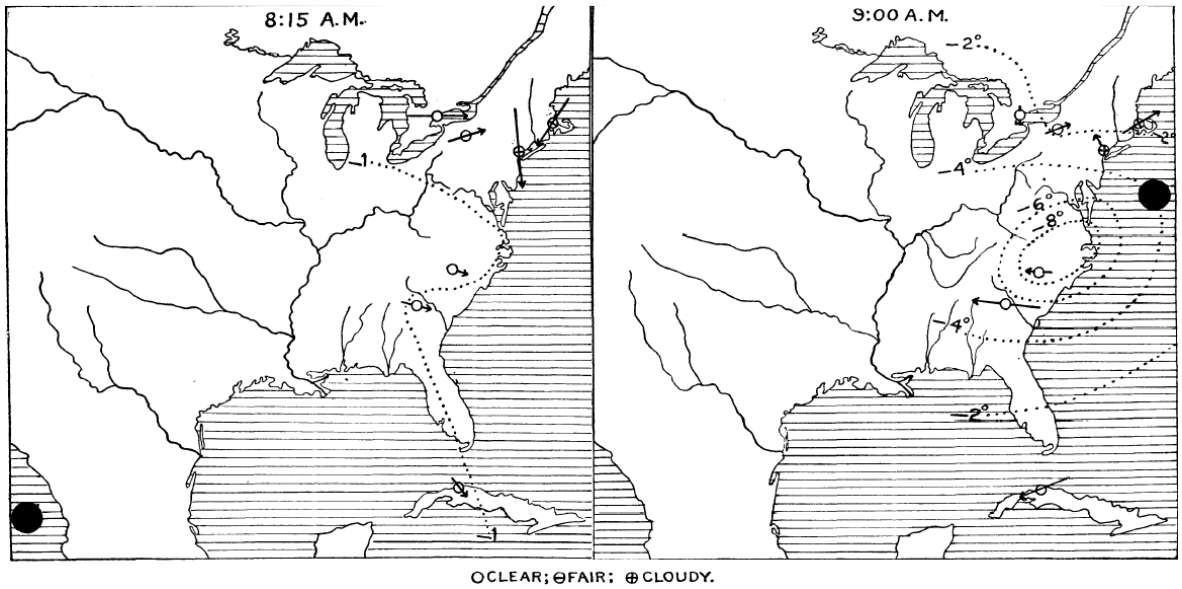

Figure 2.5 Plots of temperature depression and eclipse induced wind vectors for 8:15am (left) and 9:00am (right), both on 28th May 1900. Dotted lines represent contours of equal temperature depression (isotherms) and the magnitude of this depression is shown by the numerals. Weather conditions are indicated by symbols and the velocities of the eclipse induced wind are indicated by the direction and length of the arrows. The black shaded dot represents the location of the umbral shadow at that time (from Clayton, 1901)

The distinct features of Figure 2.5 above are the reversal of the wind direction as the eclipse passed over as well as a distinct anticyclonic circulation that extended up to 3000 kilometres from the centre of the eclipse. At 8:15am the outer penumbra is somewhere over eastern US. It can be seen that only a very small cooling is observed while an outflow of wind from the penumbra prevails. At 9:00am there is an appreciable region of cooler temperatures (the magnitude of which is greater than 8 degrees Fahrenheit), which lags the umbra by about 800 kilometres. This figure gives a nice spatial idea of the temperature depression and eclipse induced wind, but the problem in this case was the scarcity of meteorological stations in the US, which would give a complete picture of what was happening across the

whole lunar shadow (umbra and penumbra). Hence this figure shows only a small part of the whole lunar shadow. (Clayton, 1901)

In order to get a better picture of what was happening in the whole lunar shadow, Clayton (1901) obtained a time series of temperature and wind data (recorded every 15 minutes) at six meteorological stations (two in the region of totality, three to the north of totality and one to the south of totality). He plotted this data into a synoptic map when the stations were successively in different parts of the lunar shadow and since the lunar shadow travelled at a speed of about 3000 km/h he obtained a lunar shadow relative map with the data at about 800 kilometre intervals.

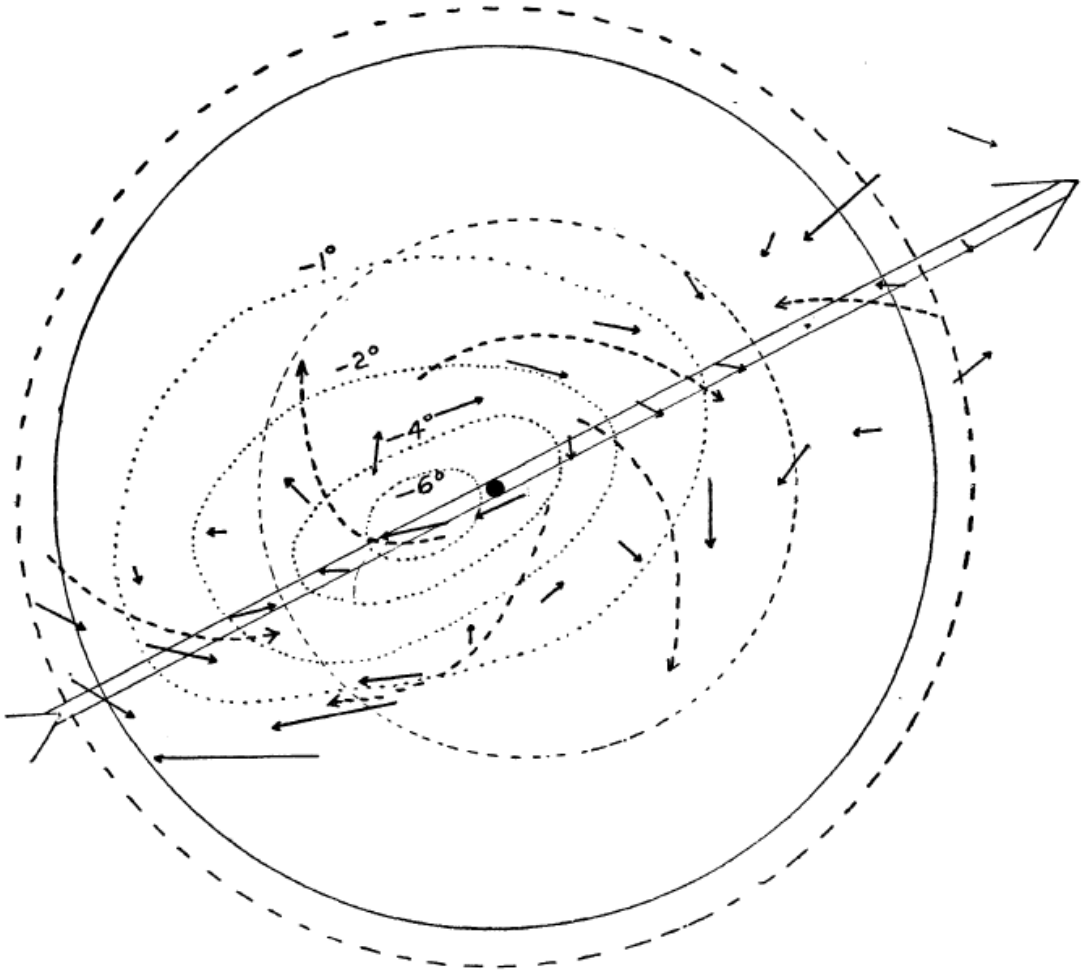

Figure 2.6: Plot of lunar shadow relative recorded values of temperature, windspeed and wind-direction. Umbra is represented by the black shaded dot while the path of totality is shown by the parallel lines forming a long arrow. Outer limit of penumbra is shown by the outer unbroken circle. The inner dashed circle represents a probable ring of low pressure and the dashed outer circle represents a probable ring of high pressure surrounding the penumbra. Dotted lines represent contours of equal temperature depression (isotherms) and the magnitude of this depression is shown by the numerals. The velocities of the eclipse induced wind are indicated by the direction and length of the solid arrows. Dashed arrows represent the average of these wind vectors. The values to the north of totality were obtained by averaging values from Ithaca, Toronto and Blue Hill; the values in totality were obtained by averaging values from Washington, Ga. and Wadesboro, N.C.; and the value to the south of totality is from Havana, Cuba (Clayton, 1901)

Figure 2.6 shows the measured temperature and wind direction patterns obtained by Clayton's (1901) technique described above. There is an elliptical area of cold air centereds about 800km behind the umbra, which is probably slightly displaced to the north of the centre of the path of totality. The northerly displacement of the temperature depression was likely due to the Gulf of Mexico to the south (surrounding Havana - the only used station to the south of totality), which has greater thermal capacity than the continent to the north and hence did not cool as much during the eclipse. Havana also reported more cloud than the continent and hence the radiation cooling was less effective there.

There is an anticyclonic circulation, which covers the inner half of the penumbra (stretches about 2400km (1500 miles) away from the umbra in this case). Surrounding this anticyclonic circulation is a distinct cyclonic circulation (about 1500km in width in this case), which extends beyond the penumbra. Beyond this circulation there is a hint of another ring of outflow winds.

All these measurements combined together (the induced wind direction, the temperature depression and the pressure trace) hint on a development of a cold air cyclone such as that, which was described by Ferrel (19th century) in great detail. Ferrel stated that a cyclone must have an inner area of low pressure surrounded by a ring of higher pressure. The origin of the lower pressure may be either in a temperature increasing towards the centre with approximately circular shaped maximum in the central area (warm core cyclones) or in a temperature decreasing towards the centre with approximately circular shaped minimum in the central area (cold air cyclones). Ferrel further stated about the cold air cyclones:

> "If for any reason the central part of any given portion of the atmosphere of a somewhat circular form is maintained in any way at a lower temperature than the surrounding parts, and the temperature gradient on all sides is somewhat symmetrical, we have approximately the conditions which give rise to a cyclone. In this case it is readily seen that there must be a vertical circulation, as in the ordinary cyclone, but that it is reversed, out from the centre below, and in toward the centre above, with a gradual settling down of the air in the interior to supply the outward current beneath. This vertical circulation, as in the case of the ordinary cyclone, gives

rise to a cyclonic motion in the interior and an anticyclonic in the exterior part of the air under consideration, but in this case the gyratory velocity is greatest above and is less at lower altitudes, diminishing down to the earth's surface, where it is least. In the anticyclonic part the reverse takes place, the gyratory velocity being least above and greatest down near the earth's surface. The distance from the centre at which the gyratory velocity vanishes and changes sign, is greatest above and gradually becomes less, with decrease of altitude down to the earth's surface, where it is nearest the centre. . . . The conditions of a cyclone with a cold centre which are the most nearly perfect are those furnished by each hemisphere of the globe, as divided by the equator, in which the pole is the cold centre, and the temperature gradient from the pole toward the equator is somewhat symmetrical in all directions from the centre. . . . The easterly motions in the higher latitudes and the westerly ones in the lower latitudes, in the one case, correspond to the cyclonic in the interior and the anticyclonic in the exterior part, and the belt of high pressure near the tropics to that of high pressure in the case of any cyclone with a cold centre. . . . The centre of a cyclone with a cold centre may or may not have a minimum pressure, according to circumstances. A certain amount of temperature gradient, and of pressure gradient which is independent of the gyratory motion, as explained in the case of the general circulation of the atmosphere, is necessary to overcome the friction in the lower strata and to keep up the vertical circulation, upon which the cyclone depends ; and the pressure gradient, which depends upon the temperature gradient and is independent of the gyrations, may be such that the increase of pressure in the central part due to this cause may be greater than the decrease of pressure arising from the cyclonic gyrations, especially where surface friction is great." (From Clayton, 1901, originally from A popular Treatise on the Winds, pp. 337-339)

Summarizing Clayton's theory for eclipse associated cold core cyclone, there is a thermally induced circulation in the form of a cyclonic flow in the vicinity of the umbral shadow (in the range of 100 miles), which is surrounded by an anticyclonic flow, surrounded by a further cyclonically curved flow as shown in Figure 2.7 below.

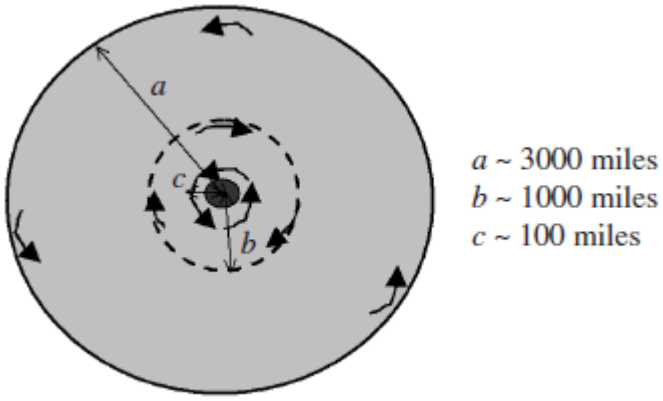

Figure 2.7: Simplified surface wind directions induced by an eclipse. The penumbra is grey and umbra is black. The arrows represent the flow direction that was predicted by Clayton's (1901) model of the eclipse induced flow (from Aplin and Harrison, 2002)

2.5.1 Objections to Clayton's (1901) model

There were, however, some, which objected to the findings of Clayton (1901) and proposed that a solar eclipse cannot on its own induce a cyclonic flow in the troposphere. One such objector was Kovner (1910), who wrote:

> "Looking at the map of the proposed cyclone and the path of the eclipse we encounter a puzzle how such an elongated path of the highly supersonic eclipse, a few hundred km wide and thousands of km long could have generated a fairly localized, moderately elliptical wind pattern only in a part of its trajectory over the North America landmass.
>
> It should also be noted that any air motion induced by reduced temperature would be very subsonic whereas the eclipse travel is very supersonic.
>
> Referring again to Ferrel, his expectation is that the region of somewhat lower temperature would be "somewhat circular" rather than very narrow and elongated.
>
> The thought that first comes to mind is that Clayton's observations in Figure 2.6 were spurious and of low statistical significance, given the scarcity of weather observations at that time. It is however possible to entertain an idea that the mild cyclonic features observed were real and that something special for this particular eclipse event may somehow relate between these features and the eclipse.

One possibility may be that the cyclone was already in the making before the eclipse and the effect of the eclipse was only to spur along the cyclonic air motion where it has already started but caused no such effect elsewhere (the south-west part of the eclipse trajectory).

Another possibility is that the cyclonic-like wind patterns might have been caused by planet surface properties such as heat capacity and topography.

At the north-east part of the proposed cyclone, the eclipse path leaves the land and continues over the ocean. As the water has substantially higher heat capacity than the dry land, any effects of the cyclone on it are reduced, so the land-sea boundary is a natural cut-off.

At the south-west end, the cyclone path followed for a while the Mexican gulf, but it entered land fully at a much larger distance from the cyclone centre than the north-east cut-off, so the Mexican gulf does not really explain the south-west boundary of the cyclone.

Another peculiarity of the topography is that a part of the south-west path was over the Mississippi basin, where as its path coincident with the cyclone was mostly over the Appalachian range. Perhaps the difference in typical height between the Appalachian range and the Mississippi basin might have contributed enough difference in atmospheric response to eclipse driving." (From Kovner, 1910)

2.6. Lower tropospheric changes associated with eclipses

There are also other effects that have been observed and studied during eclipses in the surface layer of the boundary layer such as changes in concentrations of various gases. Measurable changes in CO2 fluxes occur in case of a region that is dominated by vegetation. This is caused by the fact that photosynthesis is taking place during the daytime hours (when light is incident on plants) and as the umbral shadow approaches, the rapid reduction in solar light causes an abrupt shut down of the photosynthesis process so that plants stop absorbing CO2 and breathe in the same way as other living organisms (animals, humans, etc.) and actually produce CO2. This shift normally happens a few minutes before totality

and the photosynthesis resumes a few minutes after totality when enough solar radiation becomes incident on the plants. (Foken, et al. 2001)

Concentrations of other gases, such as surface ozone, can also be affected by total solar eclipses. The concentration usually increases around the time of totality and this is true in case of gases that are continuously being emitted from the ground. Before and after totality these gases are well mixed due to the solar heating induced turbulence. With the onset of totality and reduction in turbulence these gases concentrate near the surface until turbulence sets in with increasing surface heating after totality. (Foken, et al. 2001

3. Chapter 3: The total solar eclipse of 11th August 1999

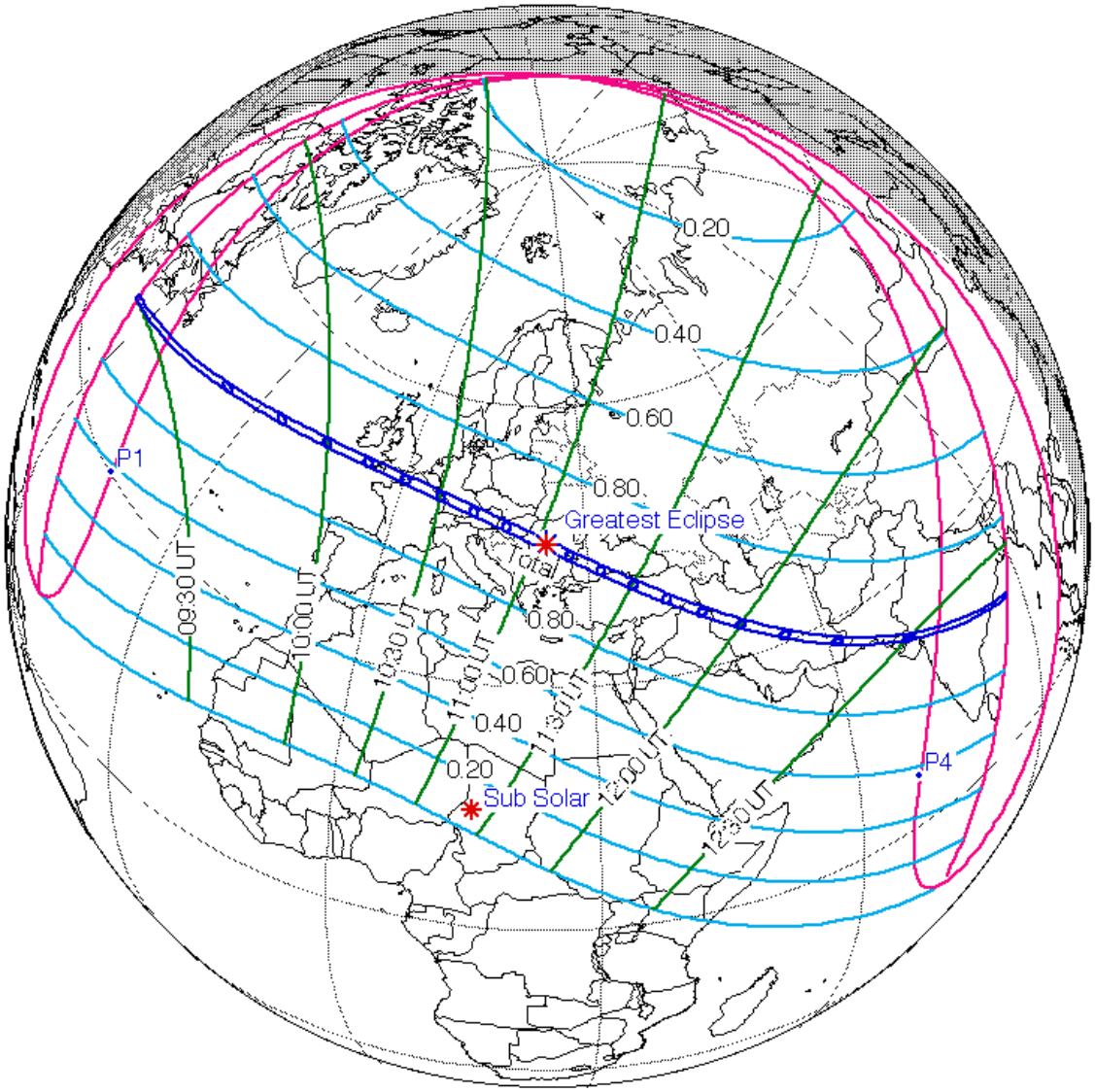

Figure 3.1 Map showing details for the total solar eclipse of 11th August 1999. Dark blue lines indicate path of totality. Light blue lines indicate limits of the given fraction of Sun obscured at maximum eclipse (e.g. 0.80 stands for limit of 80% eclipse). P1 indicates where penumbra first fell upon Earth's surface and P4 indicates where penumbra left Earth's surface (from Espenak @ http://eclipse.gsfc.nasa.gov/SEplot/SEplot1951/SE1999Aug11T.GIF downloaded on 11th August 2010)

On 11th August 1999 a total solar eclipse occurred. As can be seen in Figure 3.1 its path of totality crossed the Atlantic, western and central Europe, Balkans, Black Sea, Turkey and parts of Asia all the way to India. A partial eclipse was visible from much greater region covering North Africa, whole Europe, western Asia and northern Indian Ocean.

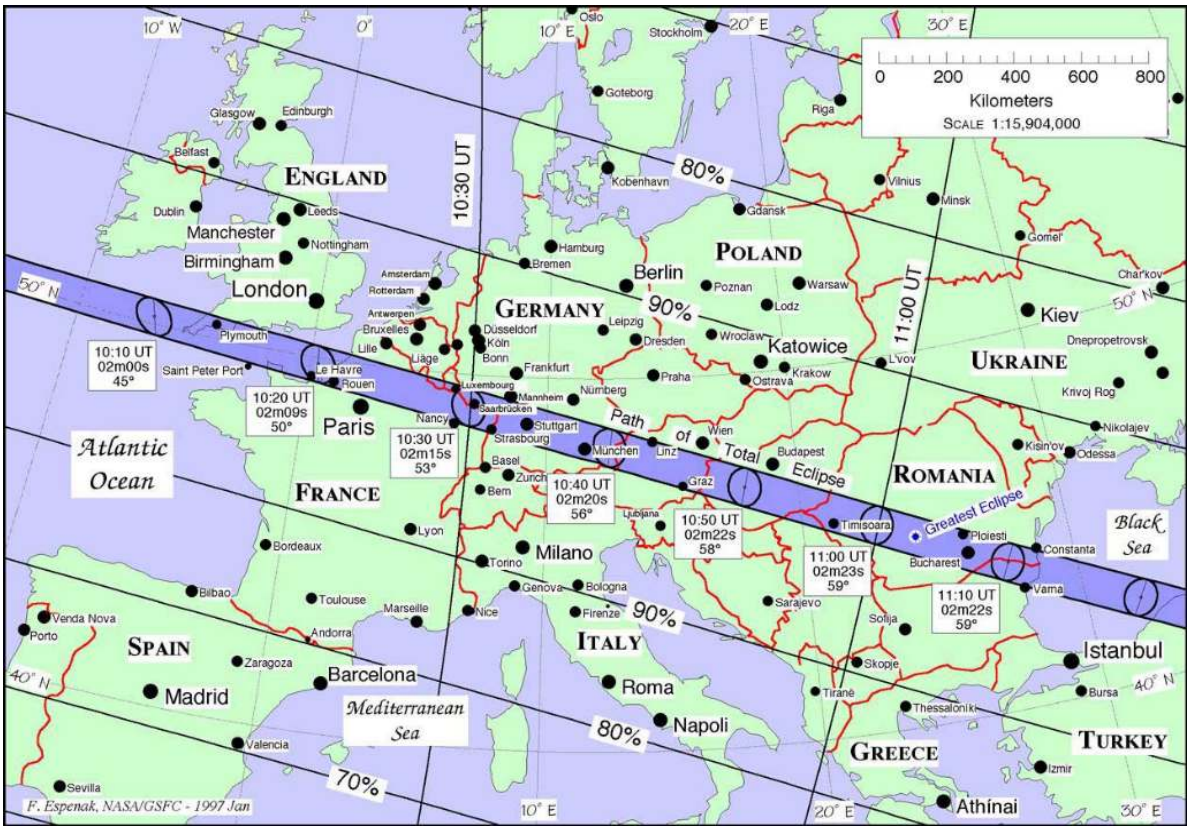

Figure 3.2: Map showing more details about the 11th August 1999 eclipse over Europe (from http://eclipse.gsfc.nasa.gov/SEmono/TSE1999/TSE1999Map/TSE1999Europe.jpg downloaded on 11th August 2010)

3.1. Meteorological measurements performed during this total eclipse

As can be seen in Figure 3.2, the total solar eclipse of 11th August 1999 passed over densely populated areas of Europe. Because of this fact, this total eclipse was the most well observed and documented total solar eclipse in history. Numerous scientific measurements for many different science disciplines were performed during this eclipse, including meteorological measurements. As an example we present here detailed meteorological measurements of a set of meteorological variables selected from 2 observation points in the UK, namely Camborne in Cornwall and Reading in Berkshire.

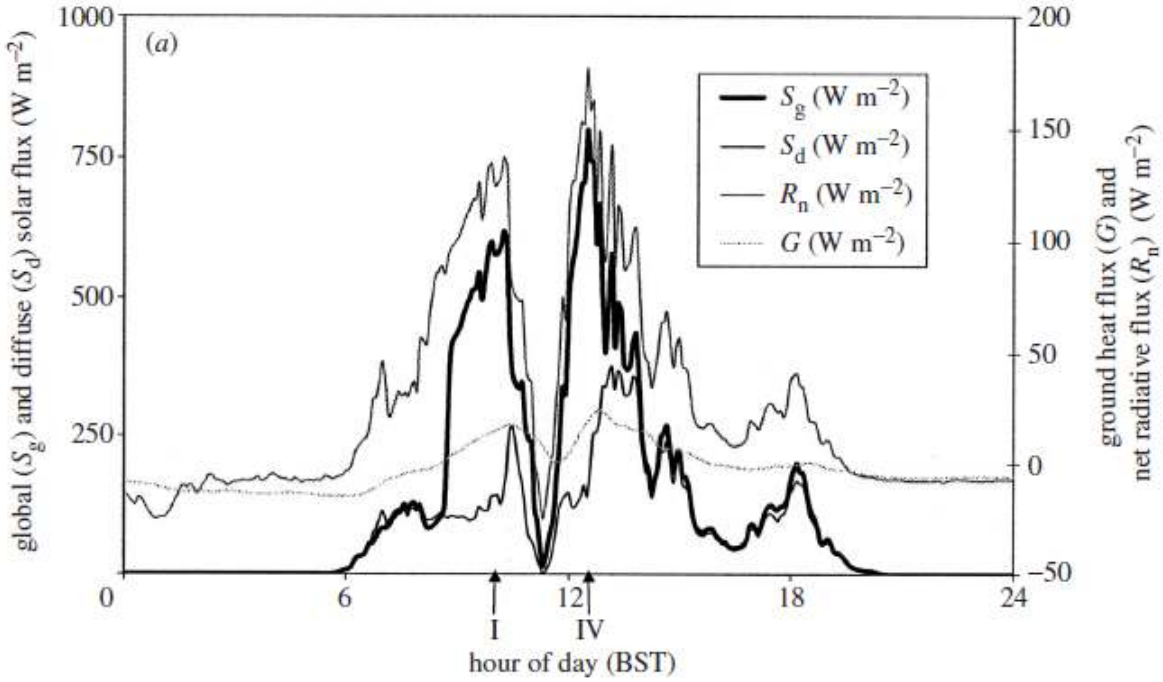

Figure 3.3: Radiative fluxes at Reading on 11th August 1999 against time. S_g stands for global solar radiation, S_d for diffuse solar radiation, R_n for net radiation and G for ground heat flux. I stands for first contact and IV for fourth contact (from Aplin and Harrison, 2002)

Since the weather at Reading remained sunny or mostly sunny for the duration of the 97% partial eclipse, data for changes in radiation and ground heat flux at that location were chosen. It can be seen in Figure 3.3 that there was a great reduction in solar radiation during the eclipse with the greatest reduction at greatest eclipse. Global solar radiation was reduced to almost zero while diffuse solar radiation was affected slightly less. Ground heat flux was also clearly reduced but the reduction was slightly delayed when compared to the solar radiation. (Aplin and Harrison, 2002)

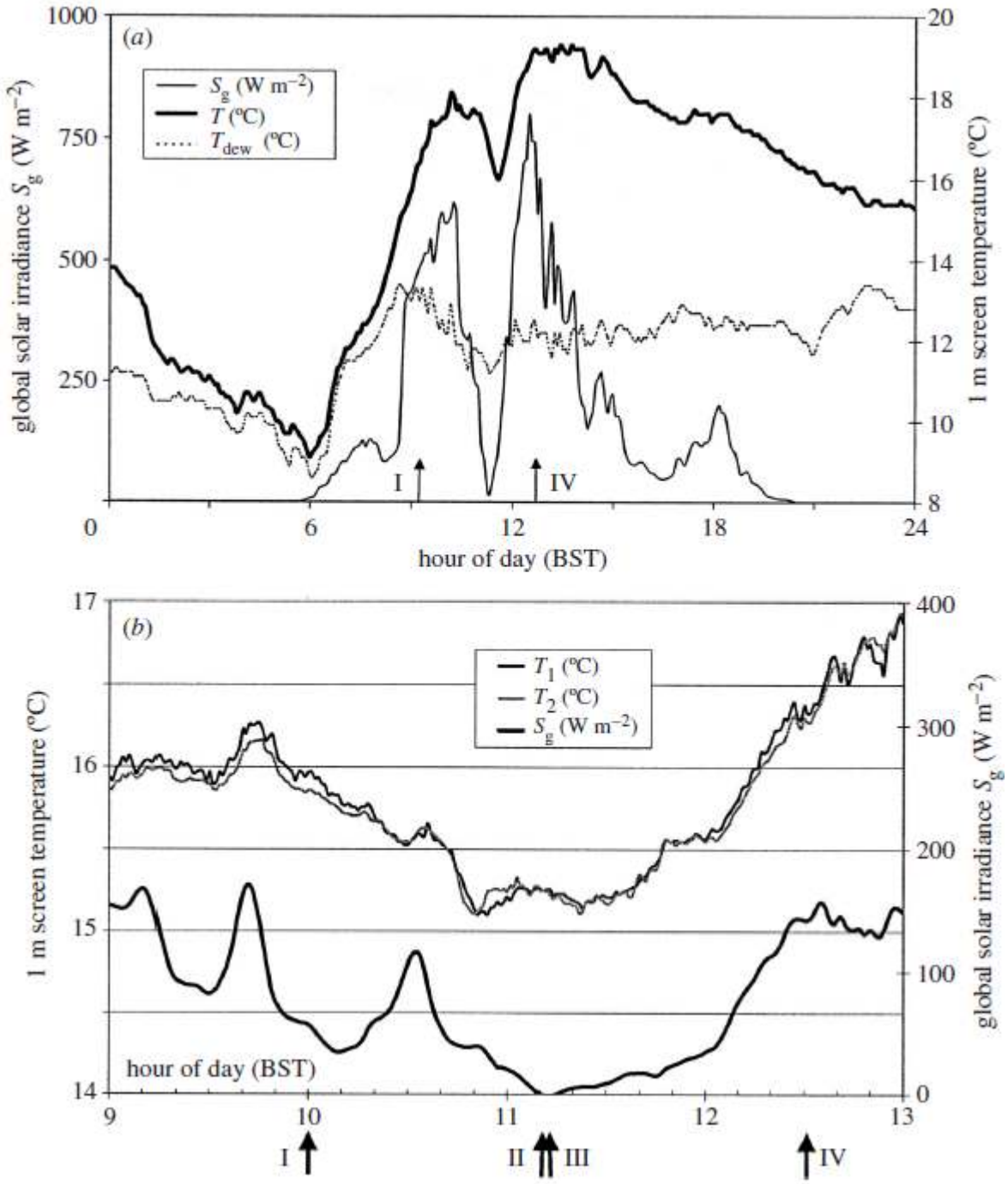

Figure 3.4: Global solar radiation, dry bulb air temperature (1 metre above ground) and dew point temperature against time for Reading (5min averages) (top) Global solar radiation and temperatures (each being measured by a different platinum thermometer) against time at Camborne (1min averages)(bottom) I, II, III and IV stands for the first, second, third and fourth contact respectively (from Aplin and Harrison, 2002)

Figure 3.4 shows two sets of data, the top one at a sunny station in a 97% partial eclipse and the bottom one at a cloudy station in the path of totality. The station in totality (Camborne) can be recognised by the fact that S_g went to zero while it did not go completely to zero at Reading. Regarding the temperature and dew point at Reading, both show a decrease at the time of maximum eclipse with a clear signal in the temperature trace. Regarding the temperature measurements at Camborne, there is no clear temperature decrease at maximum eclipse like in the case of Reading, but overall the temperature decreased by about 2 degrees during the eclipse. The minimum of temperature however occurs about 15 minutes before second contact. (Aplin and Harrison, 2002)

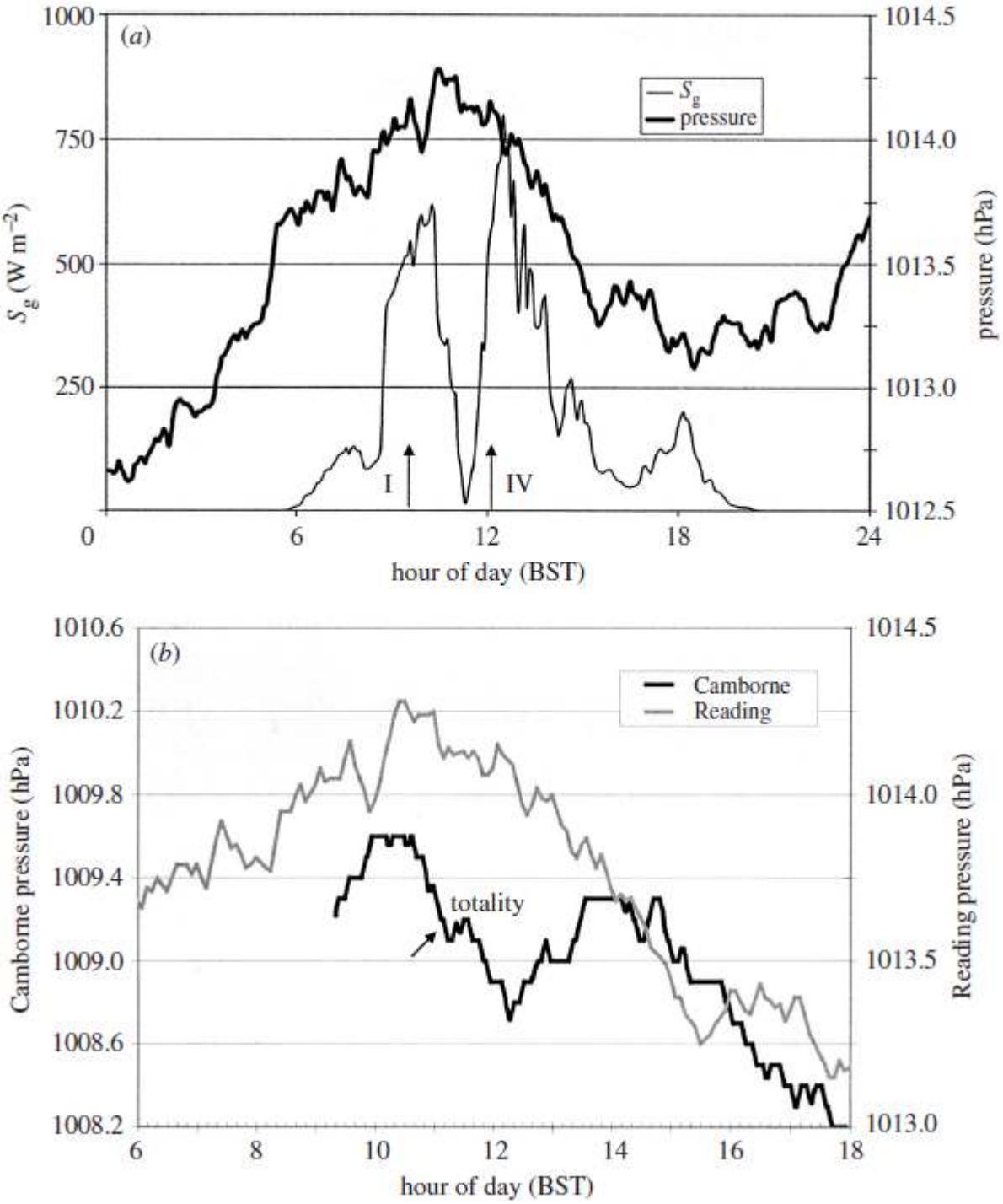

Figure 3.5: Pressure and global solar radiation against time at Reading (top) Pressures at Reading and Camborne against time (bottom) I represents the first contact and IV the fourth contact (from Aplin and Harrison, 2002)

It can be seen in Figure 3.5 (top) that overall, pressure was falling during the eclipse with no distinct minimum such as in case of Camborne (bottom). However, some fluctuations could be seen in the Reading trace with peak-to-peak magnitude of about 0.1hPa and frequency a

little smaller than 1 hour. In case of Camborne, there is a decrease in pressure during totality with a minimum about 6 minutes after totality. (Aplin and Harrison, 2002)

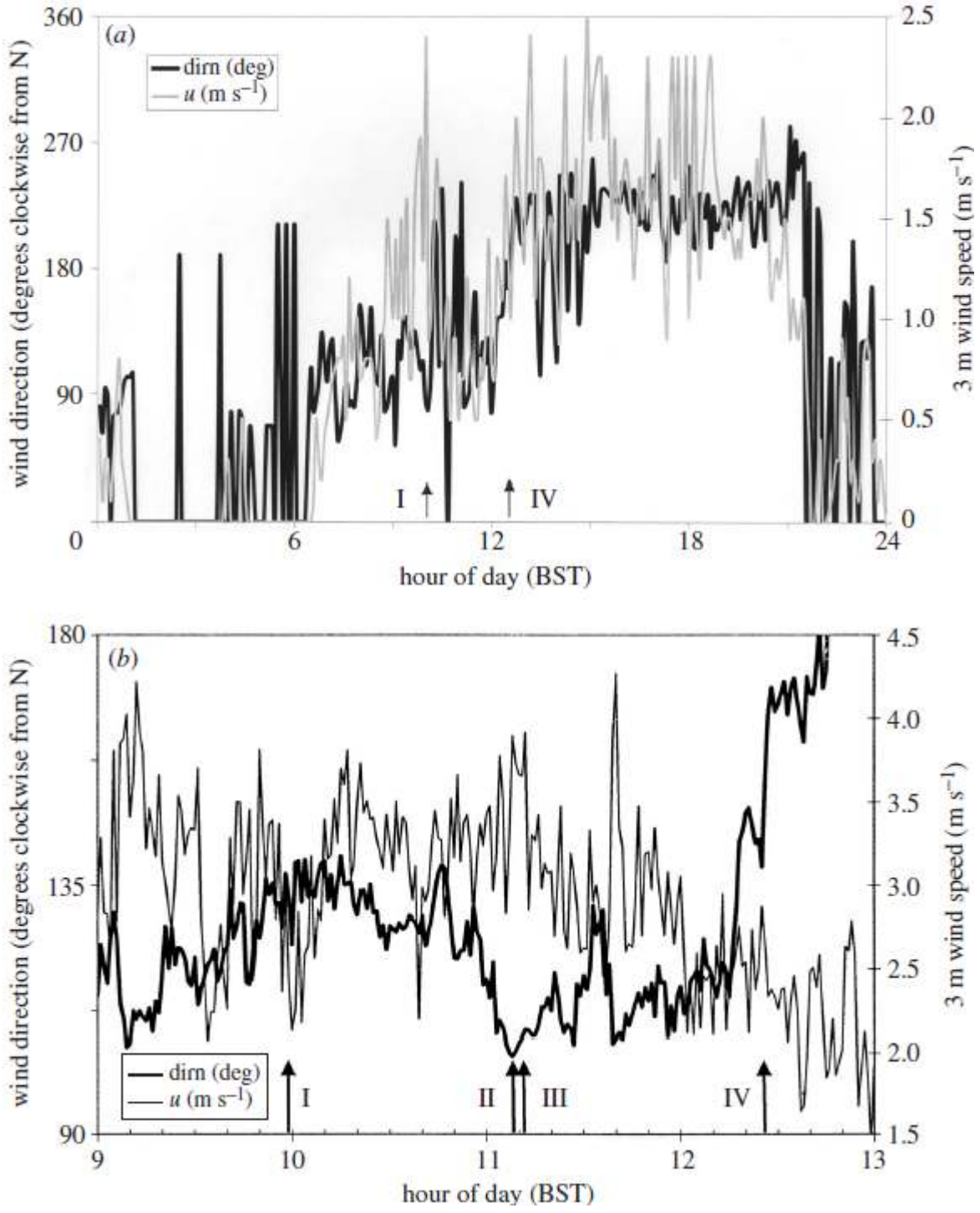

Figure 3.6: Windspeed and wind-direction measurements at Reading (5min averages of 1Hz measurements performed at 3 metres above ground) (top) and Camborne (1min averages of 1Hz measurements) (bottom) I, II, III and IV stands for the first, second, third and fourth contact respectively (from Aplin and Harrison, 2002)

Figure 3.6 shows a marked drop of windspeed at Reading during the eclipse with a minimum at maximum eclipse, which was followed by an increase to pre-eclipse values. Interesting features of the wind behaviour at Reading are wind gusts at both first and fourth contacts with the wind backing at first contact and veering at fourth contact. Similar but more pronounced changes were recorded at Camborne with the wind backing soon after first contact and reaching its most anticlockwise direction at second contact. After that the wind veered and reached its pre-eclipse direction after fourth contact. (Aplin and Harrison, 2002)

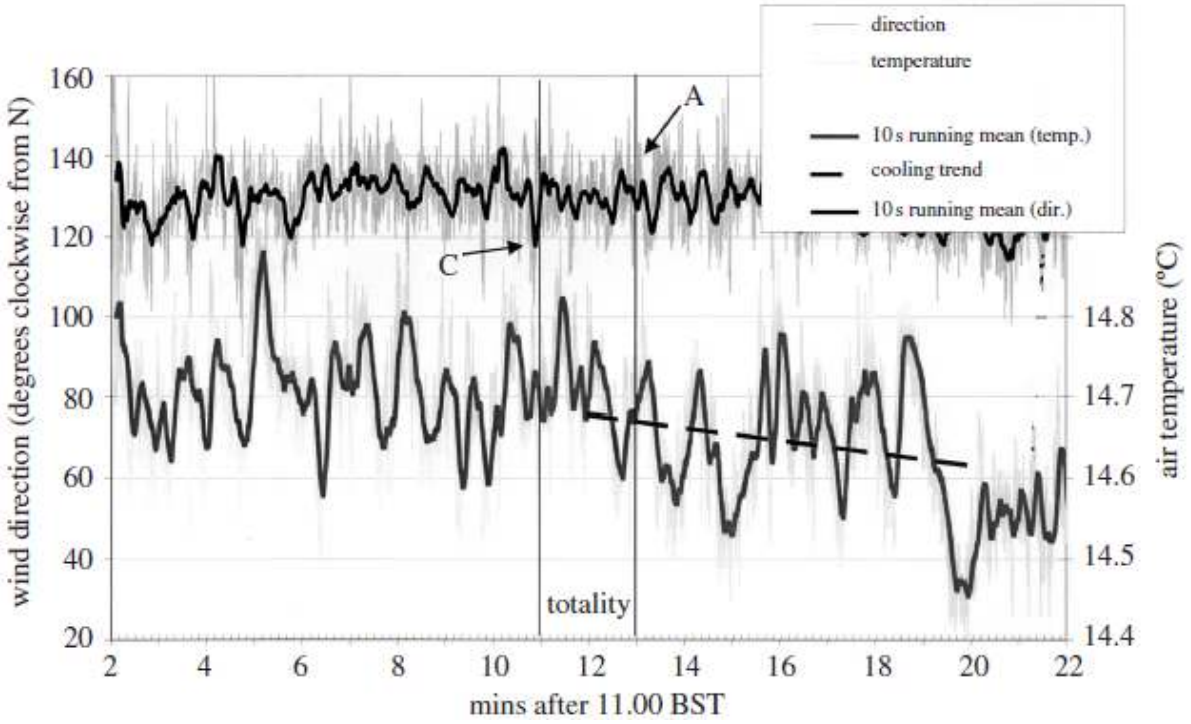

Figure 3.7: High-resolution wind direction (top trace) and temperature (bottom trace) graphs at Camborne just before and after totality. The measurements were obtained by using fine-wire thermometer and a sonic anemometer, both placed 5.8 metres above ground. The arrows C and A show clockwise and anticlockwise wind direction changes respectively, as the umbra passed over. The dashed line over the temperature trace shows the average cooling after totality (from Aplin and Harrison, 2002)

Figure 3.7 shows clockwise and anticlockwise wind direction changes just before second and just after third contact respectively. This suggests that an independent clockwise circulation is located within the umbra and perhaps surrounds it. This, however, cannot be said with a great confidence as the magnitudes of wind direction changes are comparable to background noise. Regarding temperature, there are fluctuations throughout the course of

totality with a general warming trend in the first half of totality being followed by general cooling trend, which continues until the local minimum at 11:20BST. (Aplin and Harrison, 2002)

3.2. Modelling tropospheric changes associated with the eclipse

Unlike other data analyses, which have mostly involved measurements that have been obtained at a given location in the path of the eclipse, Prenosil (2000) performed a spatial analysis of the effects of this 1999 total solar eclipse. A BLM operational weather forecasting model was used to analyse atmospheric changes that occurred during the total solar eclipse on 11th August 1999 over western, central and eastern Europe as well as over parts of Asia with the focus being mainly on the western and central European part of the eclipse including affected parts of the UK, France, Germany, Austria, Hungary and Romania. This was done in order to reproduce the features associated with the atmospheric feedback to the eclipse. These features include mainly lower tropospheric response such as modification of surface temperature and humidity as well as the behaviour of wind (both in lower and upper troposphere) and pressure. The model was initialized from low resolution data and differences between a model run when the eclipse forcing was included and a model run when there was no eclipse forcing were studied. The modelled variables that were observed to change during the eclipse were the surface temperature, mean sea level pressure, unreduced surface pressure, relative humidity, windspeed, wind direction and mid-tropospheric (500hPa pressure surface) pressure and temperature. These modelled observations were then compared to real observed and recorded data from various sites along the eclipse track. (Prenosil, 2000)

3.2.1. The model

The BLM model that was used was run on Fujitsu VPP300 mainframe. The domain that was selected for this model covered eastern half of Northern Atlantic, Western, Central and parts of Eastern Europe. The model domain was divided into a grid of grid points of 63.5km in diameter (79 x 79 horizontal grid points) and the vertical extent was divided into 25 levels with the top level being at 19km. The resolution was just high enough so that the region of

totality was within 6 grid points, which means that it just got properly resolved. The time step of the model was 1 minute. In this model the value of the solar constant was chosen to be 1320 W/m^2 and the eclipse forcing was applied in a way that the solar constant was reduced to 0% at the grid points that were affected by totality. Around these, two regions of reduction in the solar constant were applied, which represented the innermost parts of the penumbral lunar shadow. In a region surrounding the umbral shadow the solar constant was reduced to 5% of its original value and this region was surrounded by another region where it was reduced to 20% of its original value. These two regions represented 95% and 80% partial eclipse respectively. The position of this eclipse forcing was introduced as an external parameter and followed the same path as the real eclipse did (it entered the model at 09:38, reached Cornwall, UK at 10:12, went over Germany between 10:10 and 10:45 and exited the area over Romania at 11:10, all times being UTC). (Prenosil, 2000)

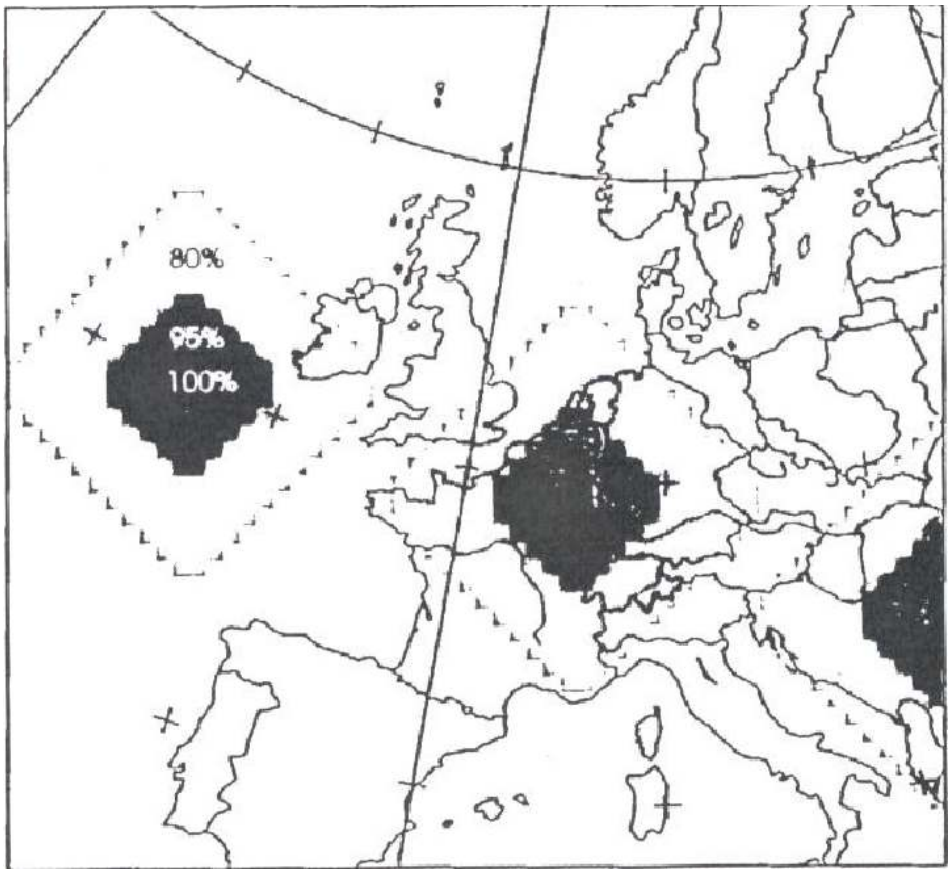

Figure 3.8: The model domain used for the simulation together with the positions of the solar eclipse at 10:00, 10:30 and 11:00 (all UTC) on 11th August 1999 (from Prenosil, 2000)

This analysis was performed with real synoptic data that was originally fed into the BLM operational forecasting model. The quantities used were surface temperature, mean sea level pressure, relative humidity, wind vectors (speed and direction), global solar radiation as well as cloud cover. The synoptic situation featured an upper-air trough over Western Europe in which three surface lows were embedded. One low was west of Ireland, another one over southern Scandinavia and one over the Adriatic Sea. (Prenosil, 2000)

3.2.2. The modelled data

The general weather pattern over Europe at eclipse time could be separated into two distinct regions. The first is over Western Europe where cool, damp and cloudy conditions prevailed and the second over Central and Eastern Europe where much warmer and clearer conditions dominated most places. For this reason two modelled meteograms, one in each region, were chosen to be analysed. The first was in Saarbrucken in western Germany and the second one in southern Romania.

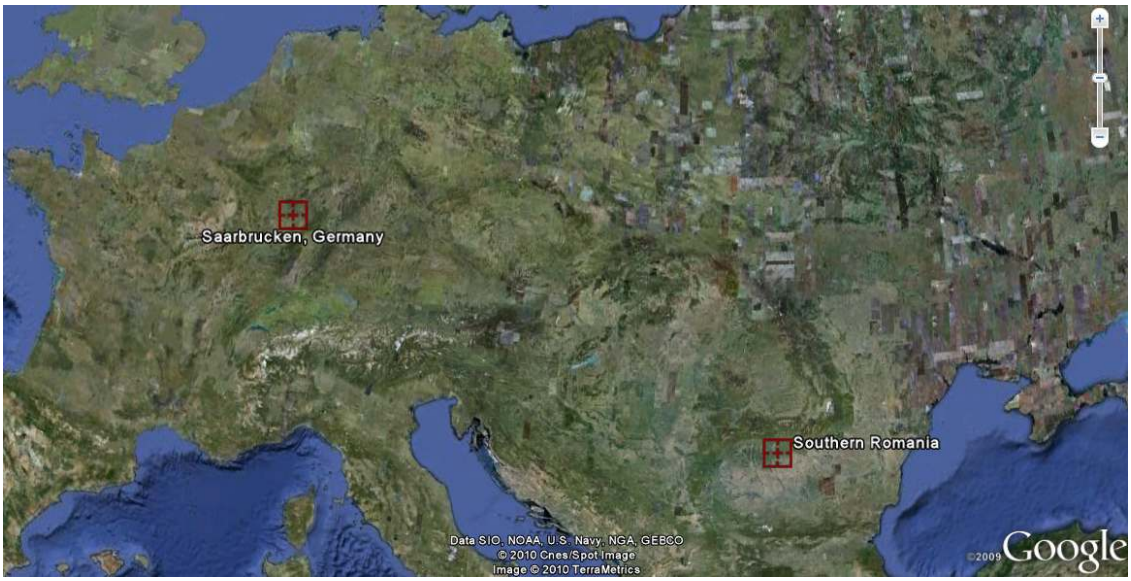

Figure 3.9: The locations of the two chosen meteograms (from Google maps @ http://maps.google.com downloaded on 25th July 2010)

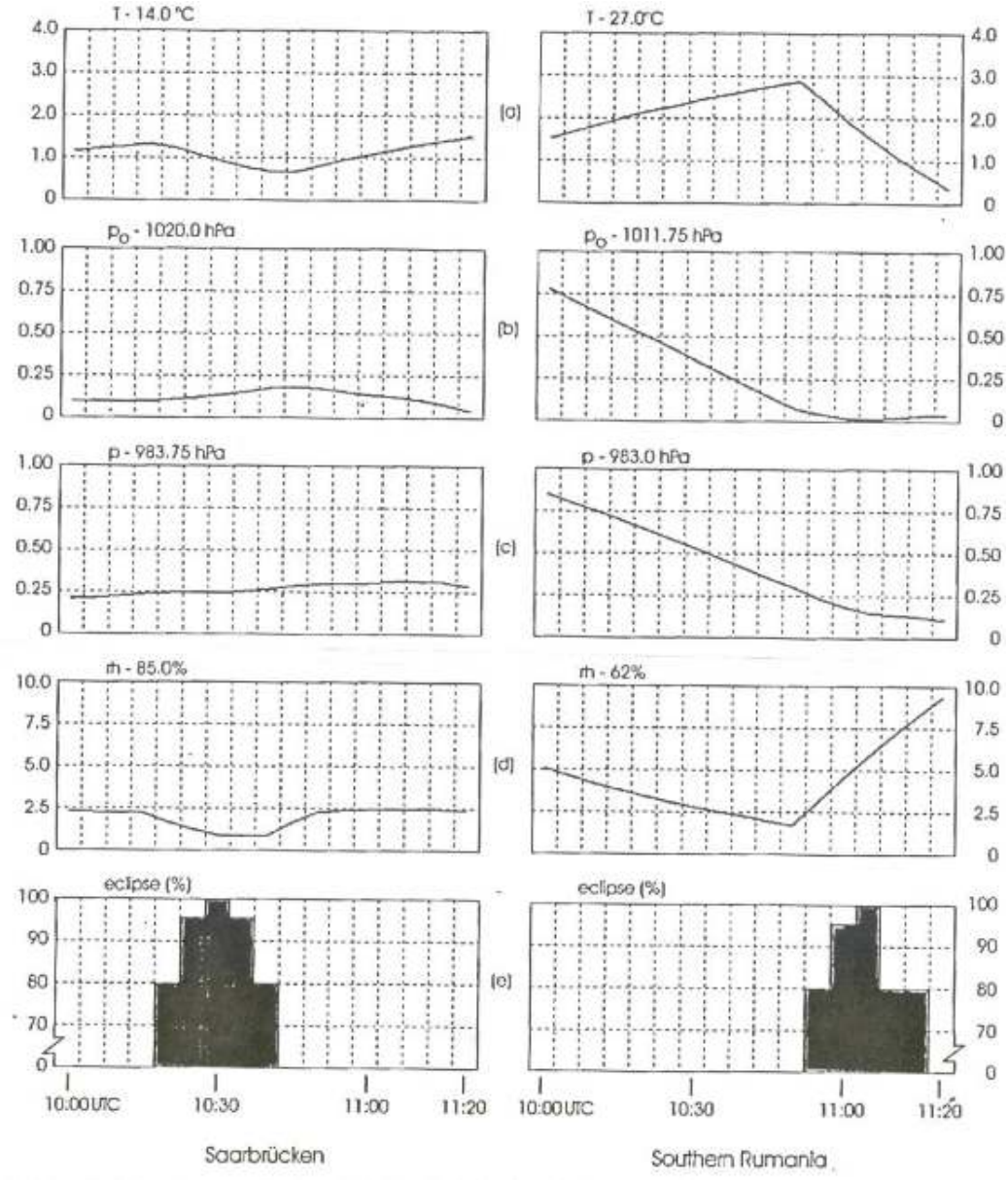

Figure 3.10: BLM meteograms for Saarbrucken (grid point 49° 26' N, 05° 51' E in western Germany) on the left and Romania (grid point 44° 35' N, 24° 02' E) on the right. (a) temperature difference from pre-eclipse temperature (modelled at 2 metres above ground), (b) mean sea level pressure difference from pre-eclipse value, (c) local unreduced surface pressure difference from pre-eclipse value, (d) relative humidity difference from pre-eclipse value (modelled at 2 metres above ground), (e) reduction in global solar irradiance introduced to the model (in %)(from Prenosil, 2000)

The German meteogram resembled a 0.6 degrees temperature decrease, which occurred 10-15 minutes after totality. The sea level pressure rose by 0.1hPa, the local surface pressure resembled a rising tendency, which temporarily stopped at eclipse time and the relative

humidity decreased by 0.25%, which is opposite of what would be expected when temperature drops. All changes are with respect to the value before the eclipse. The likely cause of the relative humidity decrease in this case was the reduction of evaporation during eclipse time. (Prenosil, 2000)

The Romanian meteogram resembled a 2.6 degrees temperature decrease with 0.75hPa pressure decrease and 7.5% increase of relative humidity. Again, all changes are with respect to pre-eclipse values. Changes in wind speed and wind direction were not tested in these meteograms. The stronger reaction of the variables to the eclipse in this case was due to the fact that the temperature in Romania was warmer (around 27 degrees before the eclipse as opposed to only 14 degrees in Germany) and hence radiative cooling was stronger (according to Stefan-Boltzmann law). Also, it was stronger due to the absence of cloudiness in Romania. The radiative cooling drives the temperature drop, which then drives changes in the other variables. (Prenosil, 2000)

3.2.3. Comparison of model data with and without eclipse

For the comparison of model outputs with and without the eclipse forcing, the Saarbrucken meteogram was replaced with a meteogram for Chiemsee area in southern Bavaria. This replacement was done due to the fact that the modelled variables on the cloudy site in Saarbrucken did not show a significant reaction to the eclipse while the Chiemsee area experienced large cloud breaks during the eclipse and the modelled variables were in good agreement with real observations from a not too distant site in Austria. (Prenosil, 2000)

The comparison was done by running the model without the eclipse forcing and then subtracting the modelled values from a run that included the forcing effects of the eclipse. From these 2 runs, difference-meteograms for the above mentioned stations were produced as well as contour plots of the whole domain that displayed pressure, temperature and wind direction changes. (Prenosil, 2000)

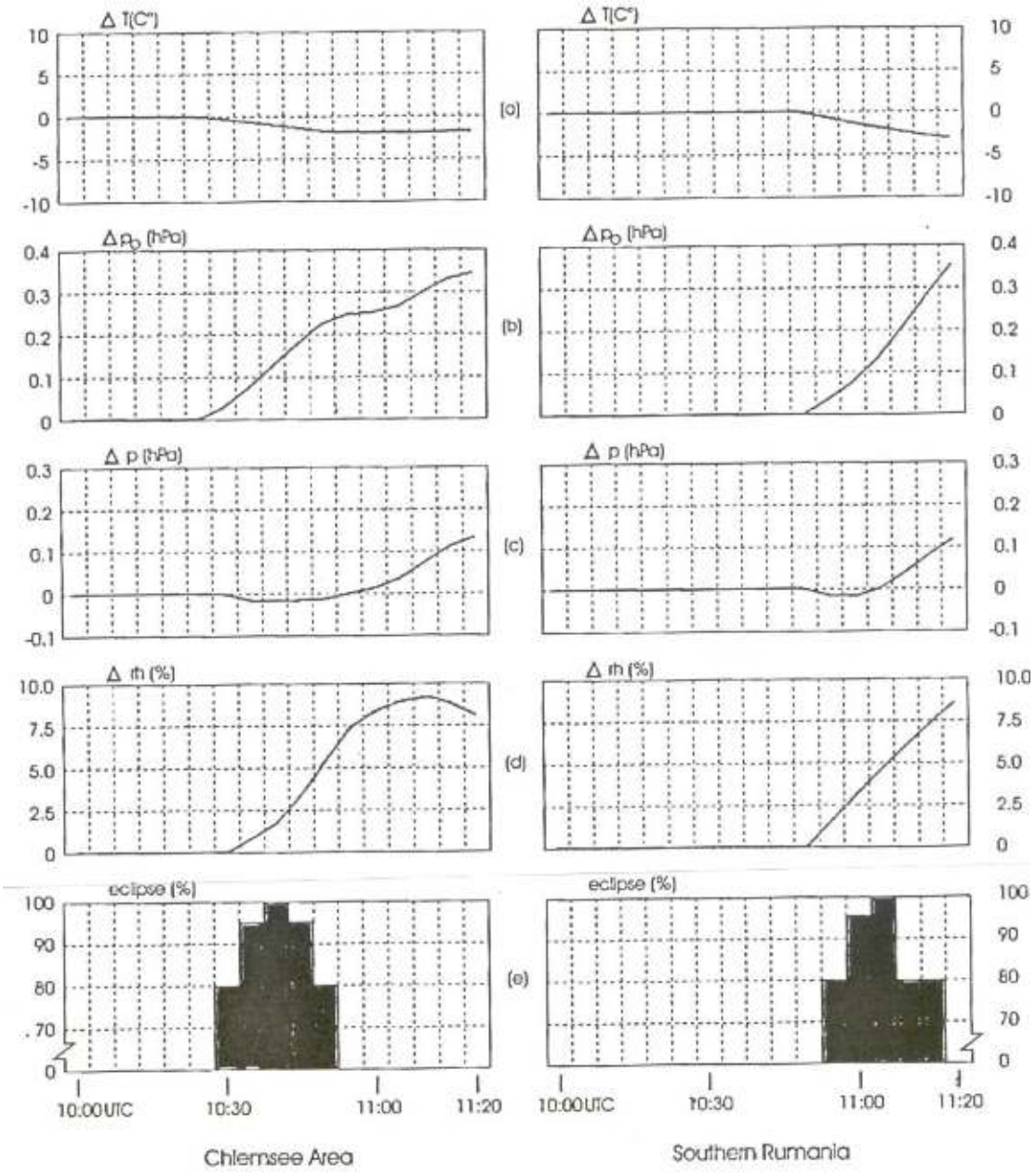

Figure 3.11: BLM difference-meteogram for the Chiemsee region (grid point 48° 26' N, 11°36' E in southern Bavaria) on the left and southern Romania (same grid point as in Figure 2) on the right. (a) temperature difference in °C (modelled at 2 metres above ground); (b) mean sea level pressure difference in hPa; (c) local unreduced surface pressure difference in hPa; (d) relative humidity difference in % (modelled at 2 metres above ground); (e) reduction in global solar irradiance introduced to the model (in %)(from Prenosil, 2000)

The Chiemsee difference-meteogram showed about 2 degrees maximum temperature difference (decrease) and about 9% maximum increase of relative humidity compared to the modelled situation had the eclipse not have occurred. The Romanian difference-meteogram

showed a maximum 3 degrees difference in temperature, which forced a maximum mean sea level pressure rise of about 0.4hPa. The greatest difference (increase) in relative humidity reached 9%, the same as in case of Chiemsee. All maxima occurred just after totality with the deviation between the two runs not starting until about 95% eclipse (which is just before totality). (Prenosil, 2000)

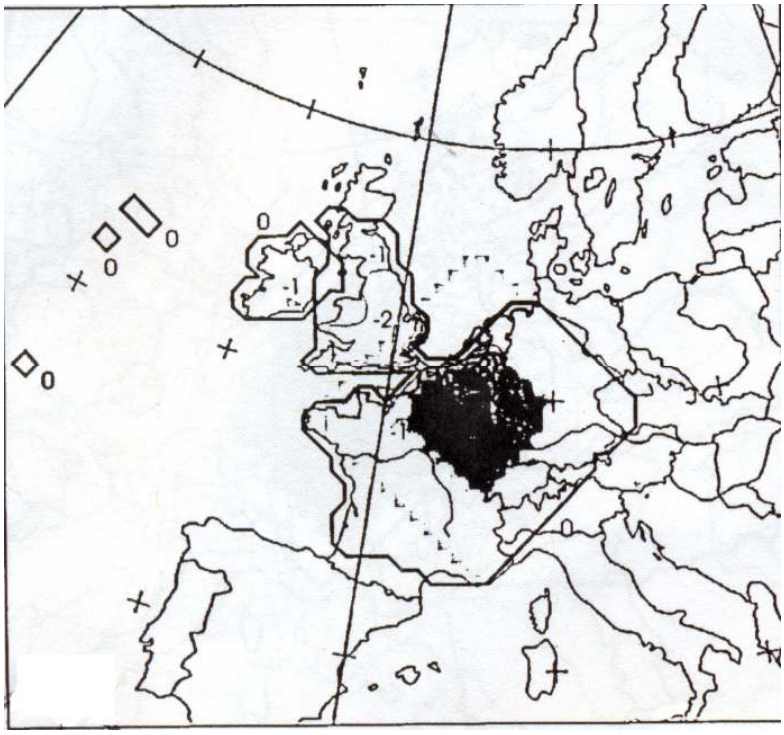

Figure 3.12: BLM model predicted temperature differences at 10:30 UTC from the simulations "with minus without eclipse". Contour interval 1°C, thick line 0°C (from Prenosil, 2000)

The contour map of thermal deficit caused by the eclipse at 10:30 UTC (when the umbral shadow was located somewhere near the French-German border) showed a maximum thermal deficit of about 2 degrees over south-east UK and north-east corner of France. The deficit was modelled only above land (not above sea), because sea surface has a large thermal capacity and hence responds only very slowly to radiation induced temperature changes. Also, areas that were modelled to be under cloud cover had only marginal (around 1 degree) modelled decrease in temperature. (Prenosil, 2000)

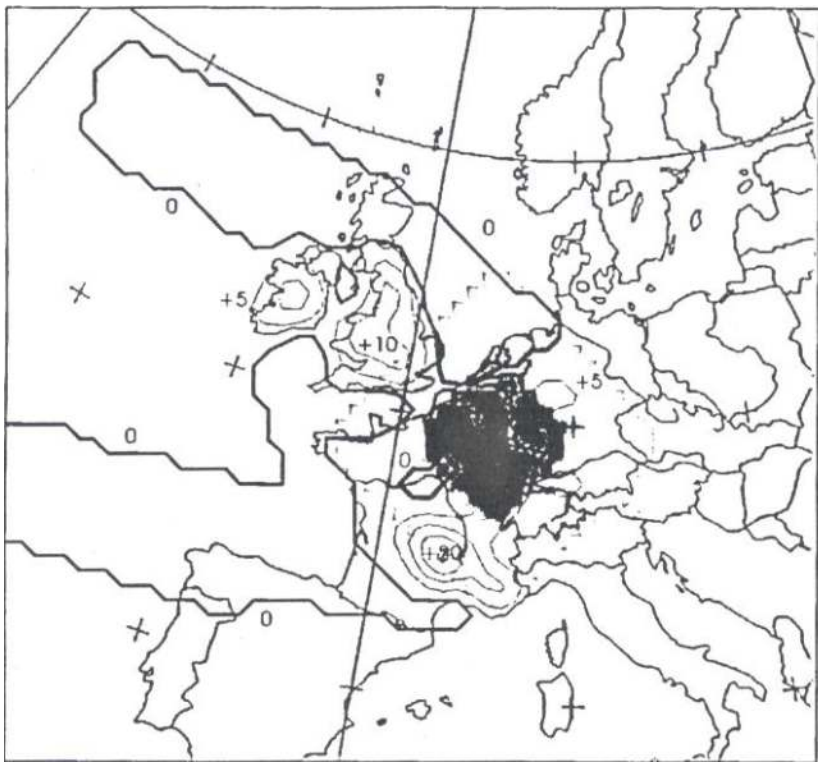

Figure 3.13: BLM model predicted mean sea level pressure differences in 1/100 hPa at 10:30 UTC. Contour interval 5/100 hPa. Negative values are within thick lines (from Prenosil, 2000)

The contour map of mean sea level pressure changes at 10:30UTC showed a pressure increase in and near the umbral region of totality as well as in areas that were located to the west (upstream) of the umbral shadow. The sea level pressure increase to the west of the umbral shadow was likely caused due to a temperature decrease, which affected the calculation of sea level pressure. This could be tested by collecting observations of unreduced pressure and temperature measured at 2 metres above ground. The mean sea level pressure increase is more pronounced over areas such as Massif Central in southern France. Over the UK, an increase of about 0.1hPa was modelled.

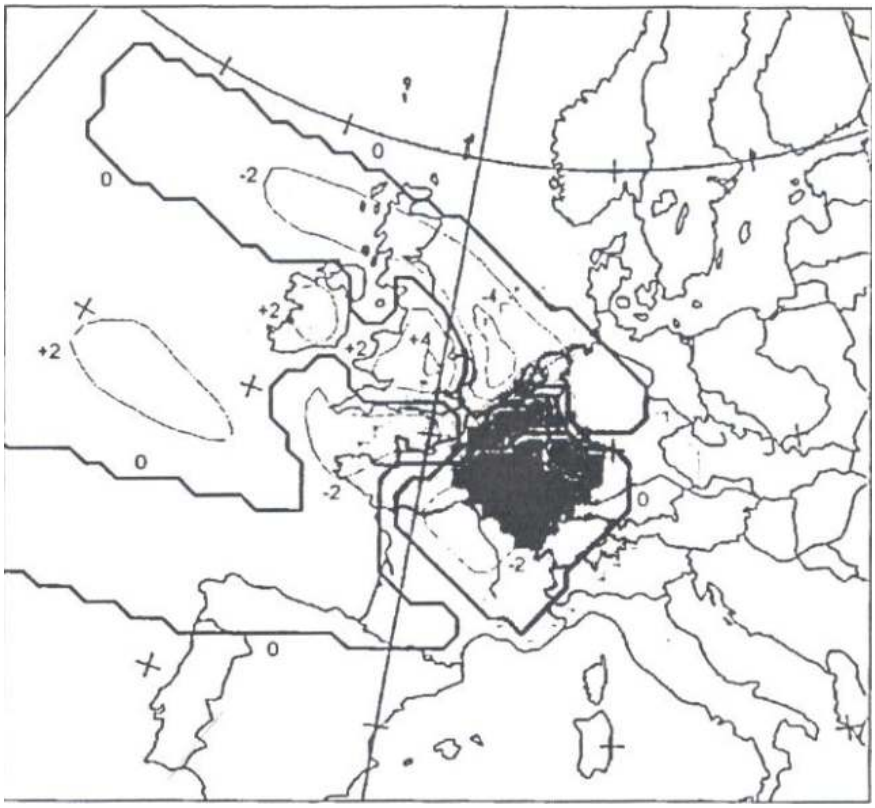

Figure 3.14: BLM model predicted local unreduced surface pressure differences in 1/100hPa at 10:30 UTC. Contour interval 2/100 hPa. Negative values are within thick lines (from Prenosil, 2000)

Figure 3.14 shows the predicted changes in unreduced surface pressure. It can be seen that there is an increase in the unreduced surface pressure in areas upstream of the eclipse. This is however of lower magnitude than the modelled increase in mean sea level pressure as unreduced surface pressure is unaffected by changes in surface temperature.

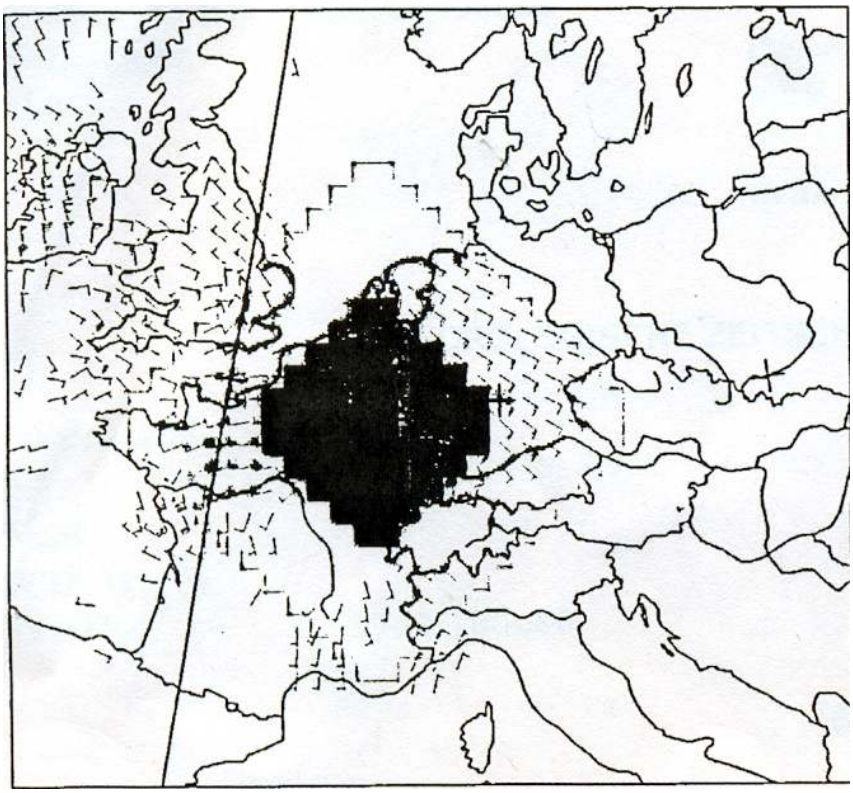

Figure 3.15: BLM model predicted windspeed and wind direction differences at 10:30 UTC (from Prenosil, 2000)

Figure 3.15 shows the modelled windspeed and wind direction changes, which resemble a cyclonic flow around the lunar shadow. These changes are modelled to occur mainly near to the lunar shadow and upstream of it. This confirms the hypothesis given by Clayton (1901) about the eclipse induced cyclone. Weaker wind changes are modelled above the sea surface, which is again likely due to the higher heat capacity of ocean. Near the coasts, it can also be seen that the eclipse wind blows towards the coast, which simply means that sea-breezes were modelled to be weakened by the eclipse.

3.3. Instrumentation that can be used to measure eclipse induced changes

Changes in atmospheric variables that occur due to a solar eclipse are minor in nature and often comparable to the random atmospheric fluctuations or noise of traditional measuring instruments. Therefore, in order to determine variations that are caused by an eclipse, sensitive and very good resolution instruments need to be used. Alternatively, averaging over a region that is affected by an eclipse needs to be performed in order to reduce random

local variability. The three most often measured quantities during an eclipse are temperature, wind direction and pressure.

As can be seen in Figure 3.4 in section 3.1, temperature variations caused by an eclipse are gradual and usually not greater than in the range of a few degrees. Therefore, a device that can measure fast and short term, but slight temperature changes would be the best to choose for eclipse induced temperature change measurements. An example would be a fine wire platinum resistance thermometer. It exploits the temperature dependent resistance properties of a metal, which is usually platinum. These thermometers are very accurate and can log the temperature at a fast rate due to the low thermal capacity of the measuring probe (a thin platinum wire), which rapidly adjusts to very small changes in temperature. (Harrison & Pedder, 2001)

For the wind direction and speed measurements a sonic anemometer is a good option to use as it can resolve changes in wind direction to the nearest 0.01 degree and wind speed changes to the nearest 0.01m/s (as opposed to a standard propeller anemometer, which is normally accurate only to the nearest 0.1-0.2m/s). A sonic anemometer can also perform several measurements per second, which is important as eclipse induced changes can occur within a second. (Wikipedia @ http://en.wikipedia.org/wiki/Anemometer) (July 2010)

It can be seen in Figure 3.5 in section 3.1 that pressure variations associated with an eclipse are very small and tend to be gradual, like the temperature variations. Therefore, any barometer or barograph that is accurate to the nearest 0.01 hPa would be satisfactory for this purpose. Its response time should however be within 1 second in order for it to respond to the rapid eclipse induced changes that occur especially during totality. (Winkler, et al. 2001)

4. Chapter 4: Time series analysis of synoptic changes caused by the 1999 eclipse

As discussed in the previous section, the total solar eclipse of 11th August 1999 was the best documented and observed total solar eclipse as it passed over densely populated areas of western and central Europe, including United Kingdom, France, Germany, Austria, Hungary and Romania. It passed through a dense network of both manned and automated weather stations, which regularly measure various meteorological variables. These provide an important source of data of short term changes in some of these variables.

In order to further investigate whether Clayton's hypothesis was correct a study was performed that would test the formation of a cyclone due to the cooling caused by the umbra. Claytons (1901) hypothesis was supported by the BLM model analysis described in the previous chapter. For this study a region covering the southern half of the UK was selected as this was the region, which was within 90% or greater partial eclipse. The path of totality crossed Cornwall and southern Devon.

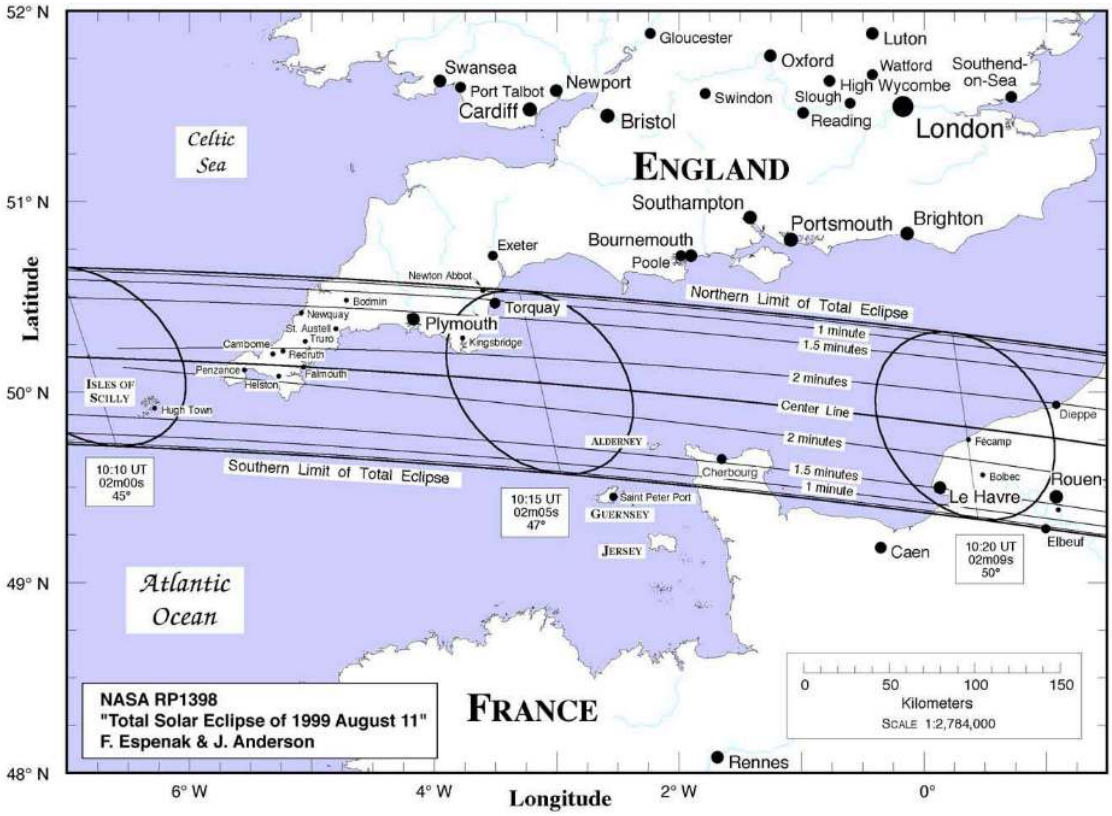

Figure 4.1: Map showing the path of totality over Cornwall, southern Devon and the English Channel. The rest of UK was within partial eclipse (from Espenak @ http://eclipse.gsfc.nasa.gov/SEmono/TSE1999/TSE1999Map/T99Fig6.jpg downloaded on 11th August 2010)

4.1. Synoptic situation on the day of the eclipse

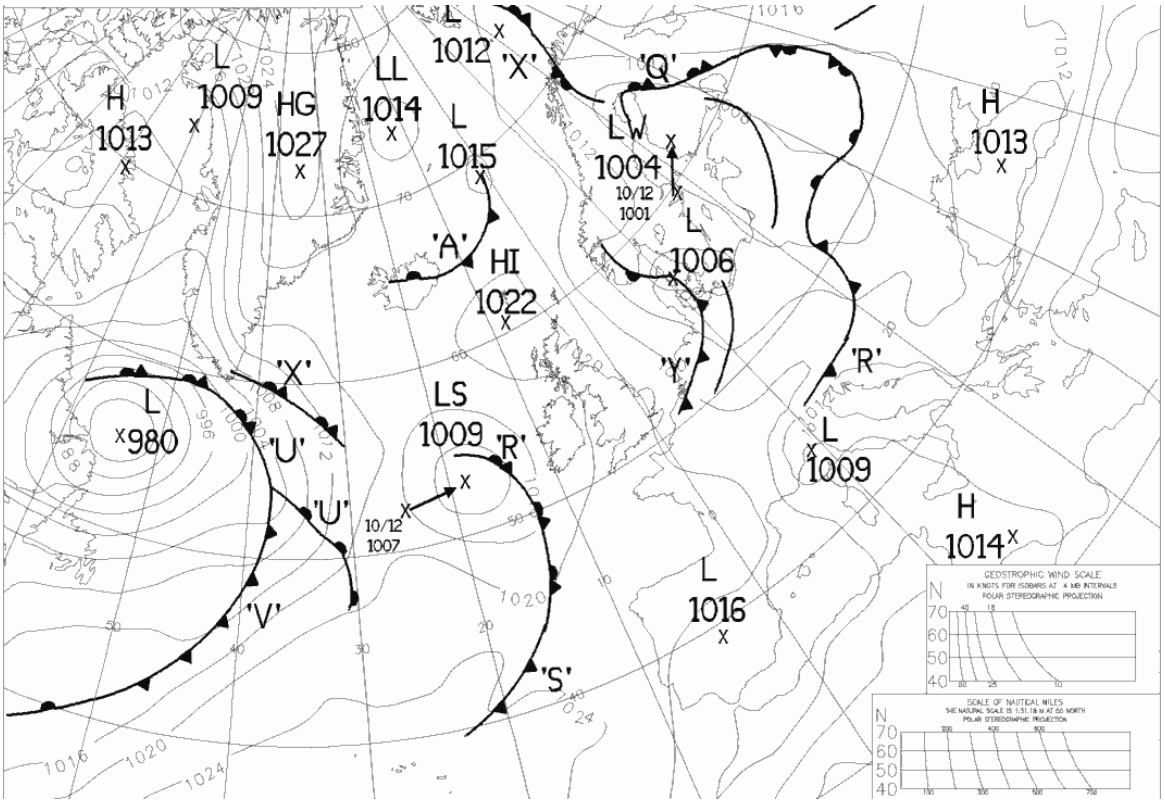

Figure 4.2: Synoptic situation for Europe and northern Atlantic at 00Z on 11th August 1999 (from http://www.wetterzentrale.de/topkarten/tkfaxbraar.htm downloaded on 13th July 2010)

It can be seen in Figure 4.2 above that United Kingdom was under the influence of a ridge of high pressure, which was moving to the east while a rather weak low pressure system with its occluded front was approaching from the west. The occluded front was located over Wales and Cornwall during the passage of totality and hence cloudy conditions prevailed in that area and the total eclipse was generally not visible. However, areas further to the northeast such as Midlands, southern England, southeast England and most of East Anglia experienced clear or mostly clear skies under the ridge.

This synoptic situation was supportive for detecting changes induced by the eclipse as weak pressure gradients prevailed, especially in eastern and northeastern parts of the UK, which means that geostrophic wind speed was not strong. Except for the occluded front in the southwest, there was no other front, trough or wind shift zone that would affect wind speed

and direction over the United Kingdom. Clear or mostly clear skies over central and southern United Kingdom meant greater changes in global solar irradiance during the eclipse and hence greater changes in temperature. Because of this synoptic setup, the very small changes in wind speed, wind direction and temperature were much easier to detect than if the synoptic situation was conductive to windy weather and well-mixed lower troposphere. Moreover, the coincidence of this synoptic setup occurring during eclipse time over a region with the availability of a dense measurement network made this eclipse a unique and very rare event, which is possible to study in great detail.

4.2. Obtaining data for the study of the 1999 eclipse

4.2.1. Meteorological variables used

In this study, the most widely measured meteorological variables were used. These are dry bulb temperature, mean sea level pressure, wind speed and wind direction. In addition to these, data for global solar radiation were obtained. Not many stations were found to have a record of global solar radiation (only 11 stations from 61 had this record), but it was used in order to see the timing of the eclipse as a change in global solar radiation is the most directly induced lower tropospheric change caused by an eclipse.

4.2.2. Meteorological stations from which data was obtained

United Kingdom has a dense network of meteorological stations that record various meteorological variables (dependent on the station) at hourly intervals. The record of these variables is being held at the BADC in a database called '*MIDAS Land Surface Stations data',* where records since year 1853 are held for all British stations being registered to that date.

61 British weather stations were chosen that were located in a region within 90% or greater partial eclipse (as discussed at the beginning of section 4) from the BADC database. A map of these stations is shown in figure 4.3 below.

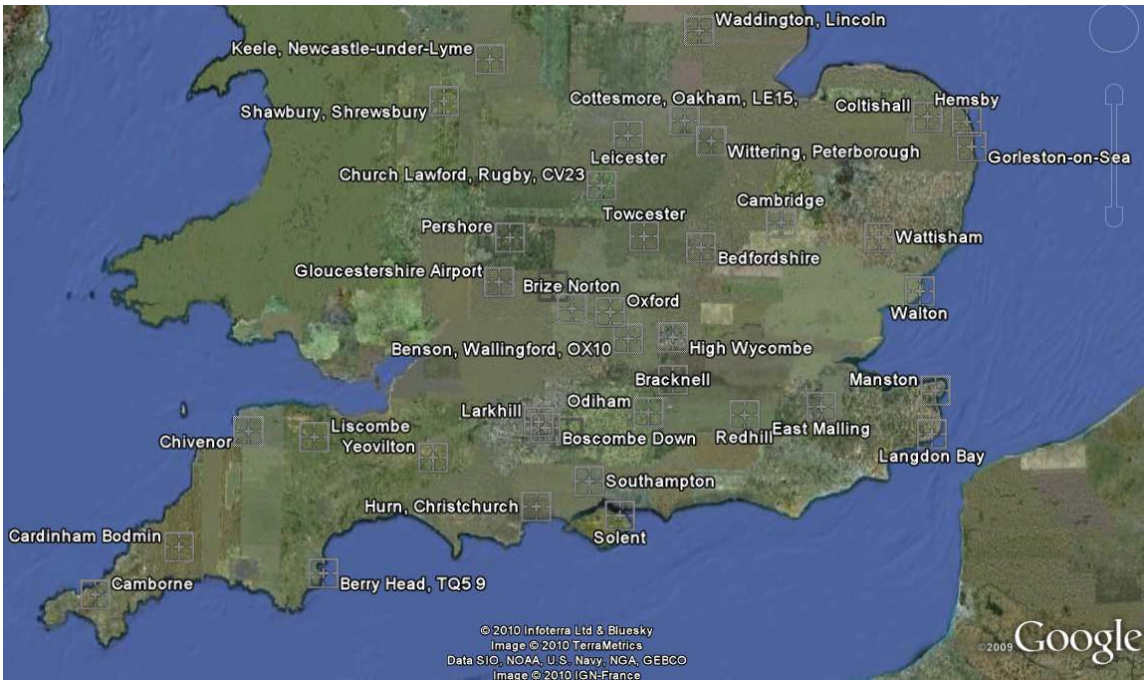

Figure 4.3: Map showing all the stations from which data was obtained for this study (from Google maps @ http://maps.google.com 10th June 2010)

4.2.3. Time range used in the study

Since this study is about atmospheric changes that were induced by the eclipse, it has to cover data for such periods that any eclipse induced changes can be compared to a large enough sample so that they can be identified and distinguished from other variations such as the diurnal cycle. This particular eclipse lasted almost 2 hours and 30 minutes over the UK and because of the reason discussed above a period covering the whole day before and the whole day after the eclipse was selected and hence the primary data obtained ranged from midnight on 10th August 1999 until midnight on 13th August 1999. The days before and after the eclipse were selected for comparison of the eclipse day with days of similar but un-eclipsed conditions.

4.3. Method for analysing synoptic changes induced by the eclipse

The variables introduced in section 4.2.1 were analysed by the method of averaging. It was performed by taking the hourly measurements from all 61 stations and calculating the average of all the station's values at each hour. If a certain station did not have a measurement recorded for the given time it was simply excluded from the averaging. By using this method, it was possible to see and study changes that were induced by the eclipse as data from individual stations could have been affected by local circumstances, but since the eclipse forcing affected the whole area averaging across 61 meteorological stations brought much clearer picture of the eclipse forcing without being greatly affected by any local effects. The averaged data was plotted against time for the time period specified in section 4.2.3 above. At each data point, error bars equalling 2 standard errors were added in order to see the possible error and certainty of the changes, i.e. to demonstrate whether changes were larger than the natural variability. Overall, 4 main plots were produced. These being temperature, mean sea level pressure, wind speed and wind direction (see Figures 4.6, 4.8, 4.10 and 4.12 respectively). In all these plots, global solar radiation was plotted in the background in order to better recognize the actual time of the eclipse (and hence distinguish those recorded measurements performed at the time of the eclipse).

$$filtered\ value = 0{,}25 * (previous\ value) + 0{,}5 * (current\ value) + 0{,}25 * (future\ value) \qquad (3)$$

In addition, a centred binomial filter with half weights at each end, as shown by equation (3), was used in order to obtain a curve that would 'smooth-out' the longer term variations in the curves obtained. An example for this equation would be a calculation for the filtered value at 12:00, where previous value is the measured value at 11:00, current value is the measured value at 12:00 and future value is the value measured at 13:00.

A graph of a difference between the actual curve and the smoothed (filtered) curve was obtained and plotted in each case in order to better see any short term and rapid changes that were caused by the eclipse and hence better recognize them from and compare with any slower synoptically or locally induced changes. In these graphs, the greater a negative

peak is the faster the decrease in the measured variable and the greater a positive peak is the faster the increase in this variable.

4.4. Results of the analysis

4.4.1. Data from all 61 meteorological stations

4.4.1.1. Mean hourly integrated global solar radiation

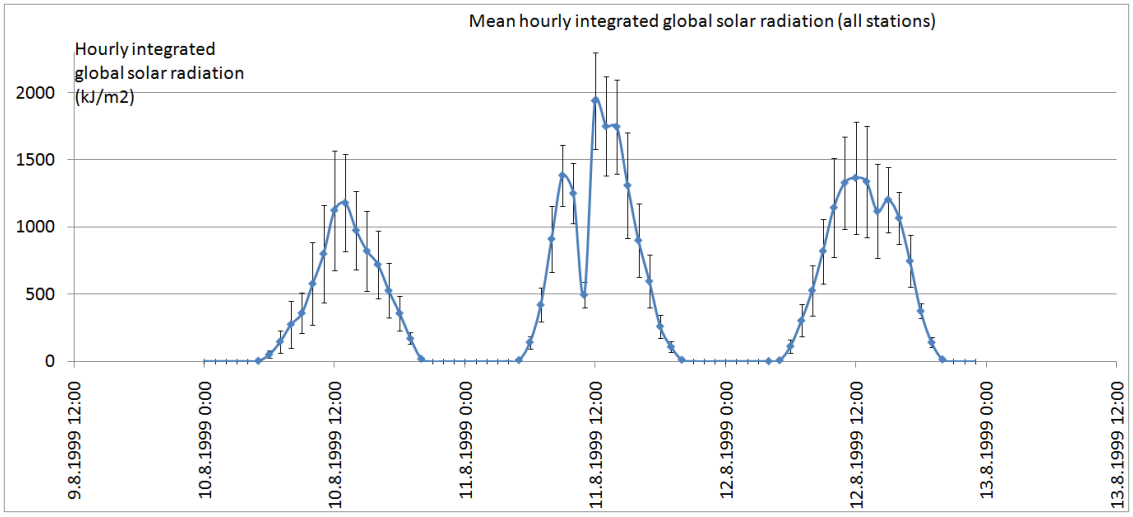

Figure 4.4: Plot of mean hourly integrated global solar radiation against time for all 61 meteorological stations. Every data point is integrated for the hour before the data point. Error bars represent 2 standard errors

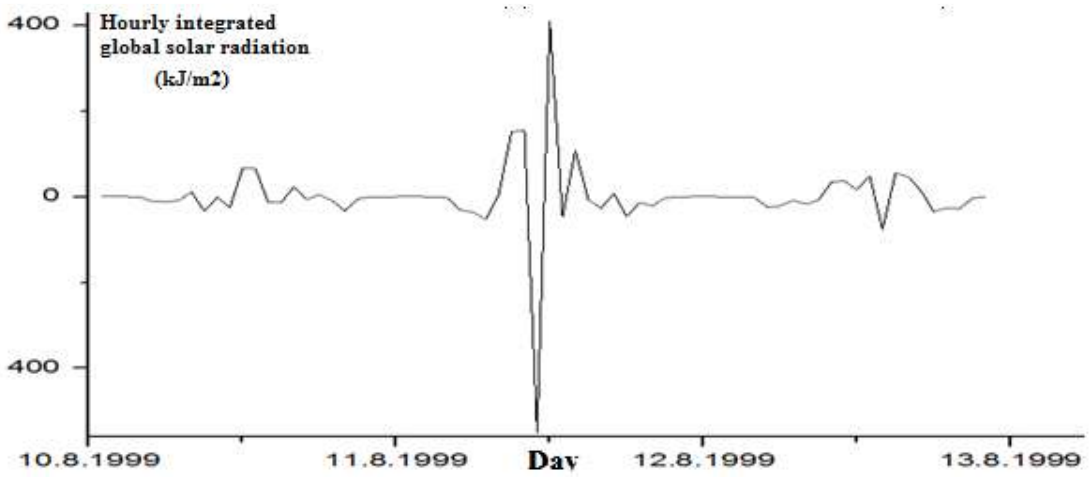

Figure 4.5: Plot of a difference between the smoothed curve and the curve in Figure 4.4

Figure 4.4 shows the change in hourly integrated global solar radiation due to the eclipse rather well. This is confirmed in Figure 4.5 by the deep negative peak being followed by a positive peak, which means that a rapid decrease in global solar radiation was being followed by a rapid increase. Both of these were more sudden than any other changes associated with diurnal variations, which is what would be expected for a solar eclipse.

The main features of Figure 4.4 are the diurnal changes with a maximum shortly after noon each day and a minimum (being zero) between sunset and sunrise. The middle peak represents the eclipse day and it can be seen that global solar radiation was strongest on the eclipse day compared to the other days (maximum hourly integrated global solar radiation on 10th August was 1232kJ/m^2 with a standard error of 204kJ/m^{2,} on 11th August 1981kJ/m^2 with a standard error of 198kJ/m^2 and on 13th August 1407kJ/m^2 with a standard error of 239kJ/m^2). The differences in its strength in between the days can arise mainly due to different amounts of cloudiness. There is a clear rapid decrease followed by a sharp increase around 11UTC on 11th August 1999, which corresponds to the time of the eclipse. The magnitude of the anomaly was 1051kJ/m^2 with a standard error of 93,2 kJ/m^2. From this graph it can be inferred with a great certainty that the change at eclipse time was caused only by the eclipse as it corresponds exactly to the time of the eclipse and its magnitude is about an order of magnitude greater than that of ordinary changes that could be associated with different amounts of cloud. Because of this certainty, this graph is shown in the background of the other graphs, as discussed in section 4.3 above, to better determine the time of the eclipse.

4.4.1.2. Mean temperature

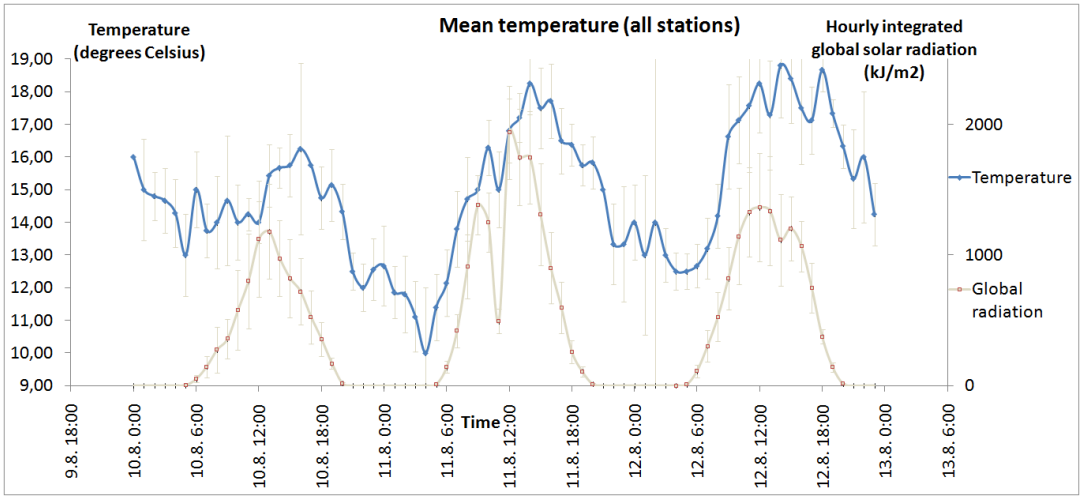

Figure 4.6: Plot of mean temperature (recorded at the hour) against time averaged across all 61 meteorological stations (blue). Plot of mean hourly integrated global solar radiation (for the hour before datapoint) averaged across all 61 stations in the background (grey) Error bars represent 2 standard errors

The main features in Figure 4.6 are again diurnal changes, which are caused by the simple fact that temperature is highest in the late afternoon due to solar radiation and lowest early in the morning due to infrared radiation out to space. The minima range between about 10 and 12 degrees Celsius while the maxima range between 16 and 19 degrees Celsius. It can be seen that the general trend in the temperature curve follows the trend in the global solar radiation curve with a slight delay of about 3 to 6 hours.

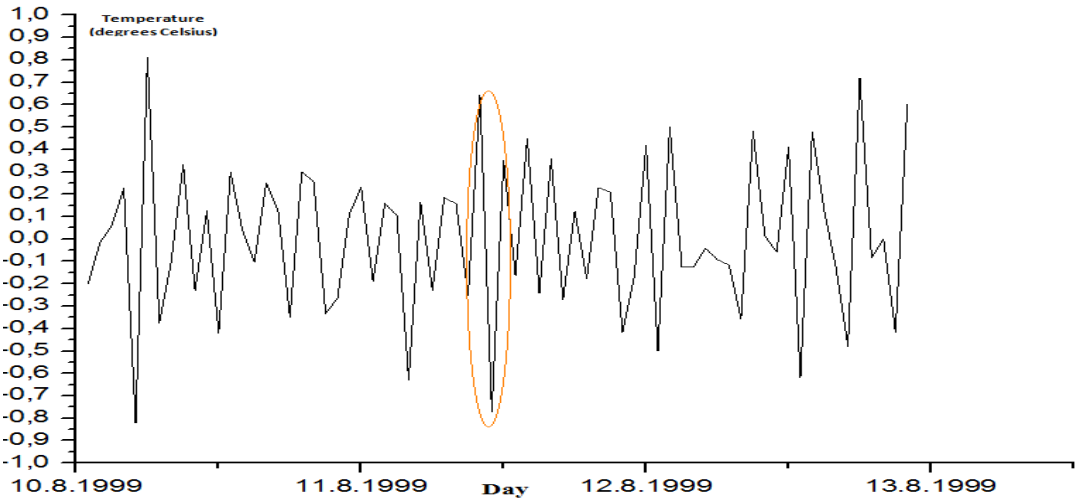

Figure 4.7: Plot of a difference between the smoothed curve and the curve in Figure 4.6

The temperature curve, however, is more variable than the global solar radiation curve, which can be seen by the variability in Figure 4.7. These frequent variations could have been caused by various effects affecting certain regions and also by the fact that temperature usually varies more rapidly on hourly basis than global solar radiation does (unless there is an eclipse). Because of this fact, it is harder to distinguish which changes were associated with the eclipse and which were caused by some other either small scale random or large scale systematic effects. The method of averaging over all the stations should have improved this. When looking at Figure 4.6 at the times where global solar radiation shows eclipse induced reduction a reduction in temperature can be identified. This has also been located in Figure 4.7 above and has been circled red. The magnitude of this reduction is 1.5 degrees Celsius with a standard error of 1.15 degrees Celsius. This is slightly larger than or at least comparable to the magnitudes of the other short term variation peaks. Because this temperature response to the eclipse is comparable in size to fluctuations its significance is low.

4.4.1.3. Mean pressure

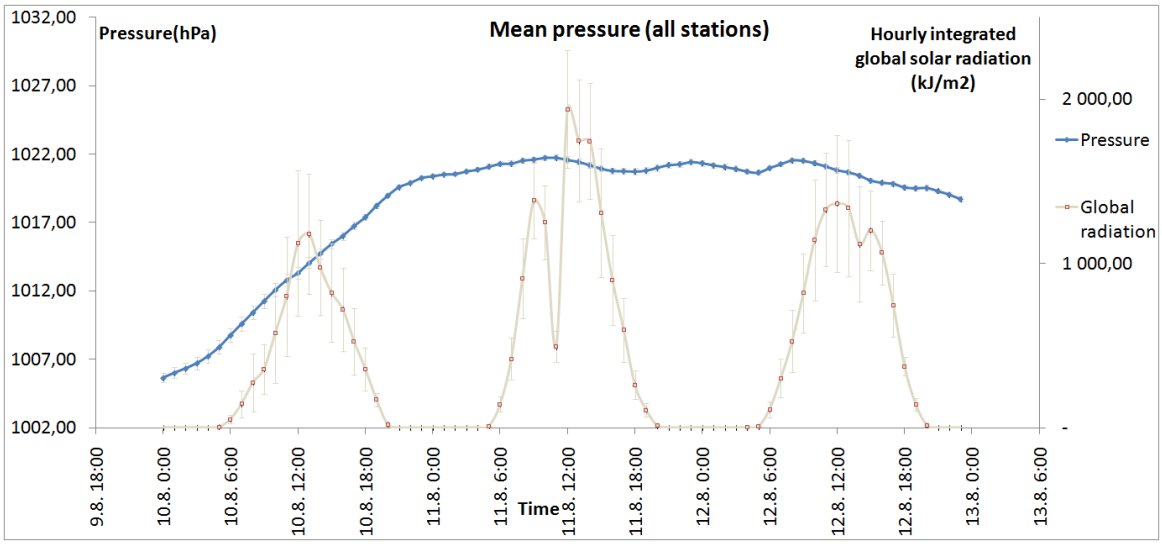

Figure 4.8: Plot of mean pressure (recorded at the hour) against time averaged across all 61 meteorological stations (blue). Plot of mean hourly integrated global solar radiation (for the hour before datapoint) averaged across all 61 stations in the background (grey) Error bars represent 2 standard errors

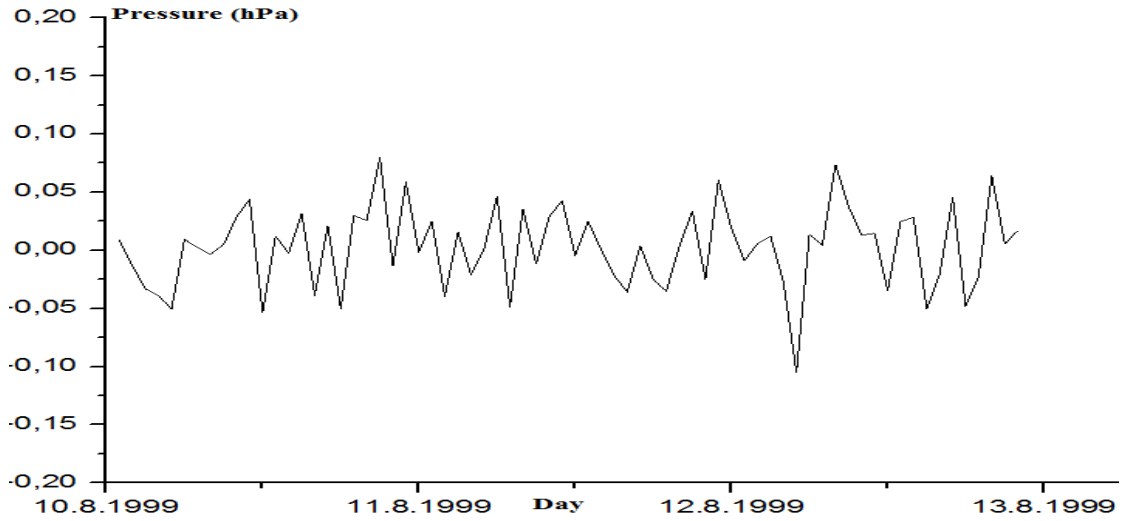

Figure 4.9: Plot of a difference between the smoothed curve and the curve in Figure 4.8

In Figure 4.8 above, the general trend of mean sea level pressure can be followed. The building of the ridge late on 10th August 1999 could be seen very well (see section 4.1 and Figure 4.2). Thereafter, pressure remained almost constant with only minor low amplitude variations. A small local maximum in the pressure track can be seen at the time of minimum global solar radiation and hence near the time of maximum eclipse. However, it cannot be concluded with a high confidence whether this maximum was caused by the eclipse or not as two other similar peaks occurred at about 12hourly intervals after this peak and hence could have been caused by some other synoptically induced mechanisms. Moreover, no distinct peak can be seen in Figure 4.9 above and hence it is very unlikely that any eclipse induced pressure changes were detected and could be displayed by this method of averaging across data that was recorded hourly.

4.4.1.4. Mean windspeed

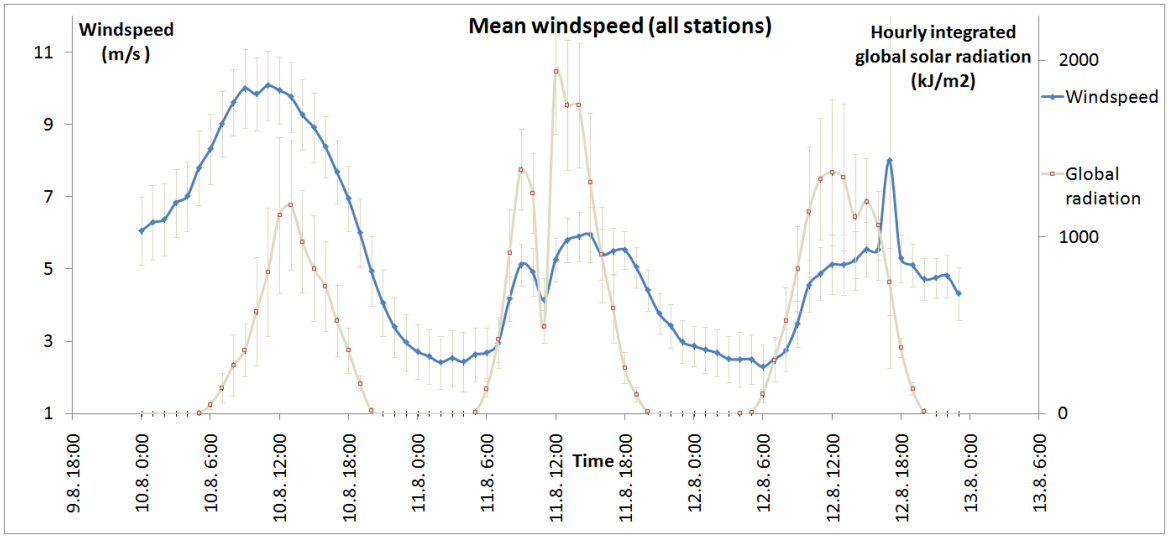

Figure 4.10: Plot of mean windspeed (averaged for the hour before data point) against time averaged across all 61 meteorological stations (blue). Plot of mean hourly integrated global solar radiation (for the hour before data point) averaged across all 61 stations in the background (grey) Error bars represent 2 standard errors

In Figure 4.10, it can be seen that windspeed also follows certain diurnal changes. Typically, there is a minimum overnight with a maximum during the day. It can be seen in the figure that windspeed had larger magnitude on 10th August before the ridge built over the UK and average windspeed decreased (see section 4.1.). The maximum hourly averaged value on the 10th was 9,46m/s with a standard error of 0,35m/s while on the 11th it was 6,41m/s with a standard error of 0,29m/s.

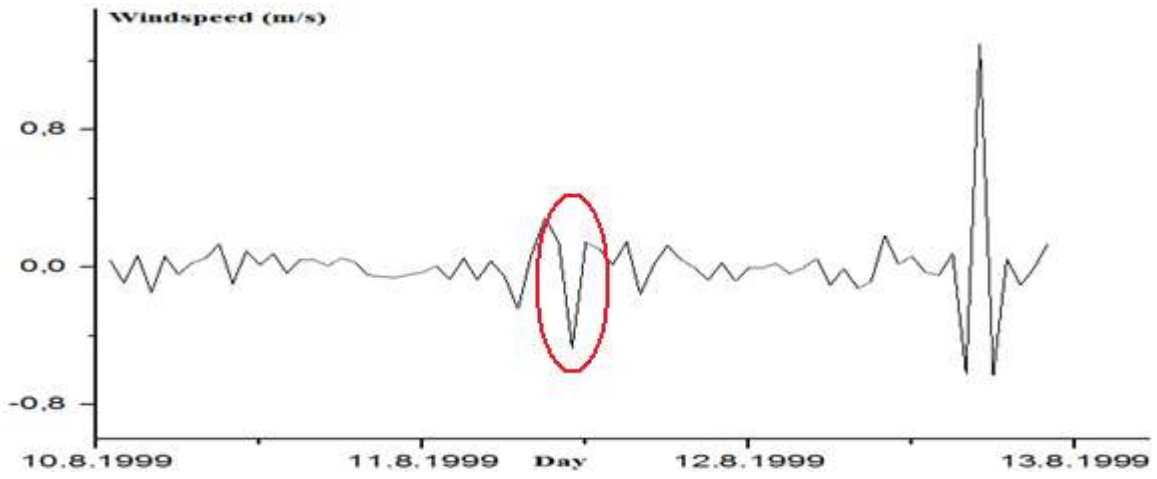

Figure 4.11: Plot of a difference between the smoothed curve and the curve in Figure 4.10

When looking at the time of the eclipse in Figures 4.10 and 4.11 above, a local minimum of average windspeed can be identified. The change at this point is greater than the other short term variations (circled red in Figure 4.11) and its magnitude is 0,8m/s with a standard error of 0,2. Only the peak on 12th August at about 18:00UTC has a larger magnitude (2,2m/s). This peak, however, has very large standard error in Figure 4.10 (3,4m/s) and therefore the magnitude of it cannot be taken into account as much. It was caused by unrealistic windspeed values being recorded likely by mistake by 2 meteorological stations, namely Hemsby and Gorleston on Sea. It can be concluded with some confidence that the wind speed minimum on 11th August was caused by the eclipse.

4.4.1.5. Mean wind direction

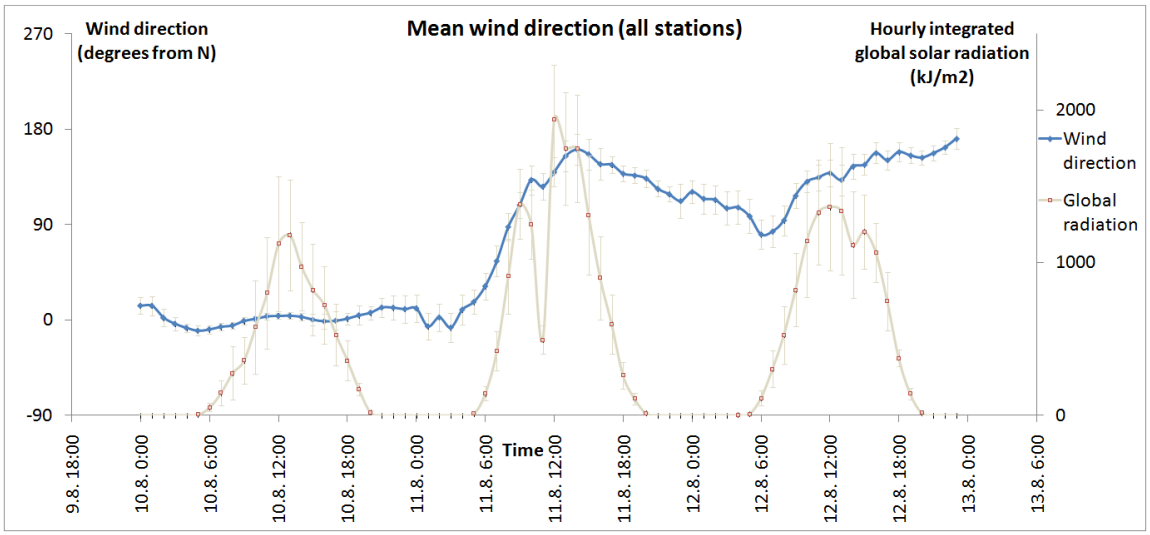

Figure 4.12: Plot of mean wind direction (averaged for the hour before datapoint) against time averaged across all 61 meteorological stations (blue). Plot of mean hourly integrated (for the hour before datapoint) global solar radiation averaged across all 61 stations in the background (grey) Error bars represent 2 standard errors

Figure 4.12 above shows very interesting results with regards to the wind direction changes. In this figure, 0 is from the northerly direction, negative values are degrees from northerly in the anticlockwise direction (backing) and positive values are degrees from northerly in the clockwise direction (veering). The wind direction on 10th August was predominantly from the northerly direction. It then veered to a prevailing easterly

direction, which was likely associated with the building of the ridge north of Scotland (see Figure 4.2). In the early hours on 12th August, there is a brief period of backed wind of magnitude of about 20 degrees. This was very likely associated with the passage of the occlusion over the UK (see section 4.1.). During the eclipse time, the wind backed by almost 10 degrees in the first half of the eclipse and then veered by about 10 degrees in the second half of the eclipse. This wind direction change was very likely associated with the eclipse as it exactly coincided with the minimum in the hourly integrated global solar radiation. This would confirm the prediction produced by the BLM model (see section 3.2.3.) and the hypothesis given by Clayton (1901).

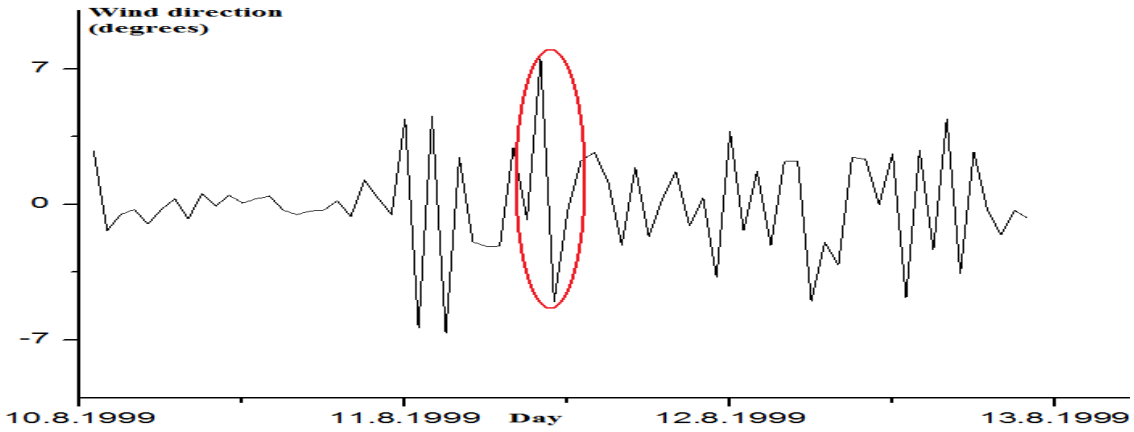

Figure 4.13: Plot of a difference between the smoothed curve and the curve in Figure 4.12

It can be seen in Figure 4.13 above that the change associated with the eclipse (circled in red) was a sudden change, which is a typical feature of the eclipse, but the magnitude of the peak corresponding to eclipse time (magnitude 13degrees with a standard error of 2,1degrees) is not that much greater than that of some of the other peaks, which means that the eclipse induced change was of a comparable magnitude to changes induced by synoptic mechanisms. With regards to the changes, a positive peak being followed by a negative peak can be seen. The positive peak means a veer in the wind direction, which occurred before the eclipse induced backing. If it were significant this veer could be a sign of anticyclonic flow predicted by Clayton (1900) that surrounds the eclipse induced cyclone.

4.4.2. Comparison of data from cloudy and non-cloudy stations

It was further investigated whether the changes associated with the eclipse that were confirmed in the main analysis were affected by the fact whether it was cloudy or sunny (mostly sunny) at the meteorological station. This investigation was performed by dividing the 61 stations into the ones that were under cloudy conditions at the time of the eclipse and those that were under sunny conditions at the same time. The same analyses as in part 4.4.1 were performed with these 2 groups of stations and the resulting graphs were then compared. The division of the stations into the 2 groups was based on 2 satellite pictures. It could have been done by the use of the measured global solar irradiance, but only a few of the stations had data for global solar radiation available.

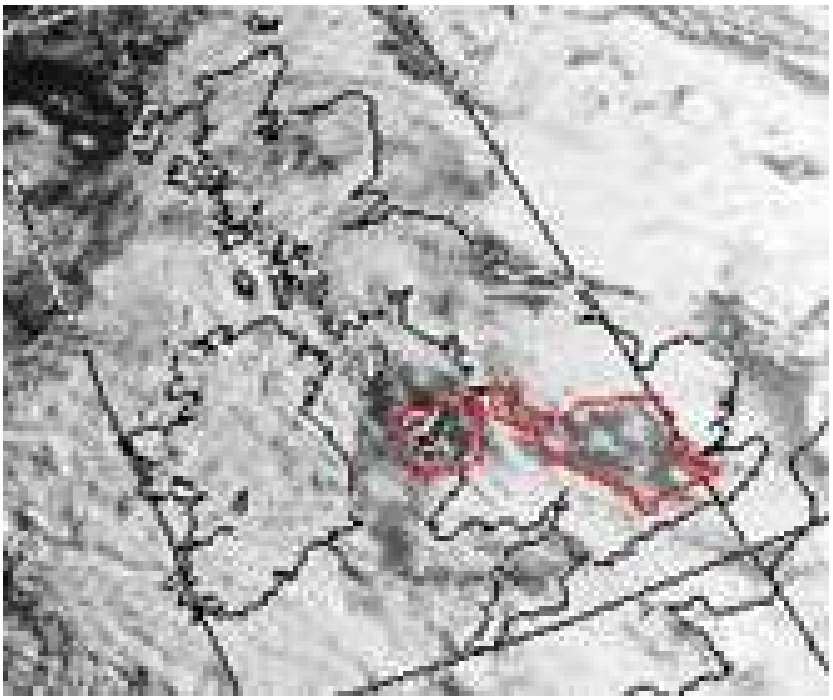

Figure 4.14: Satellite picture for 07:20UTC on 11th August 1999. Red line indicates a border between cloudy and non-cloudy regions (from http://www.sat.dundee.ac.uk/auth.html downloaded on 2nd July 2010)

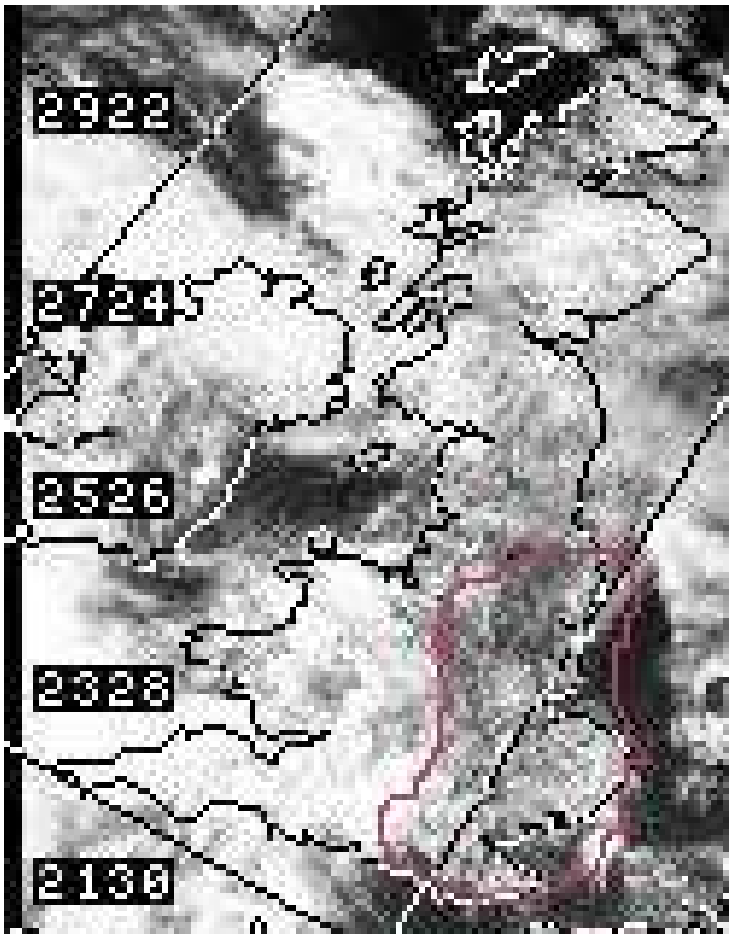

Figure 4.15: Satellite picture for 13:36UTC on 11th August 1999. Red line indicates a border between cloudy and non-cloudy regions (from http://www.sat.dundee.ac.uk/auth.html downloaded on 2nd July 2010)

Figure 4.14 above shows a satellite picture about 2 hours before the beginning of the eclipse and Figure 4.15 above shows a picture for about 1 hour after the end of the eclipse. Since most of the UK was under the ridge (see section 4.1.) it was assumed that the amount and location of the cloudiness was changing uniformly in between the time of these pictures and during the time of the eclipse. On the first image, two areas of clear or mostly clear conditions were identified (bordered by the red line) and on the second image, one large clear or mostly clear area was highlighted in the same way.

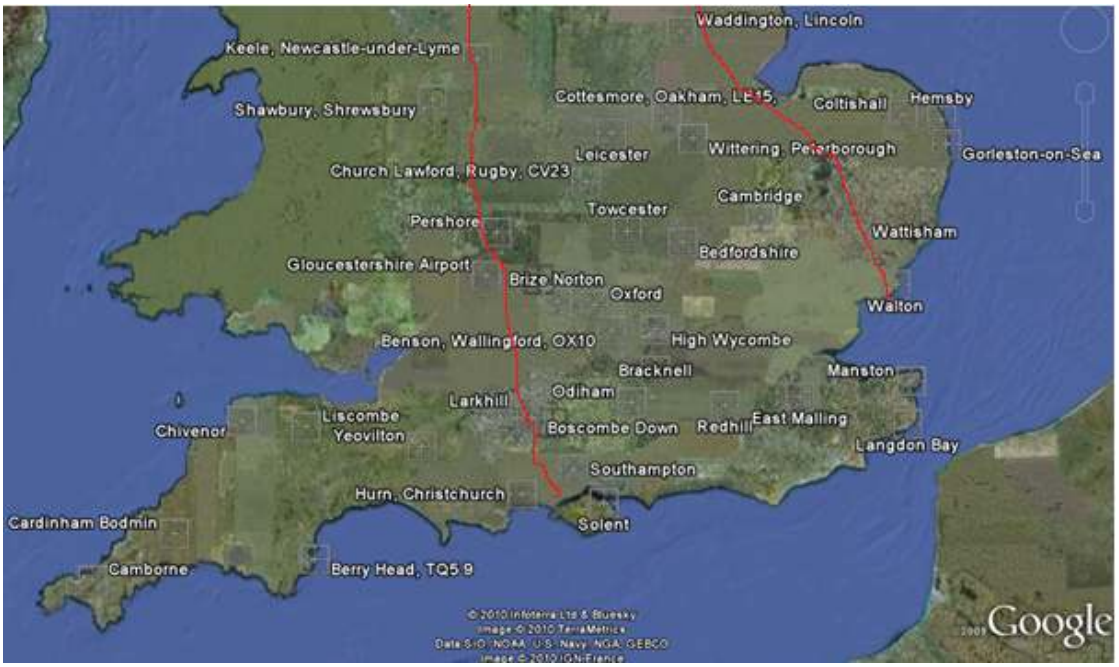

Figure 4.16: Final division of stations into cloudy stations and non-cloudy stations (from Google maps @ http://maps.google.com/ downloaded on 22nd June 2010)

Figure 4.16 above shows the final location of the boundary between those stations that were considered being under cloudy conditions and those that were considered to be under clear or mostly clear conditions during the eclipse. The cloudy stations are those located to the west of the red line that starts near the Isle of Wight and goes towards north-eastern Wales and to the east of the red line that traverses East Anglia.

In the following plots, data for temperature, pressure, windspeed and wind-direction were separated according to the cloudy and non-cloudy stations division. However, none of the stations in the cloudy division had a record of hourly integrated global solar radiation. Therefore, the averaged value that was used for the sunny stations was used for the cloudy stations as well (it is the same data of global solar radiation that was used in the analysis in section 4.4 above as there is no global radiation data for cloudy stations and cloudy + non-cloudy stations = all stations). The plots of the difference between the smoothed curves and the measured curves were zoomed in on the eclipse day in order to better see and recognize changes between the cloudy and non-cloudy curves.

4.4.2.1. Mean temperature

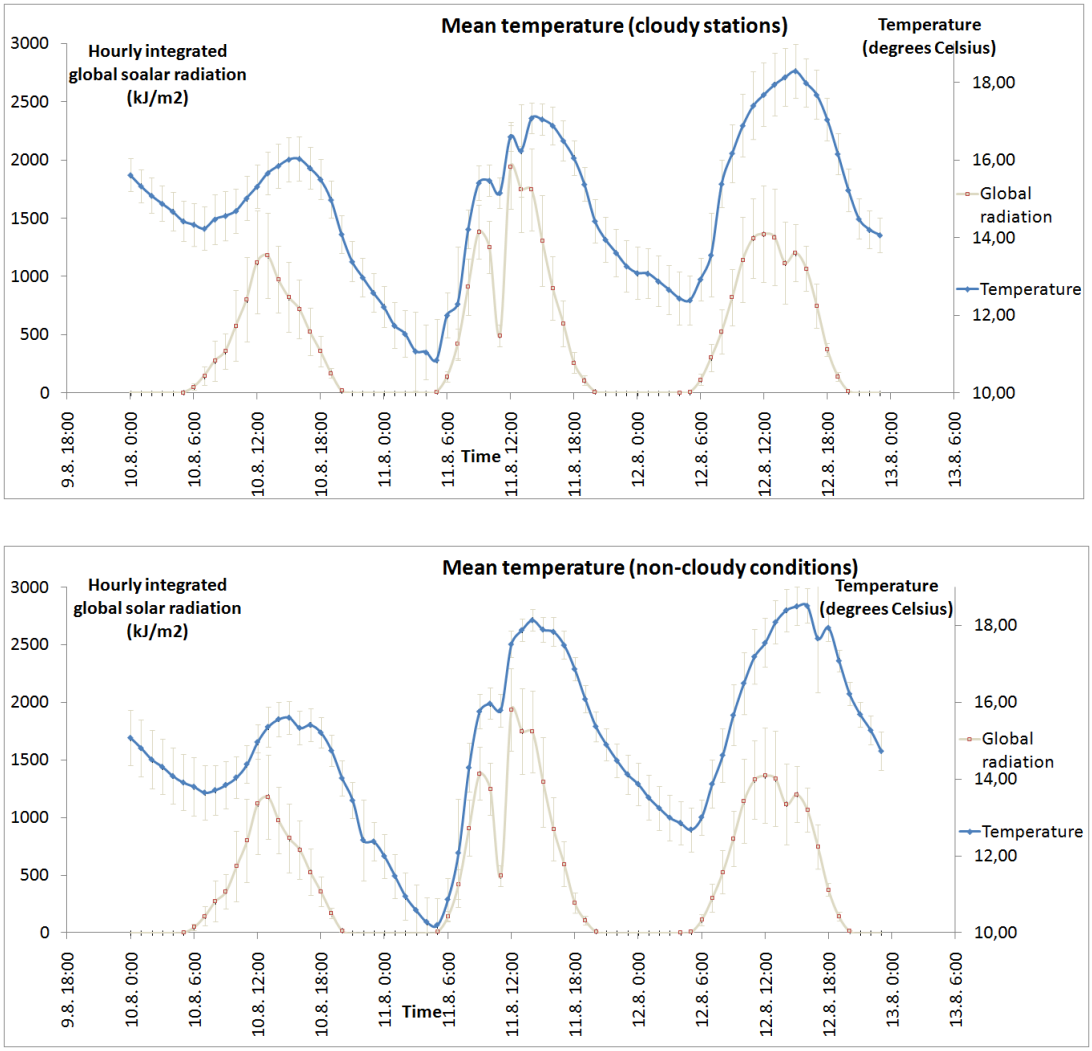

Figure 4.17: Plots of mean temperature (at the hour) against time averaged across 29 cloudy stations (top) and 32 not cloudy stations (bottom) (blue). Plots of mean hourly integrated global solar radiation (for the hour before data point) averaged across all 61 stations in the background (grey) Error bars represent 2 standard errors

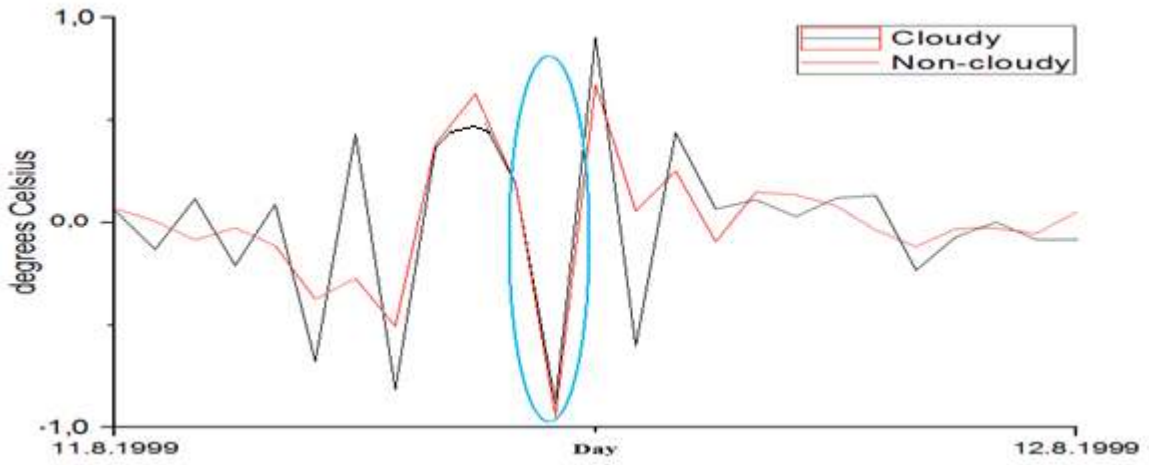

Figure 4.18: Plot of a difference between the smoothed curves and the curves in Figure 4.17 for cloudy stations (black) and non-cloudy stations (red)

The two sets of stations can be compared regarding temperature in Figures 4.17 and 4.18. In Figure 4.17 it seems that the temperature decrease is stronger in case of cloudy stations. However, if the rise in temperature onto which this cooling is superimposed is considered this shows to be not the case. Figure 4.18, which takes into account only the magnitudes of the differences shows that the relative reduction in temperature is stronger in case of non-cloudy conditions (the eclipse induced peak is circled in blue). The magnitude of the anomaly in case of non-cloudy stations was 1,6°C with a standard error of 1,19°C. In case of cloudy stations, the magnitude of the anomaly was 1,25°C with a standard error of 0,38°C. The cloudy stations have a second temperature minimum about 1 hour after the end of the eclipse the magnitude of which is smaller (namely 1,9°C with a standard error of 0,32°C) than that of the eclipse induced cooling. It cannot however be certain whether this change was somehow induced by the eclipse as the cloudy stations were mostly the ones that were located under the occluded front at the time of the eclipse and the occluded front brought some rain and possibly colder temperatures for an hour as it passed over those stations. Also, the cloudy stations seem to have greater short term variations in temperature than the sunny stations have.

4.4.2.2. Mean pressure

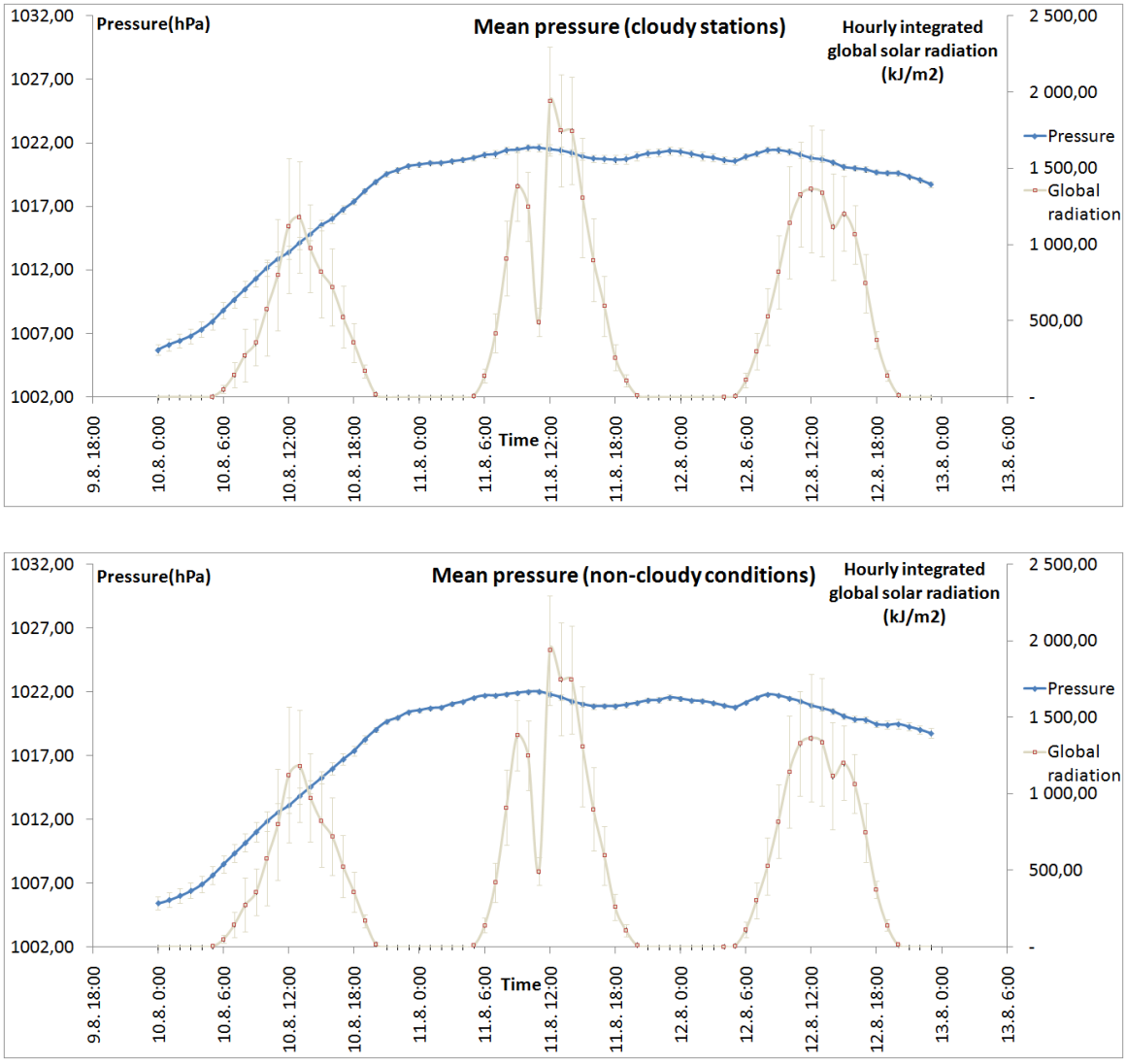

Figure 4.19: Plots of mean pressure (at the hour) against time averaged across 29 cloudy stations (top) and 32 not cloudy stations (bottom) (blue). Plots of mean hourly integrated global solar radiations (for the hour before datapoint) averaged across all 61 stations in the background (grey) Error bars represent 2 standard errors

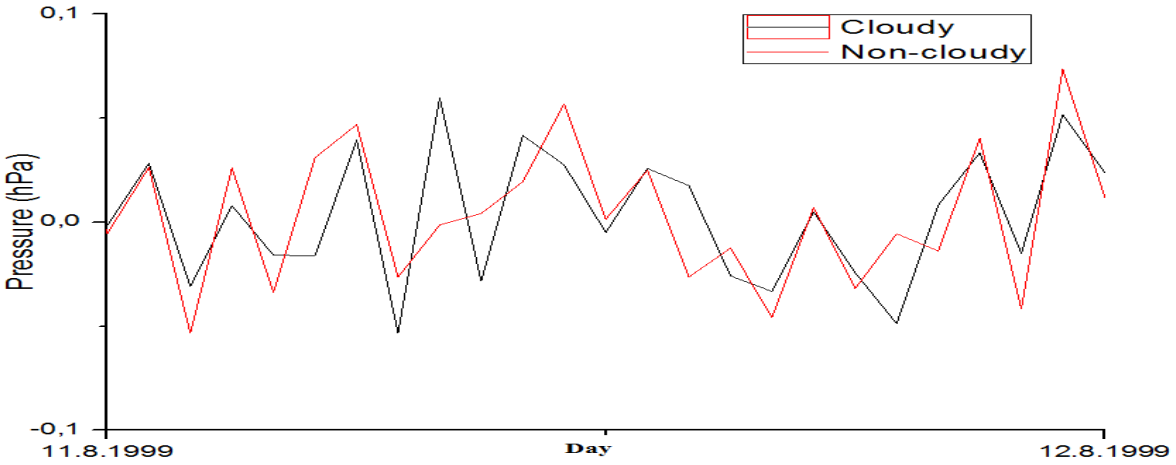

Figure 4.20: Plot of a difference between the smoothed curves and the curves in Figure 4.19 for cloudy stations (black) and non-cloudy stations (red)

Not many differences can be seen when comparing the two plots in Figures 4.19 and 4.20. Since the magnitude of the changes of the mean sea level pressure associated with the eclipse is weak (0.1hPa or less) it is difficult to distinguish this change from other synoptically induced changes. Also, this change lasts only up to several minutes and the meteorological stations record pressure just once per hour and therefore may easily miss this change. The general pressure pattern (including the two peaks in the day after the eclipse) does not reveal any major differences between the groups of stations.

4.4.2.3. Mean windspeed

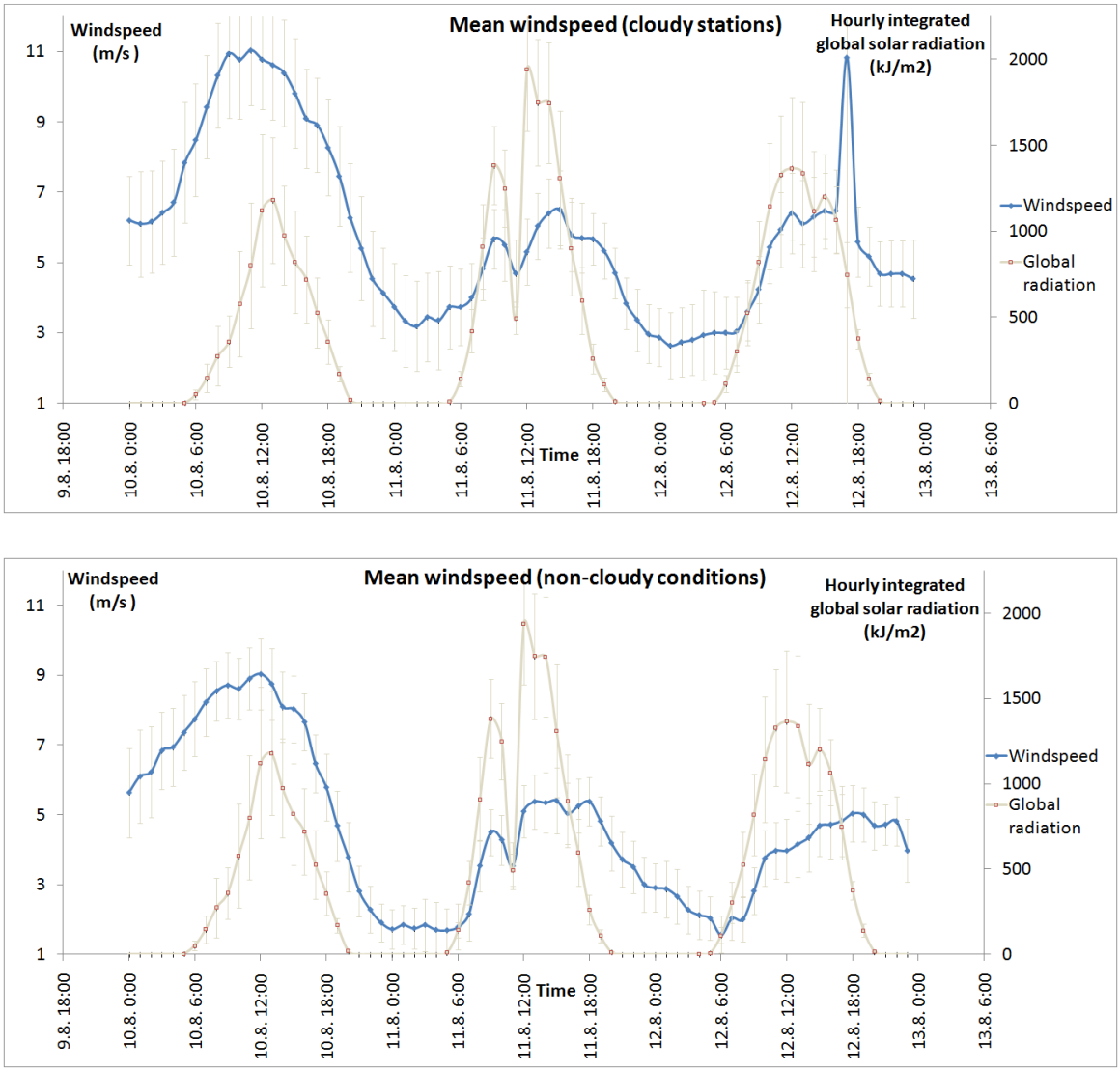

Figure 4.21: Plots of mean windspeed (averaged over the hour before data point) against time for 29 cloudy stations (top) and 32 not cloudy stations (bottom) (blue). Plots of mean hourly integrated (for the hour before datapoint) global solar radiation averaged across all 61 stations in the background (grey) Error bars represent 2 standard errors

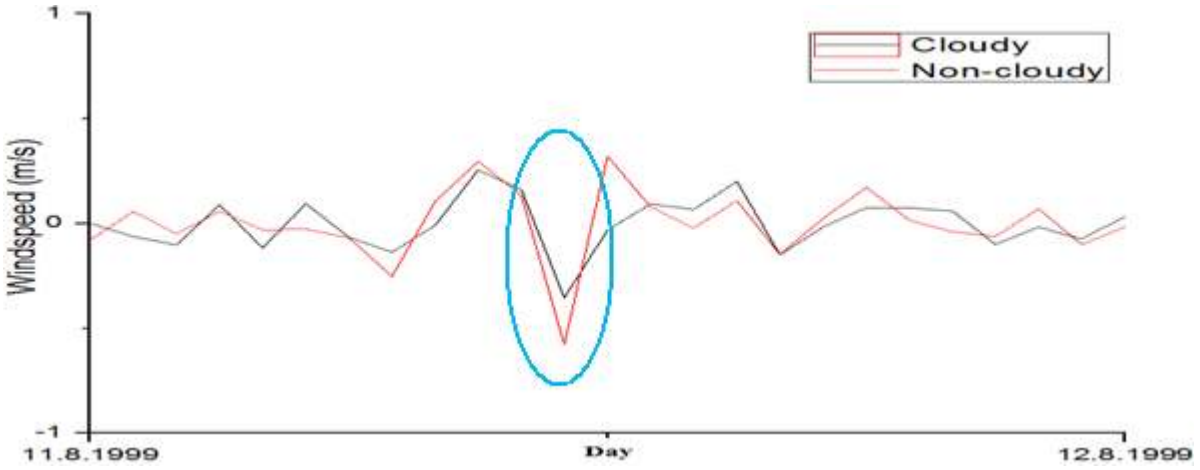

Figure 4.22: Plot of a difference between the smoothed curves and the curves in Figure 4.21 for cloudy stations (black) and non-cloudy stations (red)

The plots of windspeed in Figures 4.21 and 4.22 above do reveal a slight difference in the change of windspeed associated with the eclipse between the cloudy and non-cloudy stations. It can be seen in Figure 4.22 that in case of non-cloudy stations the eclipse induced windspeed reduction is greater (eclipse peak again circled in blue). The magnitude of the anomaly for non-cloudy stations was 0,9m/s with a standard error of 0,11m/s and for the cloudy stations 0,6m/s with a standard error of 0,08m/s. Therefore, the difference between cloudy and non-cloudy stations is not great. Overall, it can be concluded from these plots that clouds had a slight impact on the reduction of windspeed during this eclipse.

4.4.2.4. Mean wind direction

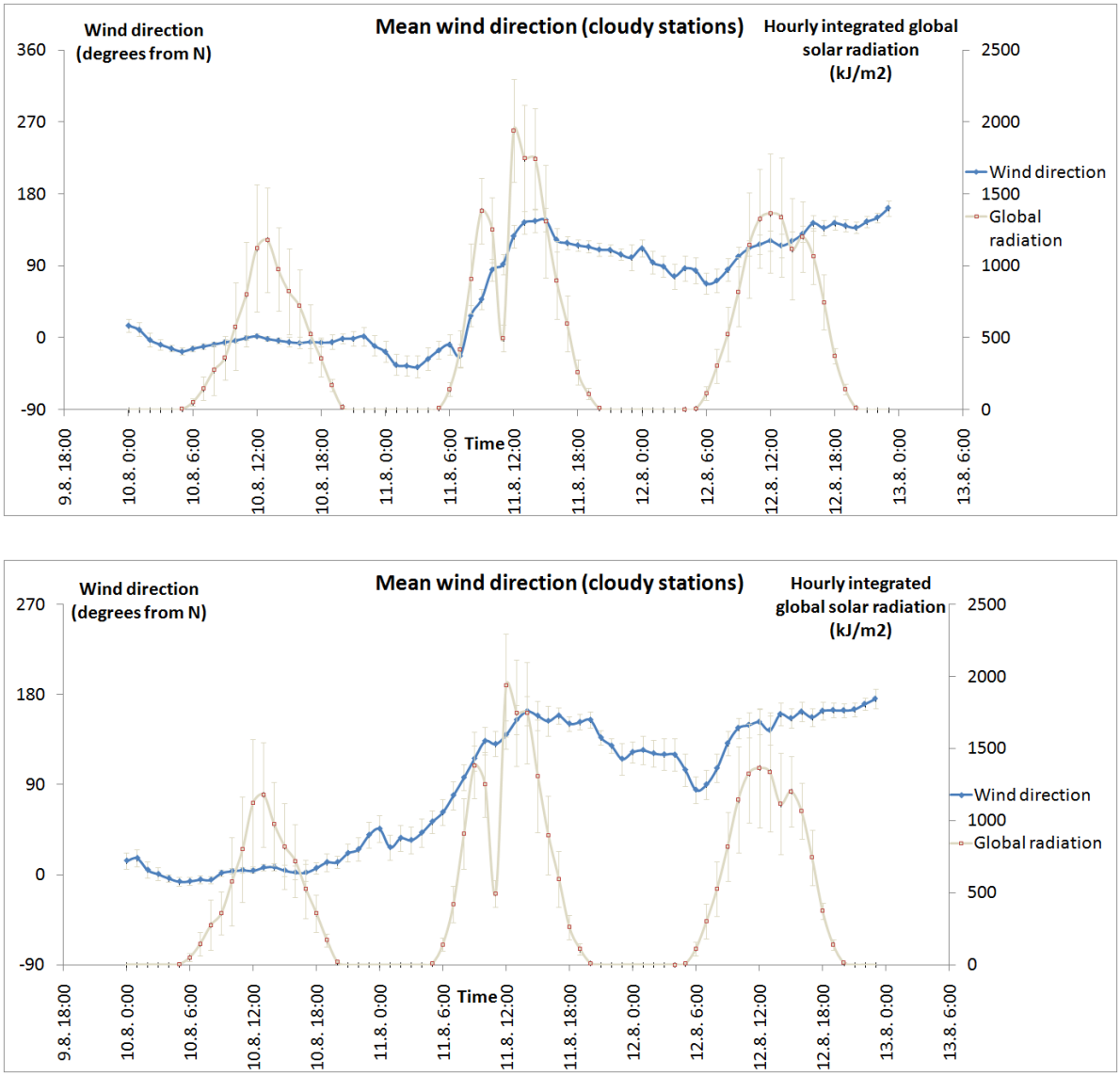

Figure 4.23: Plots of mean wind-direction (averaged over the hour before data point) against time for 29 cloudy stations (top) and 32 not cloudy stations (bottom) (blue). Plots of mean hourly integrated (for the hour before data point) global solar radiation averaged across all 61 stations in the background (grey) Error bars represent 2 standard errors

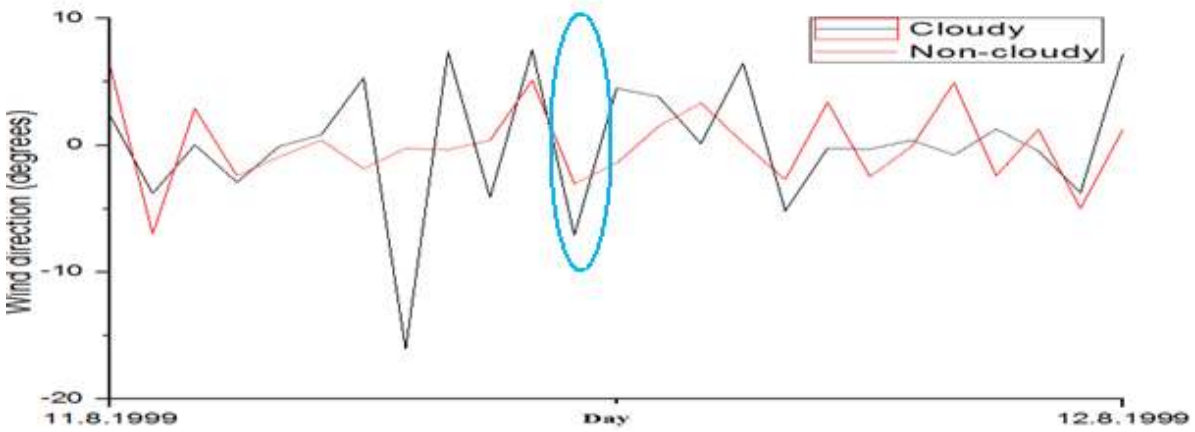

Figure 4.24: Plot of a difference between the smoothed curves and the curves in Figure 4.23 for cloudy stations (black) and non-cloudy stations (red)

It can be seen in Figure 4.24 that the eclipse-related changes in wind-direction were more pronounced in case of stations that were under cloudy conditions (eclipse induced peak again circled in blue). The magnitude of the anomaly for non-cloudy conditions was 9degrees with a standard error of 1.7degree, and for the cloudy stations 17 degrees with a standard error of 4.3 degrees.

4.4.3. Comparison of data from stations nearer to and further from totality

Another investigation that was performed with the collected data was comparison between stations that were located near to the path of totality (in deeper eclipse) and stations that were further from the path of totality and in less deep eclipse. As a borderline a line separating 97% eclipse or greater was drawn and all stations to the south of that line were selected as nearer to the path of totality and those stations to the north of that line as further from the path of totality.

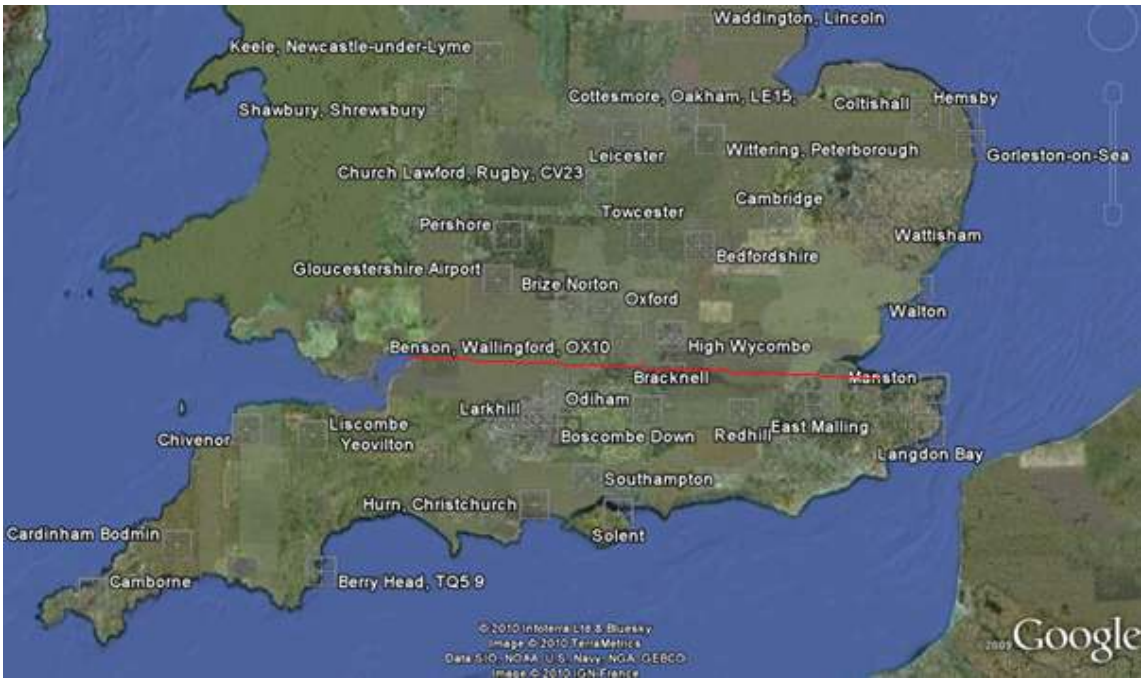

Figure 4.25: Division of stations that were considered to be near totality and further from totality (from Google maps @ http://maps.google.com/ downloaded on 22nd June 2010)

Figure 4.25 above shows the separation of the meteorological stations into the close to totality group (south of the red line) and further from totality group (north of the red line). All the plotted variables were divided according to the near to and further from the eclipse division. The plots of the difference between the smoothed curves and the measured curves were again zoomed in on the eclipse day in order to better see and recognize changes between the close to and further from eclipse curves.

4.4.3.1. Mean temperature

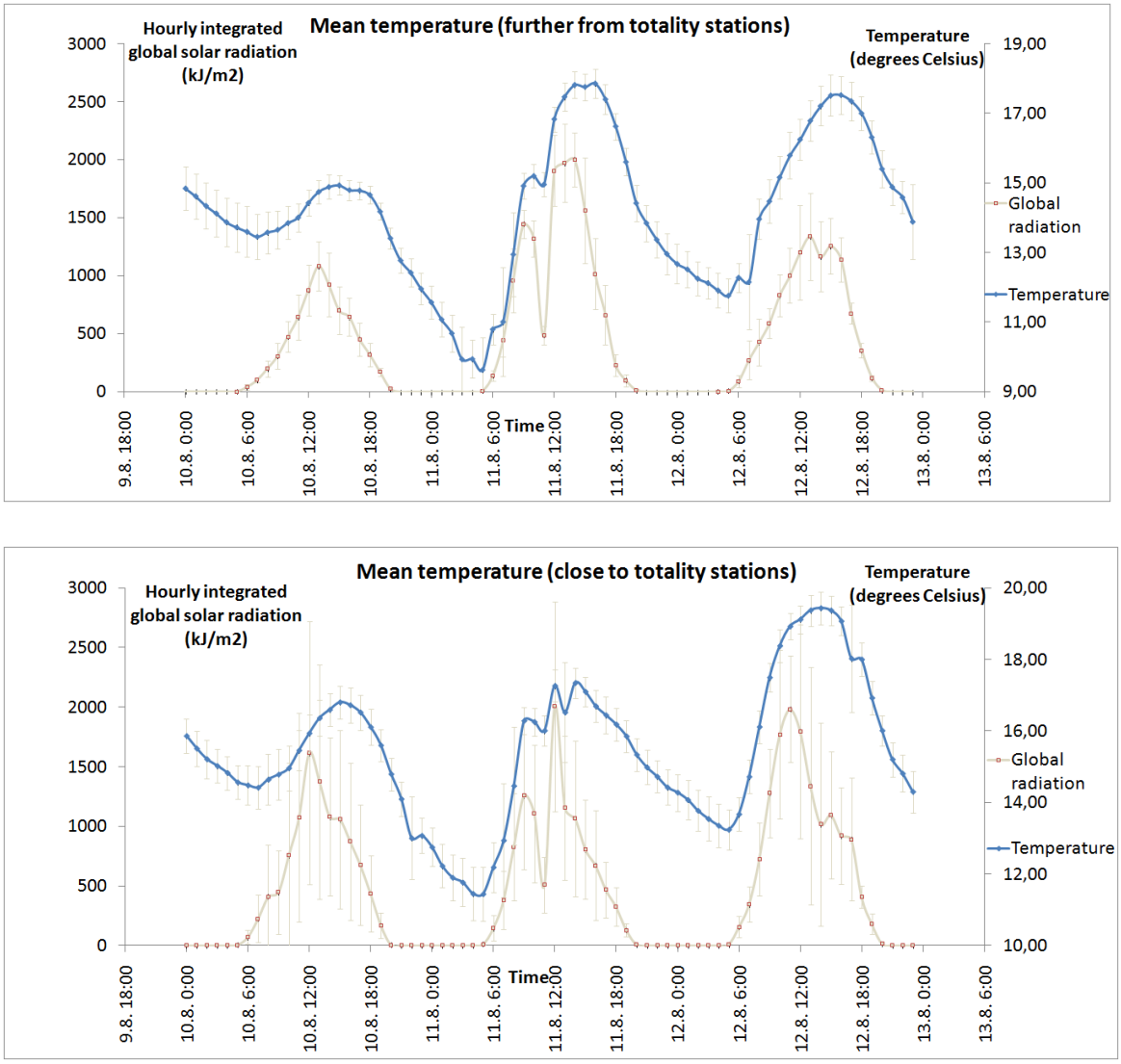

Figure 4.26: Plots of mean temperature (recorded at the hour) against time for 28 stations further from totality (top) and 33 stations close to totality (bottom) (blue). Plots of mean hourly integrated (for the hour before the datapoint) global solar radiation averaged across the stations considered in that graph in the background (grey) Error bars represent 2 standard errors

The two sets of stations can be compared in Figure 4.26. The main difference between these is the magnitude of the cooling between 9am and 11am (11am is the data point where the global solar radiation is significantly reduced). In case of stations further away the average air temperature was about 15 degrees Celsius at 9am. It then rose by about 0.3 degrees by 10am and then fell to about 15 degrees again by 11am, which is the closest

time to maximum eclipse. After that the temperature sharply rose with the end of the eclipse. According to calculation used to draw Figure 4.26 the magnitude of the anomaly for stations further away was 1.0 degree Celsius with a standard error of 0.93 degrees Celsius.

The stations closer to totality reveal an average air temperature of about 16.3 degrees Celsius at 9am. In the following hour the temperature fell very slightly (as opposed to the average temperature of stations further from totality, where it rose during this time). After that (during maximum eclipse), the average temperature fell by almost 0.8 degrees Celsius down to 16 degrees by 11am. After that the temperature rose sharply with the end of the eclipse. The magnitude of the anomaly for close to totality stations was 0.9 degrees Celsius with a standard error of 0.87 degrees Celsius. From this data it can be concluded that the eclipse induced cooling lasted longer closer to totality.

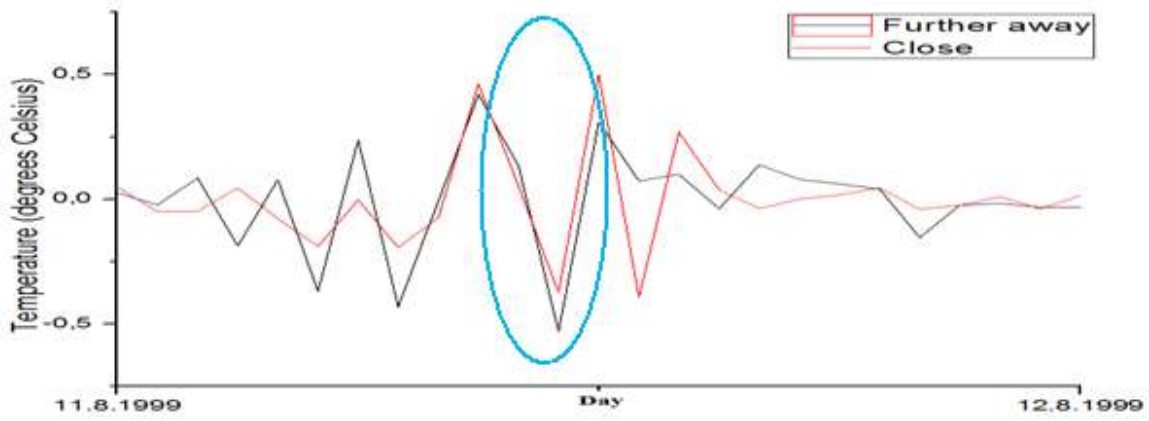

Figure 4.27: Plot of a difference between the smoothed curves and the curves in Figure 4.26 for stations further away from totality (black) and closer to totality (red)

It can be seen in Figure 4.27 by comparison of the curves at eclipse time (blue circle) that the magnitude of the temperature response to the eclipse was about the same for the stations close to the track of totality and those further away.

4.4.3.2. Mean pressure

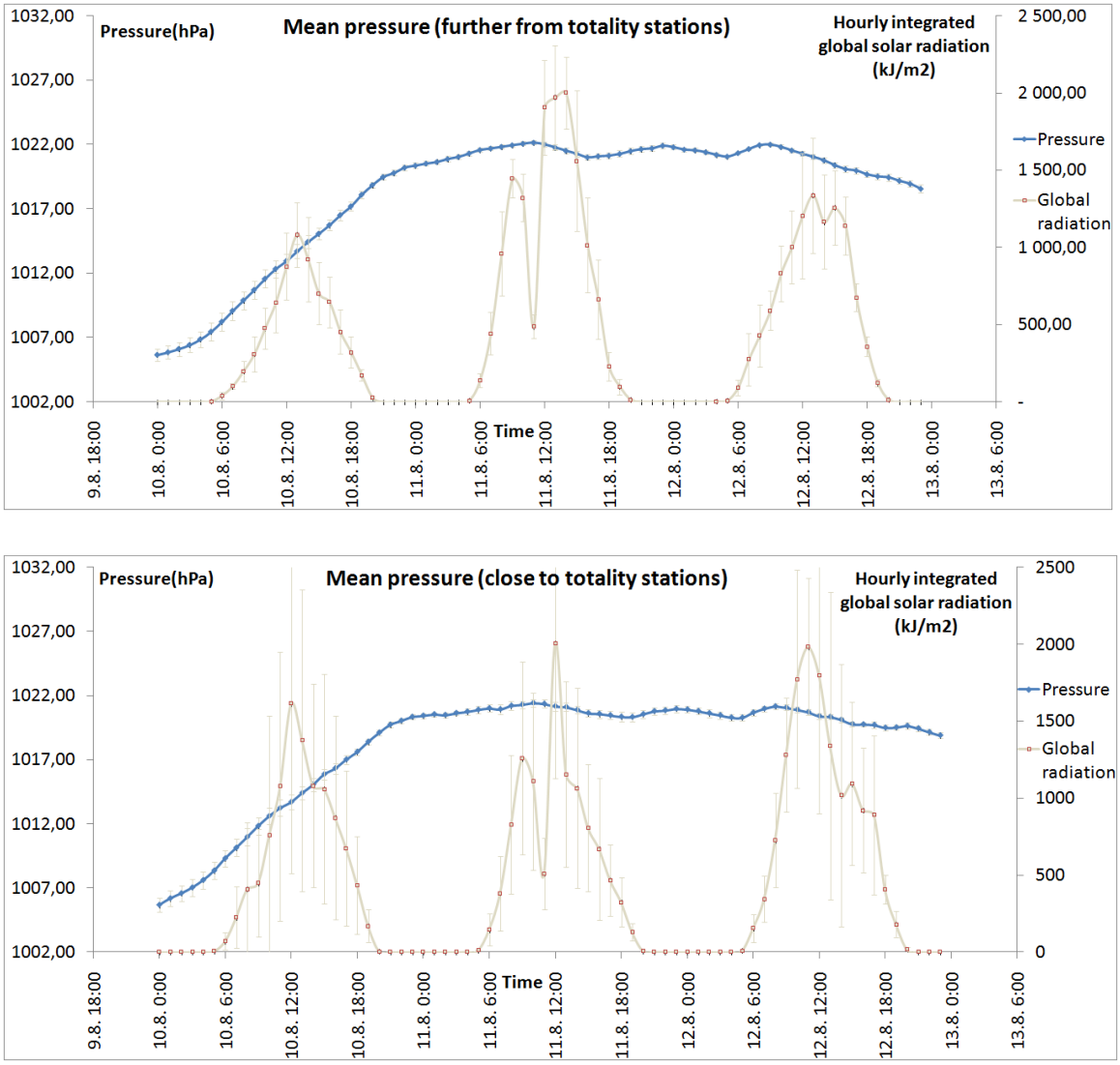

Figure 4.28: Plots of mean pressure (recorded at the hour) against time for 28 stations further from totality (top) and 33 stations close to totality (bottom) (blue). Plots of mean hourly integrated (for the hour before the data point) global solar radiation averaged across the stations considered in that graph in the background (grey) Error bars represent 2 standard errors

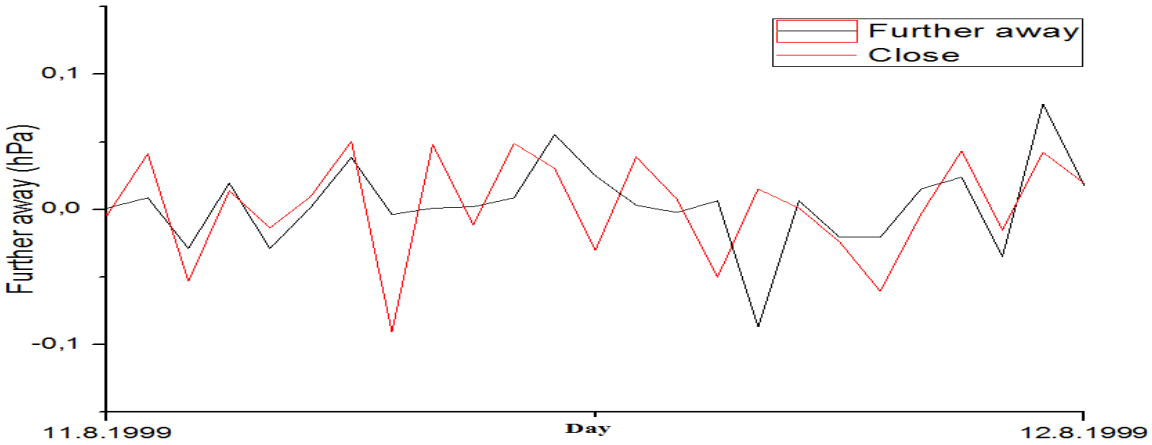

Figure 4.29: Plot of a difference between the smoothed curves and the curves in Figure 4.28 for stations further away (black) and closer to totality (red)

As in the previous comparison for pressure in section 4.4.2.2, not many differences can be seen when comparing the two plots in either Figure 4.28 or 4.29 above. This is again because the magnitude of the changes of mean sea level pressure associated with the eclipse is weak (0.1hPa or smaller) and the meteorological stations record sea level pressure to the nearest 0.1hPa at hourly intervals. Because a method of averaging is used, the pressure resolution should be greater than 0.1hPa. There should not be a problem with spatial resolution as a dense network of stations was used. However, the hourly temporal resolution is too coarse to detect eclipse related changes as they occur on a timescale of minutes. For the same reason it is not possible to differentiate whether changes were greater at stations closer to or further from totality. The general pressure pattern (including the two peaks in the day after the eclipse) does not reveal any major differences between these groups of stations.

4.4.3.3. Mean windspeed

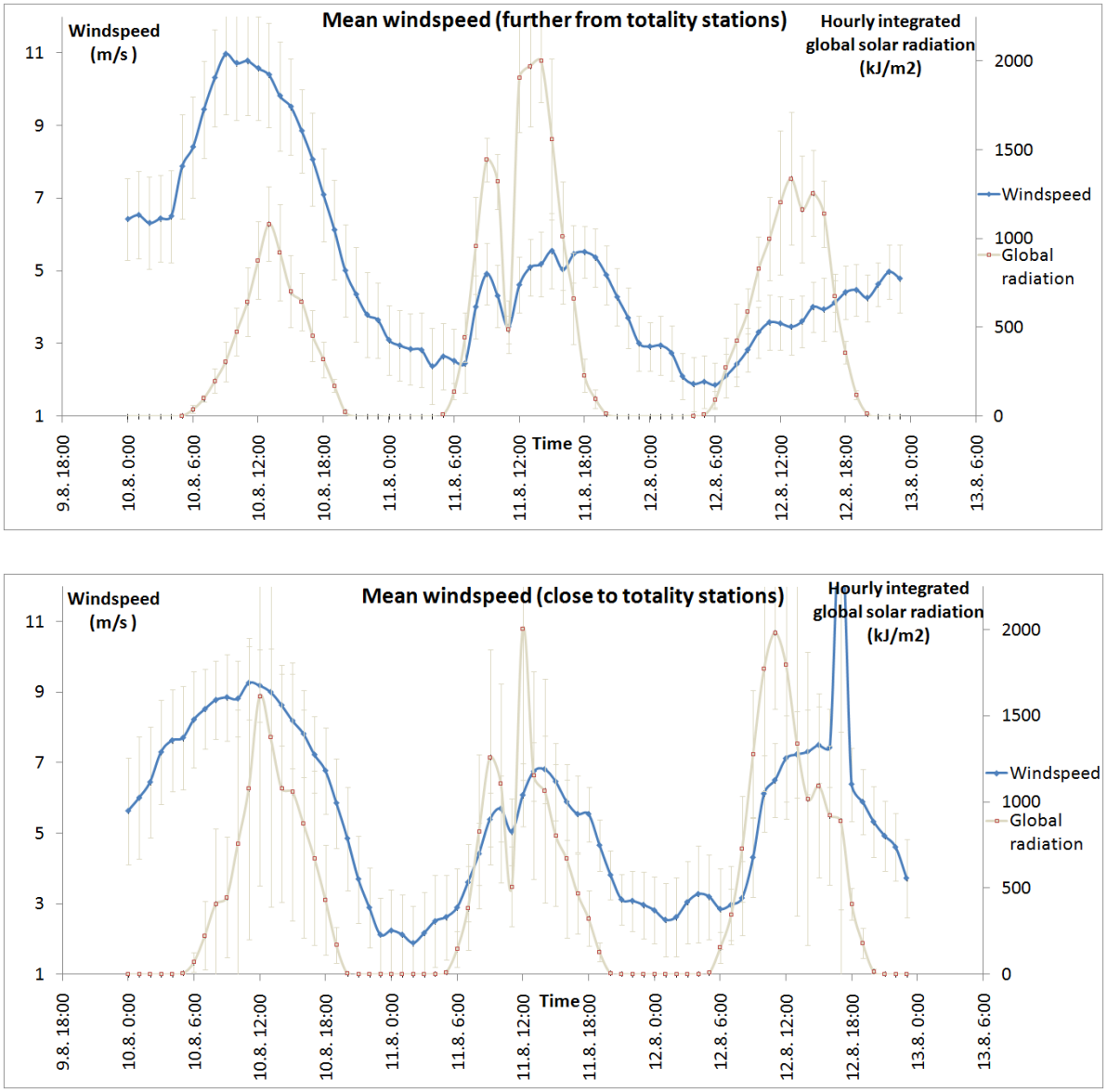

Figure 4.30: Plots of mean windspeed (averaged over the hour before data point) against time for 28 stations further from totality (top) and 33 stations close to totality (bottom) (blue). Plots of mean hourly integrated (for the hour before the data point) global solar radiation averaged across all the stations considered in that graph in the background (grey) Error bars represent 2 standard errors

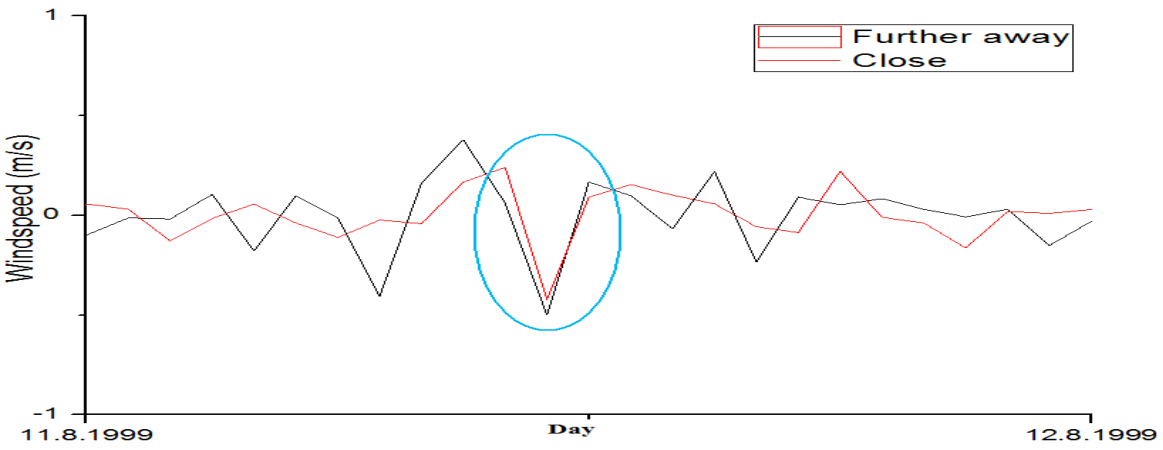

Figure 4.31: Plot of a difference between the smoothed curves and the curves in Figure 4.30 for stations further from (black) and closer to totality (red)

Figures 4.30 and 4.31 above show that the reduction in windspeed that occurred at eclipse time was about the same at stations that were located further from totality and at those located closer to totality. The magnitude of the anomaly for stations further from totality was 0,90m/s with a standard error of 0,10m/s and for stations closer to totality was 0,8m/s with a standard error of 0,13m/s. The reduction at both sets of stations was almost comparable to random or synoptically induced fluctuations.

4.4.3.4. Mean wind direction

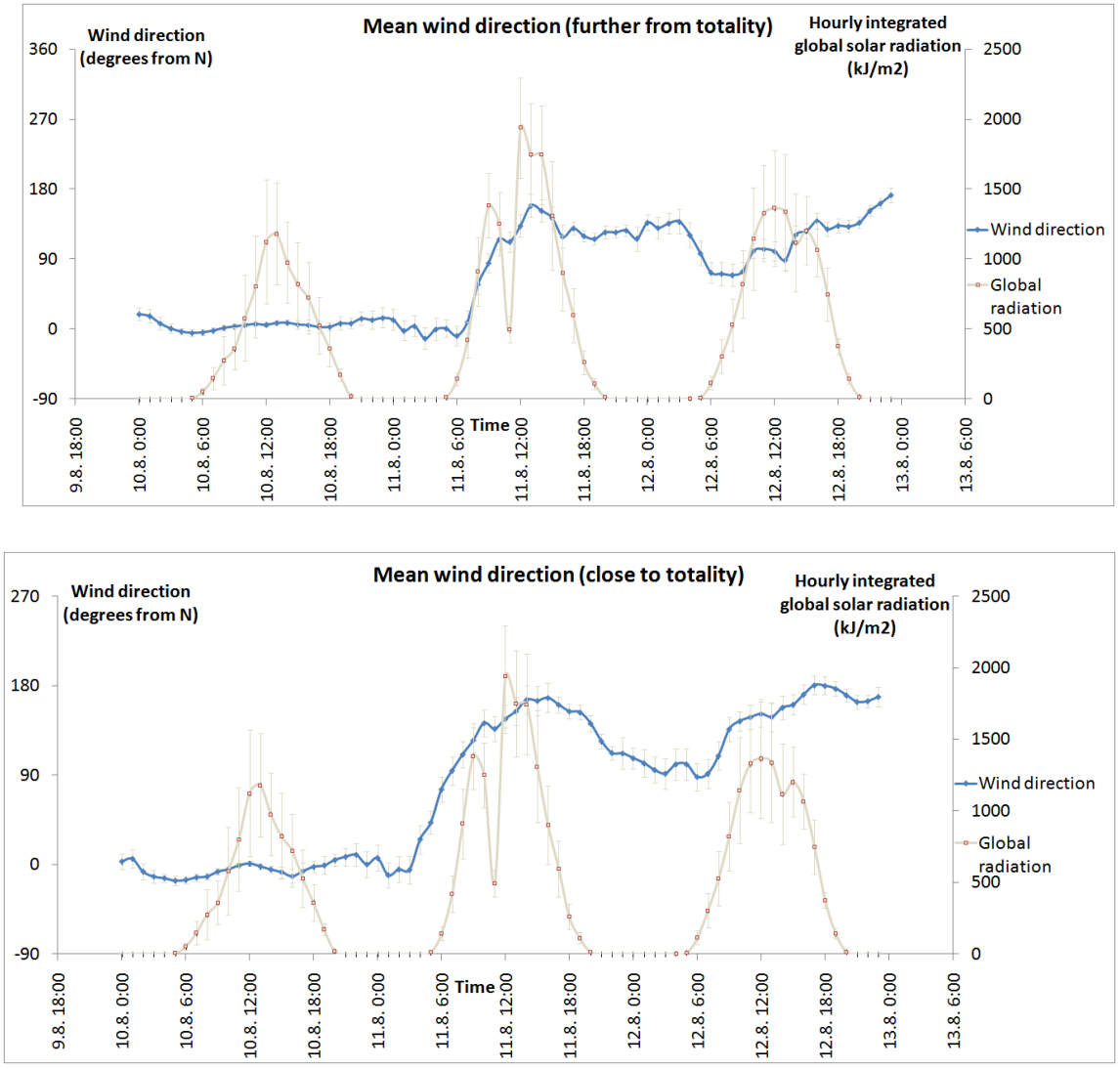

Figure 4.32: Plots of mean wind direction (averaged over the hour before data point) against time for 28 stations further from totality (top) and 33 stations close to totality (bottom) (blue). Plots of mean hourly integrated (for the hour before data point) global solar radiation averaged across all the stations considered in the background (grey) Error bars represent 2 standard errors

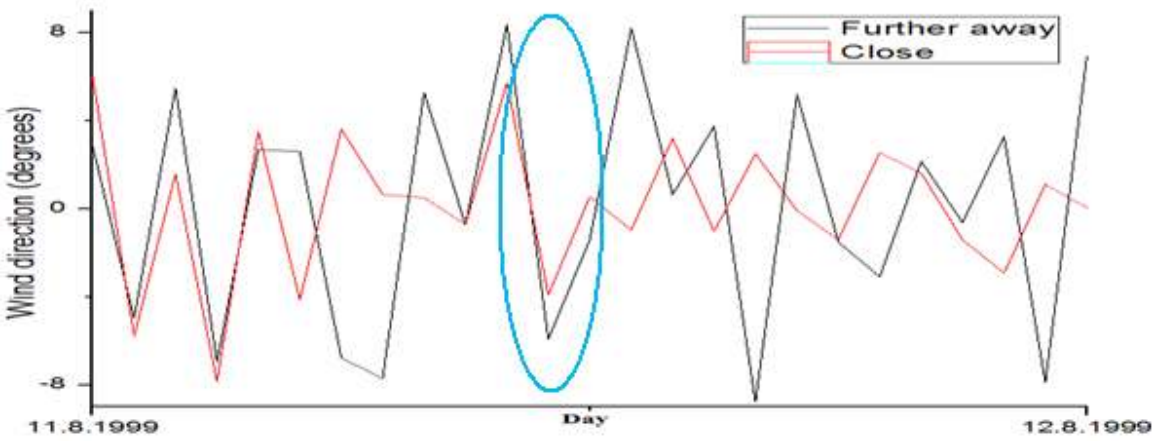

Figure 4.33: Plot of a difference between the smoothed curves and the curves in Figure 4.32 for stations further from totality (black) and closer to totality (red)

Figures 4.32 and 4.33 above show the change in wind direction due to the eclipse (blue circle in Figure 4.33). It can be seen that it was greater at stations that are located further away from totality, which is contrary to what would be expected. The magnitude of the anomaly at stations further from totality was 16degrees with a standard error of 2.8 degrees and at stations close to totality was 9degrees with a standard error of 2.6degrees. One possible explanation for this is the fact that areas further away (north) were closer to the high pressure centre and were less affected by synoptically induced wind, which enabled eclipse induced changes to be more pronounced than further south and closer to totality.

5. Chapter 5: Spatial analysis of synoptic changes caused by the 1999 eclipse

In order to better see and spatially recognise the lower atmospheric changes that were a result of the eclipse several spatial plots were created, where a map of the southern half of the UK was used and contour plots were calculated for temperature, pressure, radiation and windspeed. The contours were calculated by the use of programming language R and the data from 61 stations that were used to calculate the plots in section 4. For wind direction, vectors were used that also reflected the windspeed measured at each station. These plots were calculated for 8, 9, 10 and 11UT. The eclipse began before 9UT, maximum occurred at about 10:15UT and eclipse ended after 11UT.

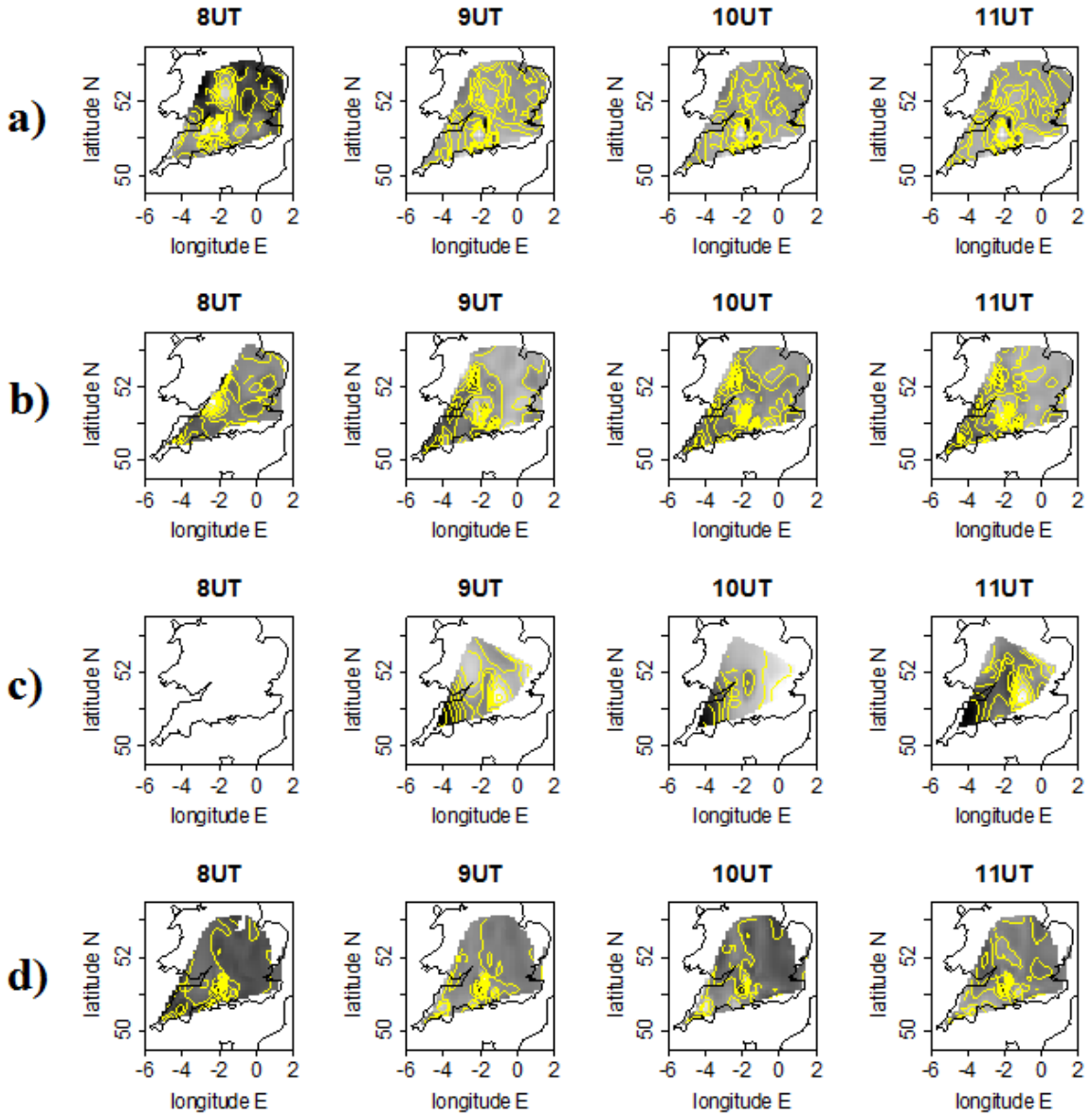

Figure 5.1: Contour plots for a) temperature, b) pressure, c) radiation and d) windspeed at 8, 9, 10 and 11UT on 11th August 1999 for southern half of UK. Dark shaded means low values and light shaded higher values of the variable concerned. Plot for radiation at 8UT missing as no information was available for that time. Maximum eclipse around 10:15UT

It can be seen in the first row of plots (for temperature) that there are initially some regional differences in temperature between the north and the south. There are lower temperatures over northern areas and inland than in the south and at the coast. This is likely an effect of nocturnal cooling, which is more pronounced in areas sheltered from marine influence and dissipates with the onset of diurnal heating. This is a typical phenomenon for clear nights and the night before 11th August was under the influence of a

ridge and hence the weather was very likely mostly clear. Otherwise, there are no other clear temperature differences that could be seen in the data for the times around maximum eclipse (10UT). There is rather high non-systematic regional variability in temperature and hence the effect of eclipse cooling (predicted by Prenosil (2000) to be 2 degrees over inland areas of the UK) does not clearly stand out in this case.

Regarding pressure, it can be seen in all four pressure plots that there is a lower pressure towards the west and higher pressure towards the north and east. This is what corresponds to the synoptic situation shown in Figure 4.2. There is a distinct area of higher mean sea level pressure somewhere in the region of Northamptonshire and this is what partly corresponds to the by Prenosil (2000) analysed mean sea level pressure change shown in Figure 3.13 in chapter 3.

Global solar radiation features generally lower values to the west and higher values to the east. This is likely a direct effect of the approaching occlusion and the cloudiness associated with it. One feature to note is an area of locally higher values of global solar radiation over central parts of England (from about Oxford southwards), which disappears in the plot for 10UTC (closest to eclipse time) where there is even a region of locally lower values in that area. This is likely a direct result of the eclipse.

Windspeed seems to be lower to the northeast, which is what would correspond synoptically to the location of the ridge. Overall, there is a decrease in windspeed at 10UTC, which is again more pronounced to the north in the areas that were closer to the high pressure centre.

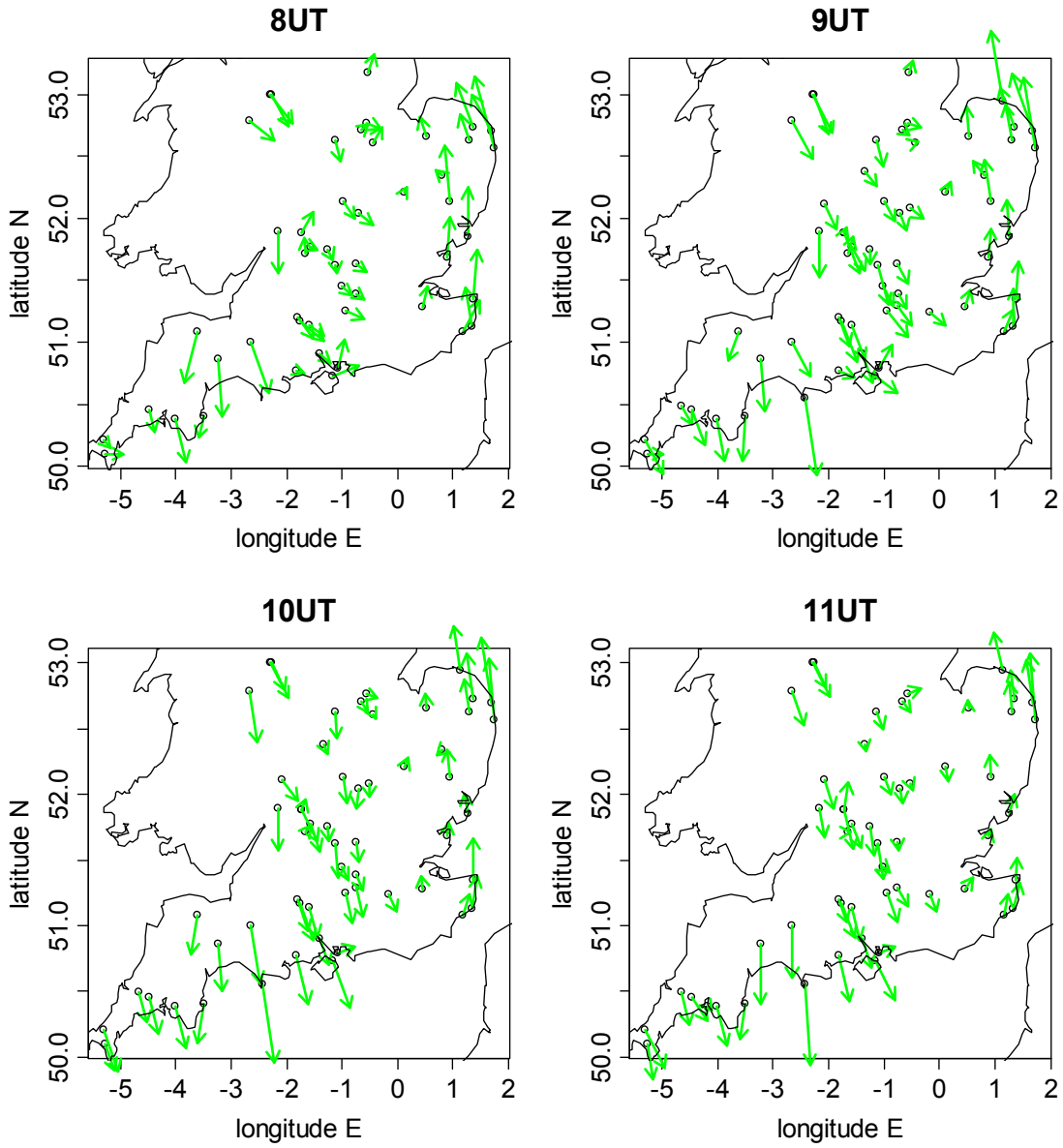

Figure 5.2: Wind vectors over the UK for 8, 9, 10 and 11UT on 11th August 1999

It can be seen in Figure 5.2 that the general wind direction distribution was from the northeast or north in the western half, more random in the eastern half with southerly on the east coast. Regarding windspeed, it was strongest in the west and weaker towards the east with the exception of a few coastal areas in East Anglia, where the windspeed magnitude was similar to the values in the west.

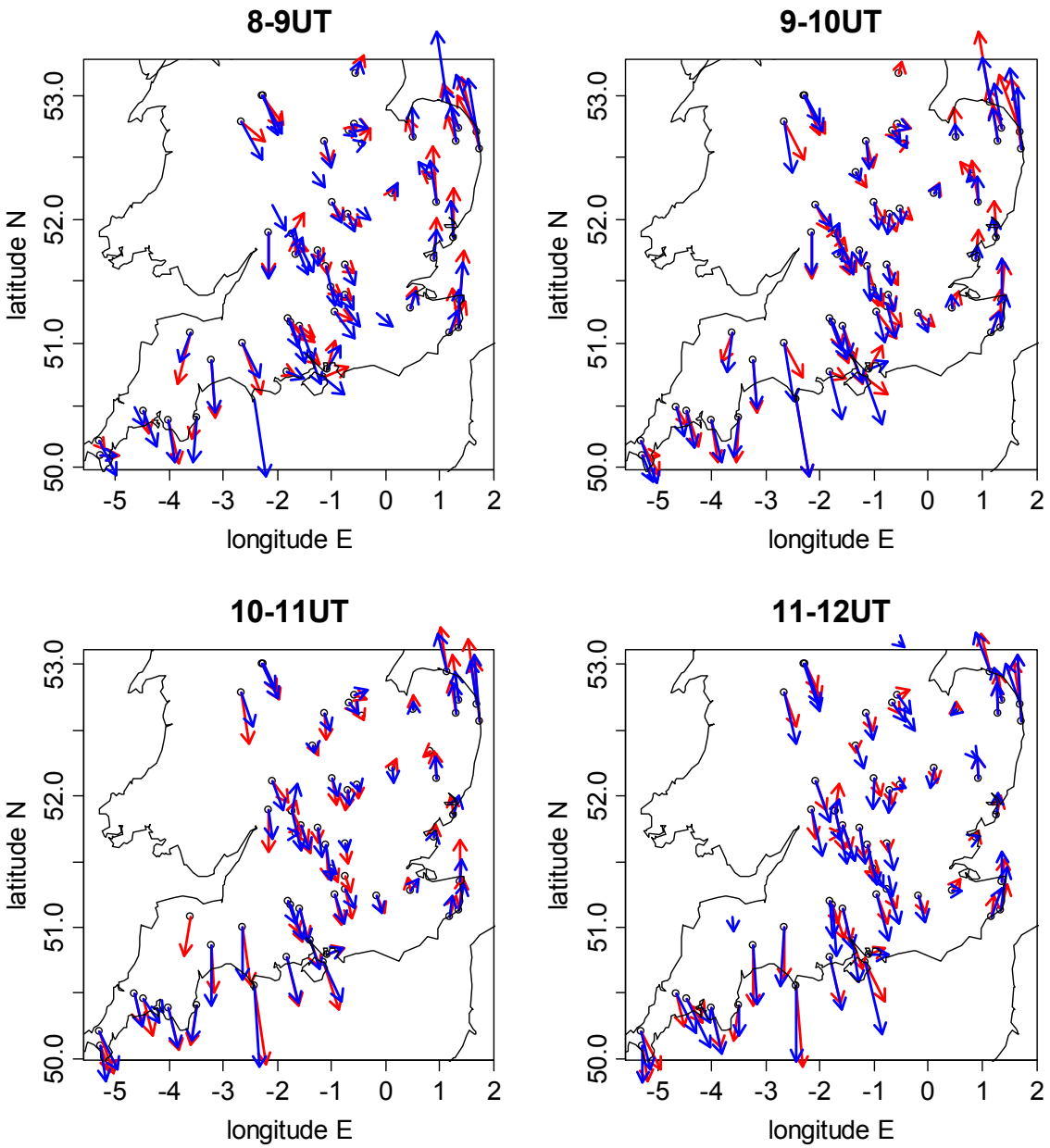

Figure 5.3: Wind vectors over the UK for two successive hours for 8-9, 9-10, 10-11 and 11-12UT on 11th August 1999. Red is for the earlier hour and blue for the later hour

In order to better see any regional changes in windspeed or wind direction, plots for two successive hours were obtained. In this way it could be more easily seen how the windspeed and wind direction changed (responded) during one hour time. The most interesting features of these graphs are the decrease of windspeed and the backing of the wind before eclipse time. The decrease of magnitude of the wind vectors is apparent at all the stations between 10UT and 11UT, even the coastal ones in Kent and East Anglia. Changes in wind direction start to be noticeable between 9UT and 10UT, especially in the

east, where almost all stations show a backing trend of the wind. The greatest wind direction changes occur between 10UT and 11UT when a veering trend is observed mainly at the stations in the southwest. A weaker veering trend follows between 11UT and 12UT mainly in the south.

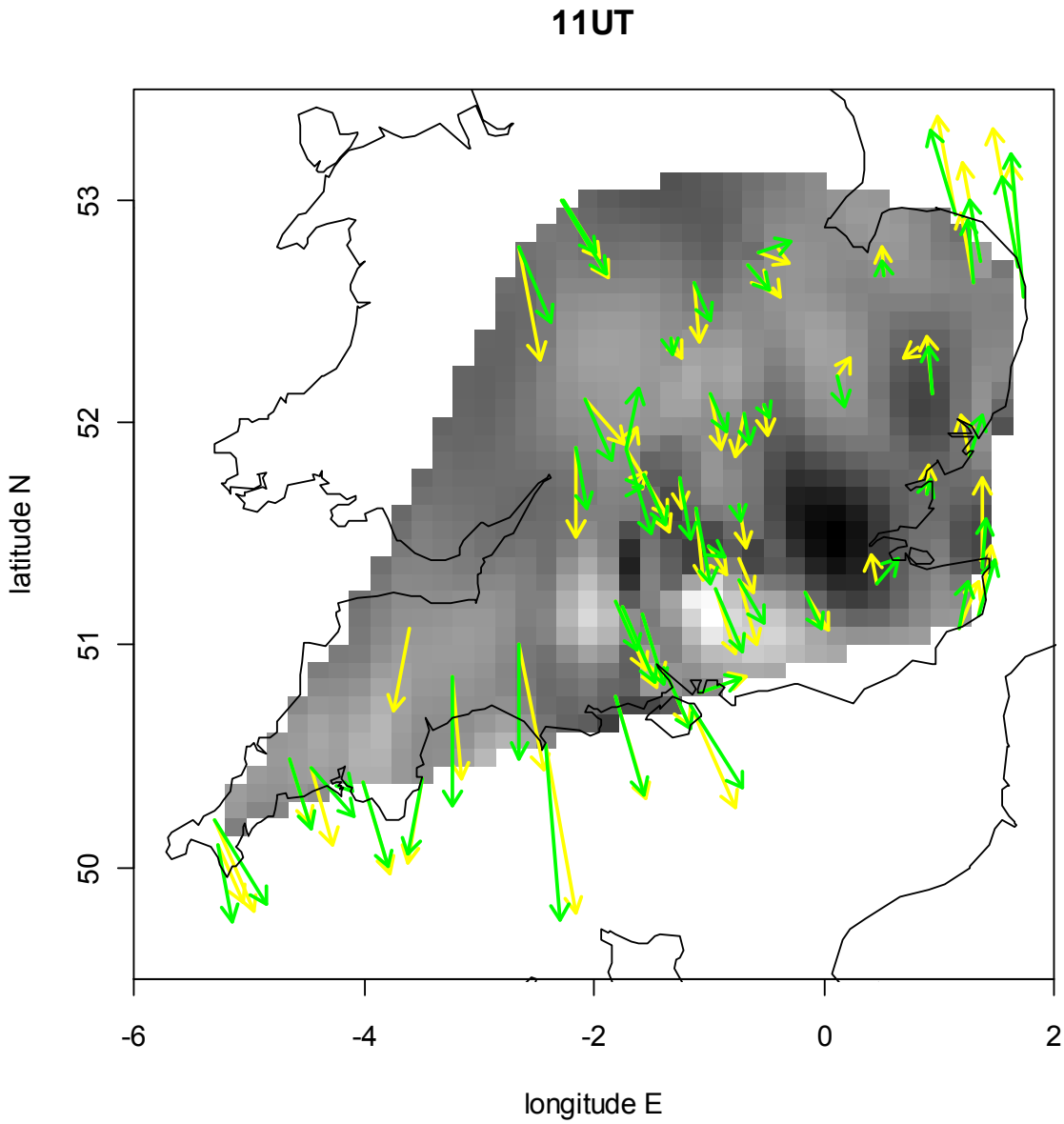

Figure 5.4: Wind vectors over the UK for 10UT (yellow) and 11UT (green) on 11th August 1999. Temperature anomalies shaded in the background. Smaller temperature anomalies (warmer relative temperatures) shaded light grey, greater temperature anomalies (cooler relative temperatures) shaded black

Figure 5.4 above is a greater and clearer version of 10-11UT in Figure 5.3 with the temperature anomaly shaded below. Regarding temperature it can be seen that there are two local minima (maximum negative anomalies) in southern England, one over the east (London area) and a second weaker one over Oxfordshire and Gloucestershire.

Regarding wind direction, it can be seen that the weaker magnitude wind vectors over the eastern half of southern UK change more than the stronger magnitude wind vectors in the southwest or near the coast of East Anglia. This is what corresponds to the results of section 4.4.3.4. The backing of the wind that is observed mainly in the east, however, is not coherent and some stations even show an opposite veering trend during this hour. This may be caused by some local variability in wind direction especially at coastal stations, which are greatly affected by land/sea breezes.

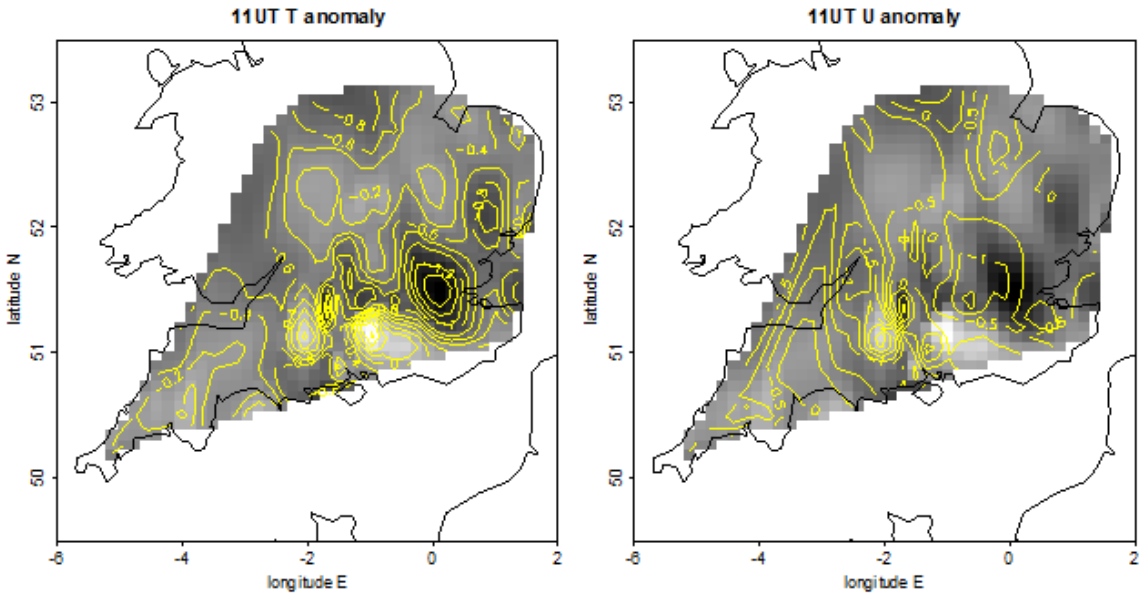

Figure 5.5: Contour plots of temperature (left) and windspeed (right) anomalies. Temperature anomalies shaded in the background of both plots. Smaller temperature anomalies (warmer relative temperatures) shaded light grey, greater temperature anomalies (cooler relative temperatures) shaded black

When looking at temperature anomalies, it can be seen that the greatest anomaly was measured over eastern parts of southeast England somewhere over the London area with lower anomalies to the north and west. The magnitude of the greatest anomaly was about 1.4 degrees Celsius. There is a second spatially smaller anomaly over East Anglia the

magnitude of which is about 0.8 degrees Celsius. When comparing this temperature plot with the results of Prenosil's (2000) study in Figure 3.12 in chapter 3 it can be seen that it does not agree well with the magnitude of the anomalies, which was modelled to be over 2 degrees for most of the area considered in this study. The windspeed anomalies show, as discussed with Figure 5.4, two local windspeed minima (maximum negative anomalies) over eastern and central England with lower anomalies to the west.

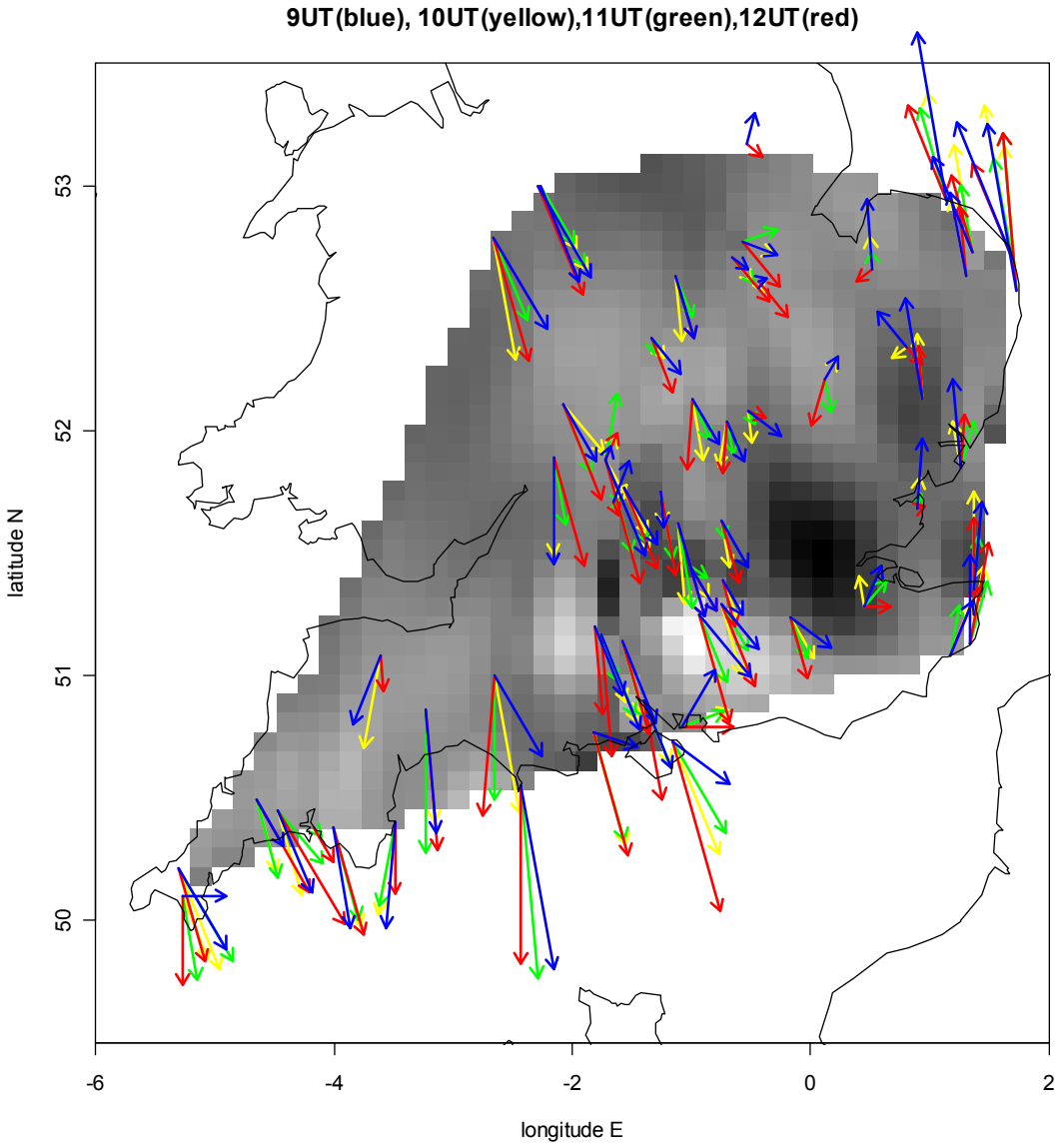

Figure 5.6: Wind vectors for 9UT (blue), 10UT (yellow), 11UT (green) and 12UT (red). Temperature anomalies for 11UT shaded below with darker areas meaning greater negative anomalies and lighter areas smaller negative anomalies

The wind vectors in the figure above show great local variability in both their magnitude and direction. There are, however, trends that can be observed at some stations. Especially the stations in the eastern half where the general magnitude of the wind vectors is low it can be seen that the wind direction backs during eclipse time (10 and 11UT) and at some stations veers between 11UT and 12UT. Towards the southwest, most of the stations are near the coast and it seems that the wind direction is still being affected by morning land breezes. The veering with time can be due to the approach of the low pressure system from the west.

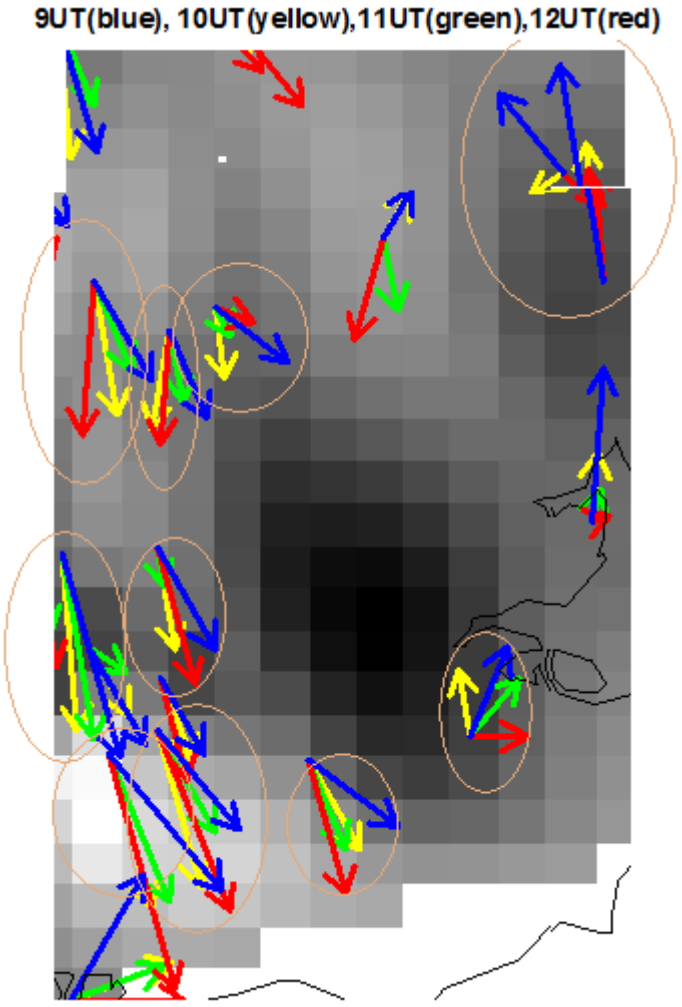

Figure 5.7: A zoom-in on the cold anomaly over southeast England from Figure 5.6. Wind vectors for 9UT (blue), 10UT (yellow), 11UT (green) and 12UT (red). Temperature anomalies for 11UT shaded below with darker areas meaning greater negative anomalies and lighter areas smaller negative anomalies. Stations that seemed to show eclipse related wind response circled in brown

Figure 5.7 shows an interesting result. A cold air anomaly has developed over eastern part of Southeast England. This was very likely a response to the eclipse and it has developed in this area due to relatively clear conditions as opposed to areas further west as well as due to its proximity to path of totality and distance from the coast.

Surrounding this cold air anomaly several stations show clear hints of an existence of an eclipse induced cold air cyclone around the time of maximum eclipse (between 10UT and 11UT). This can be seen in the cyclonic departure of the general trend of the wind between 10UT and 11UT, which is clearly visible at the stations that were circled in Figure 5.7 above. This means that the wind either backs or its veering trend is reduced between 10UT and 11UT.

6. Chapter 6: Conclusions

This project has tested a theory for eclipse induced circulation changes that was introduced more than 100 years ago by Clayton (1901). It was done by taking advantage of a rare opportunity of a total solar eclipse passing over a spatially dense network of regularly measuring meteorological stations.

6.1. Prediction and finding

The following table summarizes the results of this study and compares them to the study performed by Prenosil (2000) with the main difference between these studies being the resolution. In case of Prenosil (2000), the model grid point diameter was 63.5km while the average distance between 2 reference points (meteorological stations) in this study was 34.2km (calculated by averaging distances between neighbouring stations).

	ΔT (°C)	ΔU (m/s)	ΔWd (degrees)	ΔS (J/m2)	Δp (hPa)
Prenosil	-2	-0,51	n/a	n/a	0,1
All stations	(-1,5 ± 1,15)	(-0,8 ± 0,12)	13 ± 2,1	1051 ± 93,2	not resolvable
Cloudy	(-1,25 ± 0,38)	(-0,6 ± 0,08)	17 ± 4,3	n/a	not resolvable
Non-cloudy	(-1,6 ± 1,19)	(-0,9 ± 0,11)	9 ± 1,7	1051 ± 93,2	not resolvable
Further from eclipse	(-1 ± 0,93)	(-0,9 ± 0,1)	16 ± 2,8	920 ± 98,5	not resolvable
Close to eclipse	(-0,9 ± 0,87)	(-0,8 ± 0,13)	9 ± 2,6	1294 ± 45,9	not resolvable

Table 6.1: Comparison of results of Prenosil's (2000) study and the averaging technique used in this study together with different subsets of stations studied. ΔT stands for the temperature anomaly, Δp for pressure anomaly, ΔU for windspeed anomaly, ΔWd for wind-direction anomaly and ΔS for global solar radiation anomaly. Results of Prenosil's (2000) study in top row, results of the averaging technique study in the other rows

As can be seen in Table 6.1, there are some agreements between Prenosil's (2000) model and the results of this study, but also discrepancies. The greatest discrepancy is that Prenosil (2000) claimed 0,1hPa rise in mean sea level pressure, which was not detected in this study even by averaging 61 stations that measure changes in pressure to the nearest 0,1hPa. The resolution of the stations should have even been improved due to the averaging technique.

Spatial resolution was also much better (finer) than that used in Prenosil's (2000) model. A conceivable explanation why this change was not detected may be that it was missed by the stations temporal resolution. The stations log pressure at the hour and the maximum eclipse occurred between 10:15UT and 10:30UT. The eclipse related pressure change usually lasts only several minutes and hence it might have been missed in between the individual station measurements.

Regarding temperature Prenosil's (2000) model and this study both agree with the fact that temperature dropped during the eclipse. The magnitude of the decrease predicted by Prenosil (2000) is within the typical standard error of the results of this study. Also, it was found in this study that clouds have a significant effect on the temperature anomaly, which was found to be by about 25% greater in cloud free regions than in cloudy regions. This agrees with the results given by Aplin and Harrison (2002).

6.2. Wind effects

Many people that observe a solar eclipse and experience totality describe a gust of colder wind that occurs during or just after totality. This is generally called an 'eclipse wind'. But what is the exact effect that people describe as 'eclipse wind'? It has been suggested that the eclipse wind is the passage of the cold core cyclone and that what people feel is the change in wind direction associated with that cyclone. However, this study has shown that the eclipse related wind direction change has a magnitude smaller than 20 degrees, which is hardly recognisable by a human being without any proper measuring device.

The magnitude of the wind speed anomaly found by Prenosil's (2000) model was by about 30% smaller than the magnitude obtained in this study. It can be seen in Table 6.1 that wind speed dropped in all subsets of sites, and that clouds had a slight effect as the wind speed anomaly was greater at cloud free (and with greater negative temperature anomaly) sites. This is confirmed in Figure 5.6 of the previous section.

It was not possible to obtain the sign of the windspeed change from the Prenosil's (2000) model as well as wind direction change as the model did not give a quantitative average of change of wind direction, but only a spatial map showing wind direction anomalies. It can

however be seen in Table 6.1 that cloudy stations away from totality had a greater average wind direction anomaly. This was likely caused by the fact already discussed in section 4.4.2.4, which states that the wind changes were more pronounced in the regions closer to the high pressure centre where synoptically induced light winds prevailed as opposed to stronger winds further south and west. Therefore, it can be concluded here that in order to properly detect eclipse induced wind changes, suitable synoptic conditions have to be in place. Namely an area of light synoptically induced winds such as a high pressure or a ridge.

Figure 5.6 also confirms that the wind direction changes were most pronounced in the eastern half of southern England where light winds prevailed and in regions away from coasts. That figure also shows a cyclonic curvature of the winds around a cold region that likely evolved as a result of the eclipse over eastern parts of southern England. The curvature of the wind changes and their cyclonic nature may be challenged, but it may be claimed more solidly that there are some wind direction changes and that they look antisymmetric with respect to the (infinite) line of the eclipse passage.

Regarding windspeed, the magnitude of it decreases throughout the eclipse with a distinct minimum at maximum eclipse as can be seen in Figure 4.10 in section 4.4.1.4. The windspeed then increases again and returns to its pre-eclipse values after the end of the eclipse. The magnitude of this wind anomaly is about 1m/s, which could be felt by some people especially if there is almost no wind during totality and the windspeed returns to values around 1m/s after the eclipse. So according to the results of this study it is suggested that what people feel and describe as eclipse wind is not the change in wind direction but the increase of windspeed that usually occurs at the end of totality.

6.3. Suggestions for further work

Finally, it should be suggested how to plan an improved observation of changes that occur during an eclipse. There are several improvements that could be done. Firstly, the results would show much more detail if the recording stations recorded the data at greater time resolution so that small surface effects could be detected (e.g. recording data every 1 minute like it was performed by Aplin and Harrison (2002) in Camborne (see section 3.1)). Another improvement would be a more continental location where the study would be performed as

UK is an island and many stations here were affected by sea breezes and other land-sea interactions, which distorted the overall picture. Moreover, with a continental location much greater area could be studied both to the south and to the north of the path of totality. Also, there is some similarity between this study and Clayton's (1901) study, which is that UK is an island (landmass surrounded by ocean) and Clayton (1901) performed his study in south-east US, which is a region of landmass also surrounded by ocean in the southern and eastern half. A study that would better test Clayton's hypothesis would be performed in a more continental location, such as central or northern US.

Another improvement would be a use of instruments with greater resolution, such as sonic anemometers, which can detect very small changes in both windspeed and wind direction. The use of fine wire thermometers would be best to detect temperature changes at least to the nearest 0,01°C. Also, the measurements would be better the denser the network of meteorological stations.

6.3.1. Future potentially suitable eclipses for atmospheric research

Figures 6.1 to 6.6 show several future total and annular solar eclipses that will occur over densely populated areas with dense networks of regularly recording meteorological stations.

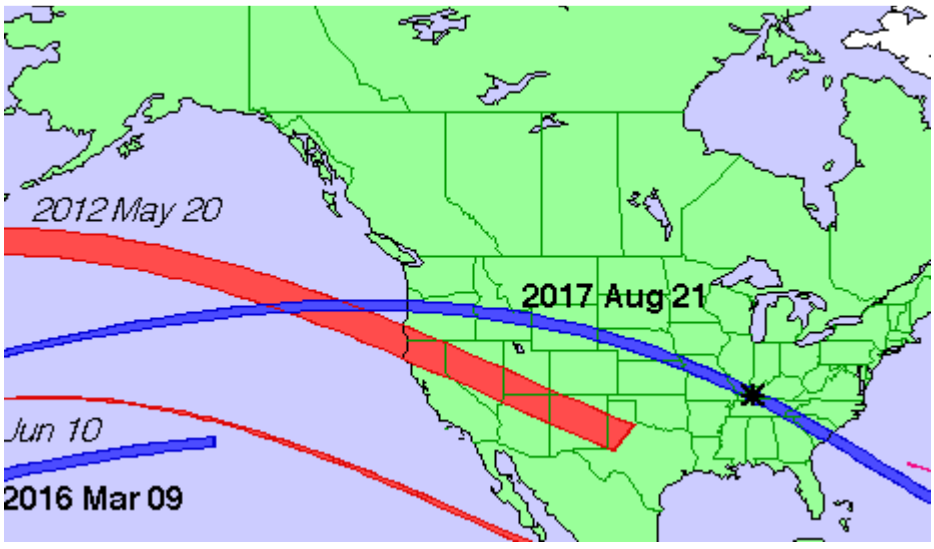

Figure 6.1: Paths of totality (blue) and annularity (red) for solar eclipses between 2010 and 2020 for the United States. Points of greatest eclipse shown by a black star (from Espenak @ http://eclipse.gsfc.nasa.gov/solar.html downloaded on 12th August 2010)

The next potentially interesting eclipse is the annular eclipse of 20th May 2012 as shown in Figure 6.1, which will pass over California and south-western states of the US, such as Arizona and Nevada. This may not be ideal in terms of coverage of meteorological stations as most of the area is desert. However, this area experiences strong diurnal heating and great temperature differences between day and night in May, which may be supportive of strong eclipse related temperature anomalies and other associated atmospheric changes.

The next total eclipse that passes over a dense network of recording stations is the one on 21th August 2017 as shown in Figure 6.1. This total eclipse will cross the entire United States and will very likely be observed, documented and studied at least to the same extent as the 1999 total eclipse was. Moreover, the eclipse will pass over a continental location, which is more suitable location than UK to test Clayton's (1901) hypothesis as discussed in section 6.3 above.

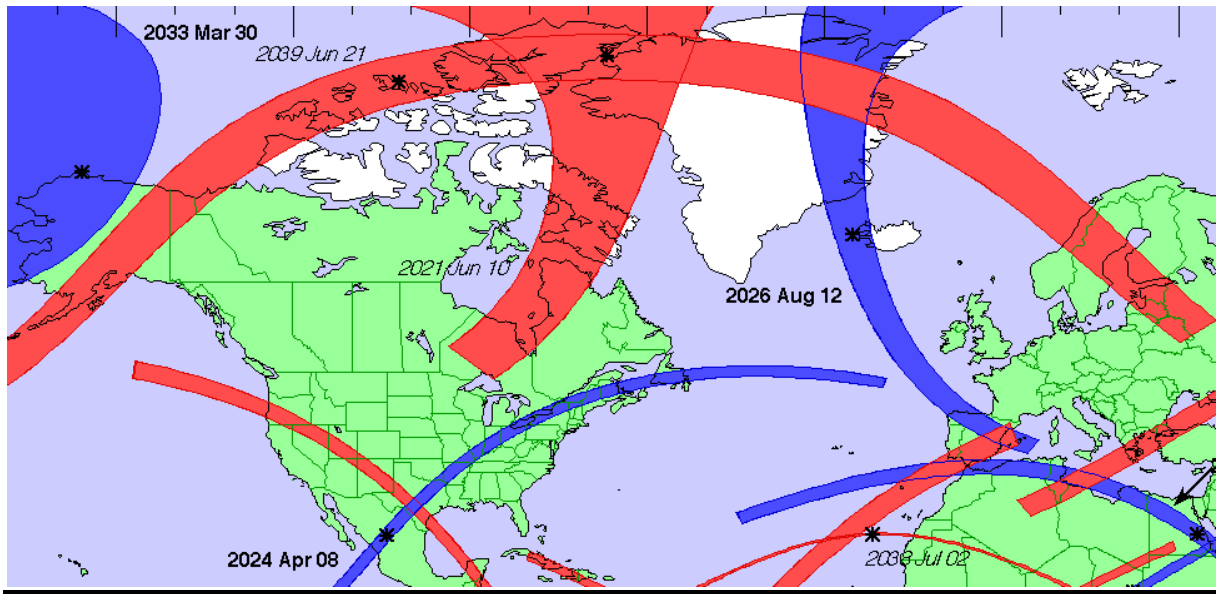

Figure 6.2: Paths of totality (blue) and annularity (red) for solar eclipses between 2020 and 2040 for the United States and Europe. Points of greatest eclipse shown by a black star (from Espenak @ http://eclipse.gsfc.nasa.gov/solar.html downloaded on 12th August 2010)

Figure 6.2 shows further eclipse opportunities in the 2020s. The best one seems to be the Apr 08 2024 total eclipse that also crosses the US and will likely be very well documented.

Another total eclipse crosses Spain in 2026, which gives the next European total eclipse opportunity to be studied.

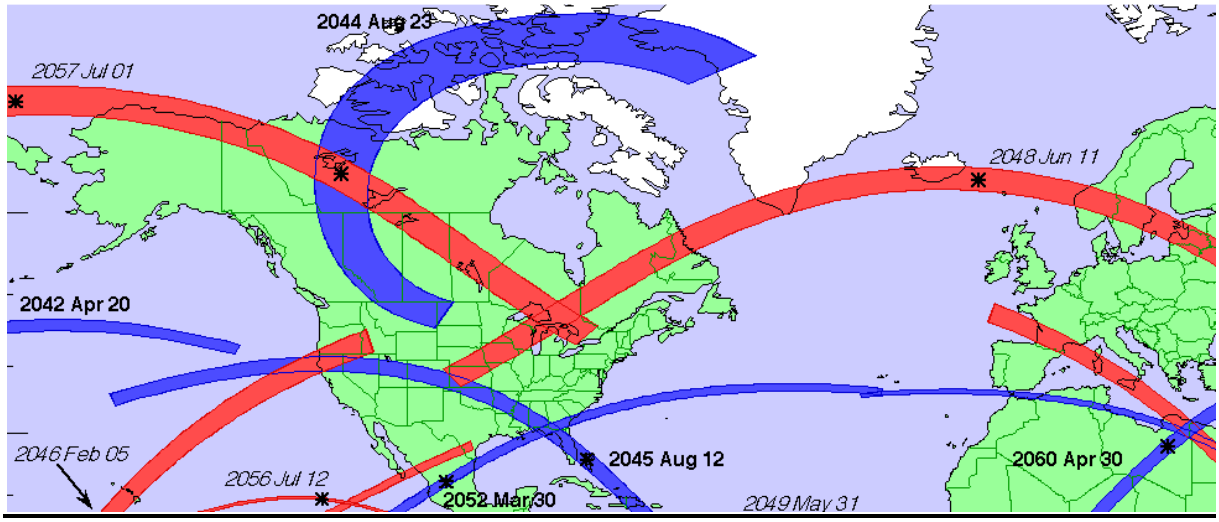

Figure 6.3: Paths of totality (blue) and annularity (red) for solar eclipses between 2020 and 2040 for the United States and Europe. Points of greatest eclipse shown by a black star (from Espenak @ http://eclipse.gsfc.nasa.gov/solar.html downloaded on 12th August 2010)

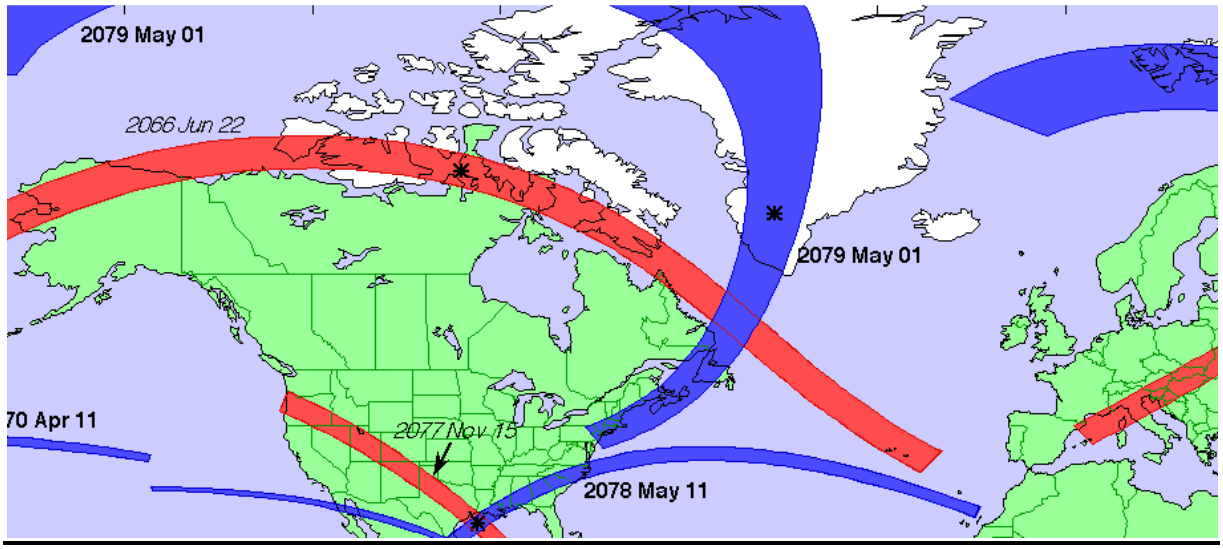

Figure 6.4: Paths of totality (blue) and annularity (red) for solar eclipses between 2020 and 2040 for the United States and Europe. Points of greatest eclipse shown by a black star (from Espenak @ http://eclipse.gsfc.nasa.gov/solar.html downloaded on 12th August 2010)

Figures 6.3 and 6.4 show some more distant eclipse opportunities. The most promising of these are probably the total eclipses of 2045, 2052 and 2078 over the US. Two eclipses, one

annular and one total, occur over the US in 2077 and 2078 respectively that are separated by less than half a year. This means that a great amount of data could be gathered at these two events and perhaps differences between effects associated with a total and an annular eclipse could be analysed and studied in this case.

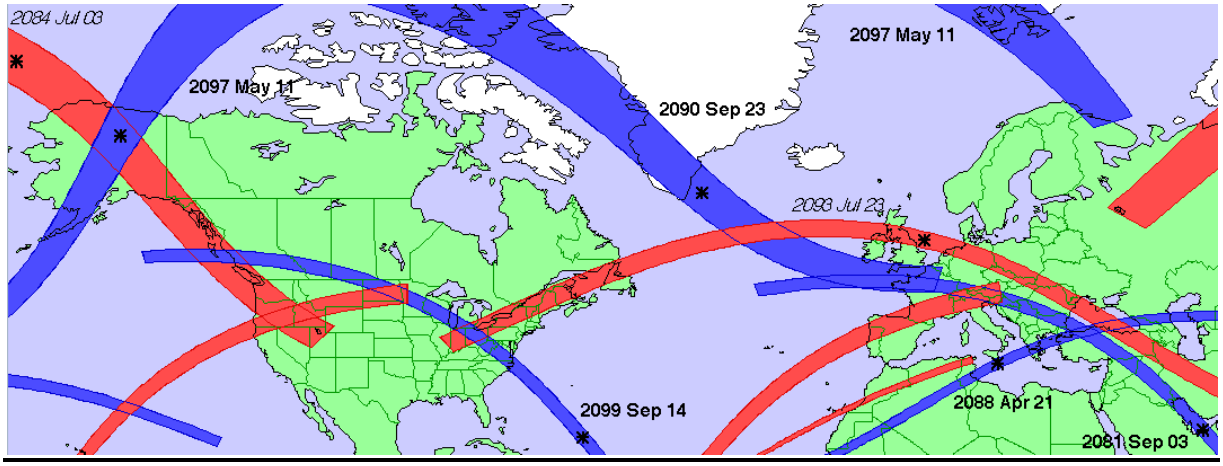

Figure 6.5: Paths of totality (blue) and annularity (red) for solar eclipses between 2020 and 2040 for the United States and Europe. Points of greatest eclipse shown by a black star (from Espenak @ http://eclipse.gsfc.nasa.gov/solar.html downloaded on 12th August 2010)

Figure 6.5 shows the next total eclipses that will occur over the UK, namely the ones of Sep 03 2081 and Sep 23 2090, both in southern UK. An annular eclipse will also affect northern UK on Jul 23 2093. Only the annular eclipse, however, will cross the UK. The umbral shadows of the two total eclipses will only partly fall on southern UK in the same way as the umbral shadow of the 1999 eclipse did.

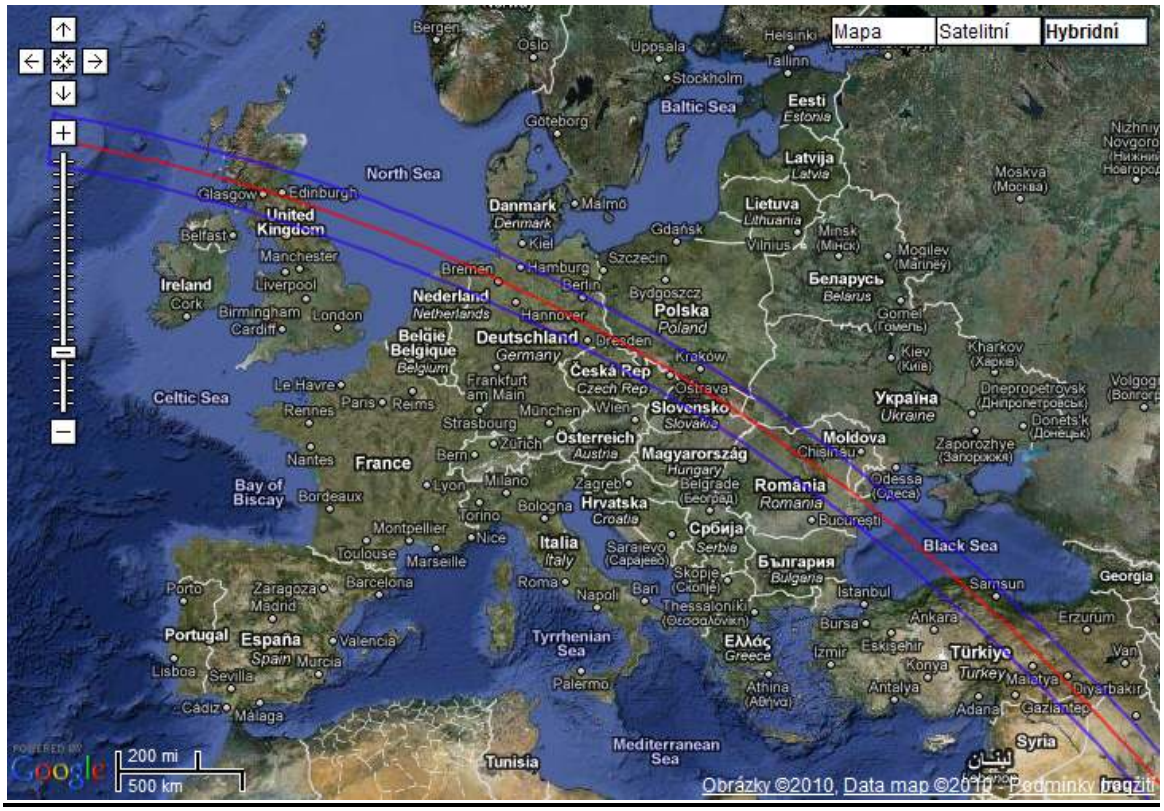

Figure 6.6: Path of totality of a total solar eclipse of 7th October 2135 over Europe. Centre of the path denoted by red line and limits of the path by blue lines (from Espenak @ http://eclipse.gsfc.nasa.gov/SEsearch/SEsearchmap.php?Ecl=21351007 downloaded on 12th August 2010)

Figure 6.6 above shows the path of totality of the total solar eclipse of 7th October 2135, which is the next total solar eclipse, whose umbral shadow will wholly cross the UK and hence measurements to the north of the path of totality as well as to the south of the path of totality would be obtainable from UK meteorological stations. This eclipse will be another good European opportunity as it will cross central Europe on quite a similar track to the total eclipse of 11th August 1999.

As can be seen in the Figures 6.1 – 6.6 above, the next century will give us several opportunities to further study atmospheric changes that are associated with eclipses. These will mostly be over the US, but several eclipses will occur over Europe as well. In the meantime, observing networks in all the countries that are to be affected by these eclipses could be improved to standards described in section 6.3 so that more precise and detailed measurements of effects associated with eclipses could be obtained in the future.

References

Abbot, W. N. 1958. On certain radiometric effects during the partial eclipse of February 25, 1952. *Geofisica Pura Appl.* **39**, 186-193

Adeniyi, J. O., Radicella, S. M., Adimula, I. A., Willoughby, A. A., Oladipo, O. A., and Olawepo, O.: Signature of the 29 March 2006 eclipse on the ionosphere over an equatorial station, *J. Geophys. Res., 112, A06314, doi: 10.1029/2006JA012197, 2007.*

Afraimovich, E. L., Palamartchouk, K. S., Perevalova, N. P., Chemukhov, V. V., Lukhnev, A. V., and Zalutsky, V. T.: Ionospheric effects of the solar eclipse of March 9, 1997, as deduced from GPS data, *Geophys. Res. Let., **25(4),** 465–468, 1998.*

Aplin K. L. and R.G. Harrison, 2002 Meteorological effect of the 1999 eclipse, *Proc. R. Soc. Lond. A (2002)*

Bojkov, R. D.: The ozone variations during the solar eclipse of 20 May 1966, *Tellus, **20**, 417–421, 1968.*

Chakrabarty, D. K., Shah, N. C., and Pandya, K. V.: Fluctuation in ozone column over Ahmedabad during the solar eclipse of 24th October 1995, *Geophys. Res. Lett., **24(23)**, 3001, 1997.*

Clayton, H. H. 1901, the eclipse cyclone and the diurnal cyclones. *Ann. Astron. Observ. Harvard College* **43**, 5–33

Espenak, F 2009 @ http://www.mreclipse.com/Special/SEprimer.html (May 2010)

Espenak, F 2009 @ http://eclipse.gsfc.nasa.gov/SEsaros/SEsaros.html (May 2010)

Espenak, F 2010 @ www.eclipse.gsfc.nasa.gov/SEgoogle/SEgoogle1951/SE1999Aug11google.html (July 2010)

Espenak, F 2010 @ http://eclipse.gsfc.nasa.gov/SEplot/SEplot1951/SE1999Aug11T.GIF (August 2010)

Espenak, F 2009 @ http://eclipse.gsfc.nasa.gov/SEmono/TSE1999/TSE1999Map/T99Fig6.jpg (August 2010)

Espenak, F 2009 @ *http://eclipse.gsfc.nasa.gov/SEmono/TSE1999/TSE1999Map/TSE1999Europe.jpg (August 2010)*

Farges, T., Jodogne, J. C., Bamford, R., Roux Y. Le., Gauthier, F., Vila, P. M., Altadill, D., Sole, J. G., and Miro, G.: Disturbances of the western European ionosphere during the total solar eclipse of 11 August 1999 measured by a wide ionosonde and radar network, *J. Atmos. Sol.-Terr. Phy., **63**, 915–924, 2001.*

Foken T., Wichura, B., Klemm, O., Gerchau, J., Winterhalter, M. &Weidinger, T. 2001, Micrometeorological measurements during the total solar eclipse of August 11, 1999, *Meteorol. Z.* **10**, 171–178

Gerasopoulos E., C. S. Zerefos, I. Tsagouri, D. Founda, V. Amiridis, A. F. Bais, A. Belehaki, N. Christou, G. Economou, M. Kanakidou, A. Karamanos, M. Petrakis, and P. Zanis, *Atmos. Chem. Phys., **8,** 5205–5220, 2008*

Google maps @ http://maps.google.com/ (June 2010)

Le, H, L. Liu, X. Yue, & W. Wan 2008. The ionospheric responses to the 11 August 1999 solar eclipse: Observations and modelling. *Ann. Geophys., **26,** 107-116*

Harrison, R. G. & Pedder, M. A. 2001 Fine wire thermometer for air temperature measurements at Poona during the solar eclipse on 14th December 1955. *Ind. J. Meteorol. Geophys.* **8**, 93-98

Jagannathan, P., Chacko, O. & Venkiteshwaran, S. P. 1956 Insolation measurements at Poona during the solar eclipse on 14th December 1955. *Ind. J. Meteorol. Geophys.* **8**, 93-98.

Kazantzidis, A., Bais, A. F., Emde, C., Kazadzis, S. and Zerefos, C. S.: Attenuation of global ultraviolet and visible irradiance over Greece during the total solar eclipse of 29 March 2006, *Atmos. Chem. and Phys., **7**, 5959–5969, 2007.*

Kovner, I: The greatest misconceptions in atmospheric science, *Ann. Met. Observ.* **28**, 12–35, 1912

Mims III, F. M. and Mims, E. R.: Fluctuations in column ozone during the total solar eclipse of 11 July 1991, *Geophys. Res. Lett., **20(5),** 367–370, 1993.*

Prenosil, T. 2000. The influence of the 11 August 1999 total solar eclipse on the weather over Central Europe. *Meteorol. Z.* **9**, 351-359

Tomas, A. T., Luhr, H., Forster, M., Rentz, S., and Rother, M.: Observations of the low-latitude solar eclipse on 8 April 2005 by CHAMP, *J. Geophys. Res., 112, A06303, doi:10.1029/2006JA012168, 2007.*

Winkler P., Kaminski U., Kohler, U., Riedl, J., Schroers, H. & Anwender, D. 2001 Development of meteorological parameters and total ozone during the total solar eclipse

of August 11, 1999. *Meteorol Z.* **10**, 193–199

http://en.wikipedia.org/wiki/Anemometer (July 2010)

http://www.wetterzentrale.de/topkarten/tkfaxbraar.htm (July 2010)

http://www.sems.und.edu/index_SolarEclipse.php (Mai 2010)

http://www.sat.dundee.ac.uk/auth.html (July 2010)